LBL-22378 c.2
Preprint

Lawrence Berkeley Laboratory

UNIVERSITY OF CALIFORNIA

RECEIVED
LAWRENCE
BERKELEY LABORATORY

NOV 18 1986

LIBRARY AND
DOCUMENTS SECTION

Submitted to Nuclear Physics A

THE QUANTUM STATISTICAL MODEL OF FRAGMENT FORMATION: ENTROPY AND TEMPERATURE EXTRACTION IN HEAVY ION COLLISIONS

D. Hahn and H. Stöcker

October 1986

TWO-WEEK LOAN COPY

This is a Library Circulating Copy
which may be borrowed for two weeks.

NUCLEAR SCIENCE DIVISION

LBL-22378 c.2

Prepared for the U.S. Department of Energy under Contract DE-AC03-76SF00098

DISCLAIMER

This document was prepared as an account of work sponsored by the United States Government. While this document is believed to contain correct information, neither the United States Government nor any agency thereof, nor the Regents of the University of California, nor any of their employees, makes any warranty, express or implied, or assumes any legal responsibility for the accuracy, completeness, or usefulness of any information, apparatus, product, or process disclosed, or represents that its use would not infringe privately owned rights. Reference herein to any specific commercial product, process, or service by its trade name, trademark, manufacturer, or otherwise, does not necessarily constitute or imply its endorsement, recommendation, or favoring by the United States Government or any agency thereof, or the Regents of the University of California. The views and opinions of authors expressed herein do not necessarily state or reflect those of the United States Government or any agency thereof or the Regents of the University of California.

LBL-22378

The Quantum Statistical Model of Fragment Formation - Entropy and Temperature Extraction in Heavy Ion Collisions

Detlev Hahn and Horst Stöcker

Nuclear Science Division
Lawrence Berkeley Laboratory
University of California
Berkeley, California 94720

This work was supported by the Director, Office of Energy Research, Division of Nuclear Physics of the Office of High Energy and Nuclear Physics of the U.S. Department of Energy under Contract DE-AC03-76SF00098.

The Quantum Statistical Model of Fragment Formation - Entropy and Temperature Extraction in Heavy Ion Collisions

Detlev Hahn and Horst Stöcker

Nuclear Science Division, Lawrence Berkeley Laboratory,

Berkeley, Ca 94720 and

Institut für Theoretische Physik

Johann Wolfgang Goethe Universität, Frankfurt am Main

Abstract:

Quantum statistical model (QSM) calculations of nuclear fragment formation are presented. Various independent methods for extracting the temperature, T, and entropy, S/A, from fragment- and pion yields in heavy ion collisions are analysed. It is emphasized that stable and instable medium mass fragments play an important role in determining T and S/A: They alter the relation $S/A(R_{dp})$ dramatically and distort via feeding simple temperature measurements. However, these fragments allow by their very abundance for a variety of new, alternative methods to determine S/A from data on multifragmentation (ratios of complex fragment yields, mass yield curves, and charged particle multiplicities).

Entropy values deduced from 4π Plastic Ball data exhibit a strong multiplicity dependence. For large multiplicities the entropy residing in nuclear fragments appears to be independent of the bombarding energy and low in absolute value, $S/A \simeq 3.5$.

The corresponding breakup temperatures of the fragment conglomerate are T = 12, 16, and 20 MeV at E_{Lab} = 400, 650, and 1050 MeV/n, respectively. These values are much smaller (a factor 1/3) than the temperatures extracted from pion yields. This result can be understood only if the pions are created in the early, hot stage of the collision, while the fragments are formed after an isentropic expansion of the system at small densities where the temperature is low. This would imply that in the late stage of the reaction a large fraction ($\simeq$ 80%) of the available center of mass energy resides in (possibly isotropic) flow.

1. Introduction

Recent exclusive 4π experiments of the GSI-LBL Plastic Ball collaboration have exhibited a strong dependence of the fragment formation on the multiplicity of participant charges[1]. The experimentalists used a quantum statistical model[2] to deduce entropy values from asymptotic (i.e. extrapolated to infinite multiplicity) d-like- to- p- like ratios for the reactions Ca + Ca and Nb + Nb at E_{LAB} = 400 - 1050 MeV/nucleon. They find surprisingly low values of S/A ≈ 2.5, nearly independent of bombarding energy.

The same quantum statistical model[2] had been used previously to extract the entropy from inclusive fragment mass distributions at lower incident energies[2-4]. Similary low entropy values as in ref. 1 had been obtained then [2-4].

This quantum statistical model has furthermore been applied by other groups to determine the effects of sequential feeding on the relative population of γ-instable[5-6] and particle instable states[7] to groundstates of Li and Be fragments. Most of the population ratios are affected dramatically. Hence the original idea[5] that the ratios of γ-instable states can be useful for a temperature determination turns out to be impracticable[5,6].

Some relative populations of selected particle instable states appear to be affected only moderately for temperatures $T < 10$ MeV [2,7] and can still be useful. For measurement of higher temperatures, $T \gg \Delta E$, this method is inapplicable, since the relative populations reach the asymptotic ratio given by the statistical weights. In a recent publication[8] we have shown that higher temperatures, $T > 10$ MeV, can be determined from the observed pion - to - proton ratios.

The present paper gives a detailed discussion of the quantum statistical model used extensively in the literature (refs. 1-7). In this model a system of A nucleons is considered in the grand canonical ensemble. A large variety ($\approx$ 600) of stable and instable fragment species with the appropriate degeneracy, binding energy and quantum statistical distribution function is considered, and the thermodynamic properties of the resulting mixture of fragments are computed. The decay of the particle and γ-instable states is taken into account in the second stage of the calculation which then yields the final distributions of the $\approx$ 100 stable fragment species.

It is shown that yields of light and medium heavy fragments can be useful to determine the entropy and temperatures in heavy ion collisions in a variety of ways.

Before we come to the yields of various species (p, d, t, ^{3}He...) calculated with the quantum statistical model as a function of entropy and temperature, we want to discuss in some detail the entropy creation in heavy ion collisions. In particular we study how the entropy distributes over the various hadronic channels in the initial hot, compressed stage of the reaction.

2. Hadronization in Nuclear Shock Waves

Entropy is created in heavy ion collisions predominantly during the stage of highest compression and thermal excitation[9]. A measurement of the asymptotic entropy value can yield information on this initial stage if there is only a moderate increase of entropy during the expansion of the system. Recent three dimensional (3-D) fluid dynamical and Vlasov- Uehling- Uhlenbeck calculations have

indicated that there is a moderate ~ 10% increase of the entropy due to nonequilibrium effects (viscosity), and that simplified 1-D shock wave calculations give values for the entropy per nucleon, the maximum achievable temperature and the achievable compression which are compatible with the results of the 3-D calculations.[9]

In a recent paper[8] we studied the connection between the pion multiplicities and the thermodynamic quantities density, temperature and compressional energy in the energy region from 30 MeV/n to 30 GeV/n. We also analyzed the importance of massive baryon resonances, heavy mesons and the Bose condensation of pions, which decrease the temperature in the system substantially. The main point of that paper was to extract the temperatures in the moment of highest compression from the pion data. We used a relativistic quantum statistical approach to describe the state of the system in the moment of the pion freezeout. We will employ this model here to estimate the achievable entropy values in the collisions of heavy nuclei. The main input into the calculation is[8-11]

i) The pions emerge from the high density stage of the reaction with a multiplicity given by the chemical equilibrium value of the pion plus Δ and N^* abundance at the given thermal energy[8-11].

ii) All the available c.m. energy resides exclusively in thermal and compressional energy at one - namely the maximum achievable - density in the moment of the pion, Δ, and N^* chemical freeze-out.

iii) The density and temperature in this moment of highest compression and excitation is given by a simplified one dimensional hydrodynamical calculation using the Rankine- Hugoniot equations for two colliding equal nuclei[9-11].

These assumptions are qualitatively supported by cascade and VUU calculations[9,11-13]. They are certainly not quantitatively fulfilled in the experiment. Nevertheless, they serve as a convenient method to guide the search for the principle physical effects of the compression on the bombarding energy dependence of the thermodynamic quantities.

Let us briefly recapitulate the relativistic Rankine- Hugoniot equation which is used to connect the dynamical variables with the thermodynamical ones[8-11]. It is derived from the conservation of baryon number, energy and momentum on the two sides of a shock front:

$$W^2 - W_o^{\ 2} + P\left(\frac{W}{\rho} - \frac{W_o}{\rho_o}\right) = 0 \qquad (1)$$

where W_o = 939 MeV - B, B = 16 MeV and ρ_o = 0.15/fm^3. This equation relates the total energy per baryon, $W(\rho,T)$, in the high density phase - equated in the one dimensional model with the incident c.m. energy per nucleon - to the baryon density ρ. The pressure P is given by the isentropic derivative of W. Then all the properties of the high density region are given through the solution of eq.(1) for a prescribed constituitive equation, say $W(\rho,T)$. The total pion multiplicity is given as the sum of the pions which emerge from the decay of the baryonic and mesonic resonances taken into consideration plus the thermal gas of pions created in the reaction volume.

In ref. 8 we have included the 23 lowest-lying well established nonstrange resonances of the nucleon, as well as the pion and the η-meson (m_η = 549 MeV). We have shown that the inclusion of the heavy resonances plays an important role for the achievable temperature and

the absolute pion yields even at rather moderate energies. Masses and statistical weights of the nucleonic resonances are taken from ref. 14. The pion production rates are calculated from the branching ratios of ref. 14. High lying resonances increase the pion - multipli-city by $\approx$ 10 % at $E_{Lab} \simeq 1$ GeV/n, even more at higher energies, and must therefore be taken into account.

To solve the Rankine-Hugoniot equation (1), the energy per baryon as a function of temperature and density, $W(\rho,T)$, has to be related selfconsistently with a particular baryon density at a given total energy E_{lab}. A thermal energy can always be defined by subtracting the compression energy at zero tempe-rature from the total energy per baryon at finite temperature:

$$W(\rho,T)= E_T(\rho,T) + E_C(\rho) + W_o \tag{2}$$

where $E_C(\rho) = W(\rho,T=0)-W(\rho_o,T=0) = W(\rho,T=0) - W_o$ is defined to be the compressional energy. Two commonly used functional forms for $E_C(\rho)$ have been used:

$$E_C^l(\rho) = \frac{K_l(\rho-\rho_o)}{18\ \rho\rho_o} \tag{3a}$$

$$E_C^q(\rho) = \frac{K_q(\rho-\rho_o)^2}{18\ \rho_o^2} \tag{3b}$$

the first being referred to as the linear - and the second as the quadratic EOS, respectively, in accord with their different asymptotic increase with density.

The total energy per baryon can, on the other hand, also be

written as an expression involving kinetic and potential terms and, using relativistic Fermi- and Bose - distributions (in the fragment calculation presented below, nonrelativistic quantum distributions are used), we get

$$W = U + \sum_{i=1}^{\sigma_b} \left[\frac{\rho_i^o m_i c^2}{\rho} + \frac{4\pi g_i}{(2\pi\hbar c)^3} \frac{1}{\rho} \int_{m_i c^2}^{\infty} \frac{\epsilon^2 \sqrt{(\epsilon^2 - m_i^2 c^4)}}{\exp(\epsilon/T) - 1} d\epsilon \right] +$$

$$+ \sum_{i=\sigma_b+1}^{\sigma} \frac{4\pi g_i}{(2\pi\hbar c)^3} \frac{1}{\rho} \int_{m_i c^2}^{\infty} \frac{\epsilon^2 \sqrt{(\epsilon^2 - m_i^2 c^4)}}{\exp[(\epsilon + U - \mu)/T] + 1} d\epsilon \qquad (4)$$

where the first sum runs over the Bose - degrees of freedom, the pion, the η-meson and the photons, the second sum runs over the 24 states of the nucleon. It is assumed that all nucleonic resonances feel the same interaction energy per particle U, which depends only on the total baryon density ρ. The potential energy must be included into the relativistic Fermi-Dirac distribution function in a selfconsistent manner.

The baryons are assumed to be in chemical and thermal equilibrium and have the same chemical potential μ. Both the chemical potential and the interaction potential for the Bosons are taken to be equal to zero. ρ_i^o is the contribution of the Bose groundstate to the density of the boson species. The connection between the baryon density and the chemical potential reads

$$\rho = \sum_{i=\sigma_b+1}^{\sigma} \frac{4\pi g_i}{(2\pi\hbar c)^3} \int_{m_i c^2}^{\infty} \frac{\epsilon \sqrt{(\epsilon^2 - m_i^2 c^4)}}{\exp[(\epsilon + U - \mu)/T] + 1} d\epsilon \qquad (5)$$

The number of mesons can be calculated via

$$n_i = \frac{g_i}{\exp(m_i c^2/T)-1} + \frac{4\pi g_i V}{(2\pi\hbar c)^3} \int_{m_i c^2}^{\infty} \frac{\epsilon \sqrt{(\epsilon^2 - m_i^2 c^4)}}{\exp(\epsilon/T)-1} d\epsilon \qquad (6)$$

The connection between U and the compression energy E_C is given for T→0 by

$$(\mu - U)^2 = m^2 c^4 + (\rho C/g)^{2/3} \qquad (7)$$

with $C = 6\pi^2(\hbar c)^3$. Then

$$W(T=0) = \frac{3}{4} X + U + \frac{m^2 c^4}{8} \{\frac{3X}{X1^2} - \frac{3m^2 c^4}{X1^3} \ln[(X+X1)/mc^2]\} \qquad (8)$$

with $g = 4$, $mc^2 = 939$ MeV, the Fermi momentum $X1 = (\rho C/g)^{1/3}$, and the Fermi energy $X = \sqrt{(m^2 c^4 + X1^2)}$, assuming that for T = 0 only the nucleonic ground state is populated, which should be true for small densities. This point can be questioned, if the nucleon - Λ - interaction is much stronger than the nucleon - nucleon - interaction[15]. By comparing (2) and (8) we get the relation between U and E_C:

$$U(\rho) = E_C + W_o - 0.75X - \frac{m^2 c^4}{8} \{\frac{3X}{X1^2} - \frac{3m^2 c^4}{X1^3} \ln[(X+X1)/mc^2]\} \qquad (9)$$

The pressure is given by [16]

$$P = -T \sum_{i=1}^{\sigma_b} \frac{4\pi g_i}{(2\pi\hbar c)^3} \int_{m_i c^2}^{\infty} \epsilon\sqrt{(\epsilon^2 - m_i^2 c^4)}\, \ln(1-\exp[-\epsilon/T])d\epsilon$$

$$+ T \sum_{i=\sigma_b+1}^{\sigma} \frac{4\pi g_i}{(2\pi\hbar c)^3} \int_{m_i c^2}^{\infty} \epsilon\sqrt{(\epsilon^2 - m_i^2 c^4)}$$

$$\cdot \ln(1+\exp[(\mu-U-\epsilon)/T])d\epsilon + \rho^2 \frac{\partial U}{\partial \rho} \qquad (10)$$

and the entropy per baryon is[16]

$$S/A = \frac{P/\rho + W - \mu}{T} - \frac{\rho}{T}\frac{\partial U}{\partial \rho} -$$

$$- 1/A \sum_{i=1}^{\sigma_b} g_i \ln(1-\exp[-m_i c^2/T]) = - \left.\frac{\partial \Omega}{\partial T}\right|_{\mu, V} \qquad (11)$$

3. π/p Ratio as a Calorimeter for Heavy Ion Reactions

Let us now turn to the resulting pion yields as a function of the bombarding energy. We found that the linear equation of state, (3a), with K_l = 1400 MeV and the quadratic one, (3b), with K_q = 800 MeV fit the observed pion yields over the bombarding energy range 400 - 2000 MeV/n. Therefore, it is difficult to distinguish between the two functional forms for $E_C(\rho)$ by means of the pion multiplicity data of ref. 17.

One wonders about the large values of K but one should keep in mind that these compression constants are fitted for densities far away from normal nuclear matter density, whereas the ground state

compression constant obtained from giant monopole resonance is K = 210 $\pm$ 50MeV.

We found that the compressional energy is nearly identical for the two distinct best fitting equations of state, namely about 50% of the total available center of mass energy for all BEVALAC energies. The calculated densities, however, are in good agreement at medium energies, but they differ by about 30% at E_{lab}= 2 GeV/n. The compression energy extracted via this method is an upper bound: A delayed chemical freeze-out of the pion plus Δ and N^* degrees of freedom will yield a nonzero flow energy in the moment of freeze out, which would lower the obtained compression energy[8,9,18,19]. However, as pointed out above, cascade calculations imply that this is a rather small effect.

Fig. 1 shows the energy dependence of the thermal energy obtained from the shock calculation which best fits the pion data, using as input the linear and quadratic ansatz for E_C, respectively. Observe that the thermal energy is nearly identical for the two distinct forms of E_C. Also note that $E_T \approx \frac{1}{2} E_{CM}$, in accord with our previous finding $E_C \approx \frac{1}{2} E_{CM}$: The total available energy is shared fifty - fifty into thermal and compressional energy.

Let us now take a look from a different point of view, leaving aside the dynamical treatment of the shock compression in the reaction. Now, we inspect the dependence of the pion plus Δ and N^* abundance on the thermal energy per nucleon directly using the quantum statistical approach. This yields an extraction of the thermal energy of the system in the moment of chemical freeze-out, in close analogy to the temperature extraction performed in ref. 8: in Fig. 2 the total pion yields per baryon, including those pions originating from the

decay of baryonic resonances, are displayed as a function of the thermal energy for two fixed densities, ρ/ρ_o = 1 and 4, respectively. The yields rise nearly linearly with thermal energy. Note that the large difference in the densities has a negligible influence on the pion yields. Therefore, we can relate the pion yield per baryon directly to the thermal energy of the system in the moment of the chemical pion, Δ and N^* freeze out. This one - to - one correlation gives the thermal energy as a function of the experimentally observed pion multiplicities in the moment of the chemical freeze out of the pions and the baryonic resonances, which is close to the moment of highest density - therefore the derived thermal energy is close to the highest one in the shock-zone itself. Once the thermal energy is fixed from the experimental pion data we can compute - via the available energy E_{cm} - the nonthermal (compression plus flow) energy in the moment of pion formation.

4. The Amount of Entropy Created in the Shock Wave

Let us now come back to the entropy per nucleon which is computed from the Rankine - Hugoniot relation, again employing the two equations of state which best fit the pion data. The calculated entropy values are displayed as a function of the beam energy in Fig. 3.

Observe that the two calculations with K_q = 800 MeV and K_l = 1400 MeV result in nearly the same entropy per baryon. However, some fraction of this entropy resides in free pions and hadronic resonances. As we have dicussed above, the pions do freeze out early in the reaction, when the density is still close to it's highest

value. When the pions, including those from the decay of hadronic resonances, have escaped the hot, dense region, the entropy of the remaining nucleonic system will be lowered by an amount which can be roughly estimated from the formula for a massless pion gas $\Delta(S/A) \approx 4(\pi/A)$. At 2 GeV/n, the experimentally observed ratio is $\pi/A \approx 0.3$, therefore the entropy per nucleon residing in hadronic excitation is of the order of $\Delta(S/A) \simeq 1.2$ units.

We can also estimate the fraction of the entropy $(S/A)^{n+p}$ residing in the remaining proton and neutron degrees of freedom by taking the temperature and baryon density as obtained from the Rankine - Hugoniot relation, and calculate the corresponding entropy of a pure nucleon gas. The resulting curves are also shown in Fig. 3. The entropy $(S/A)^{n+p}$ thus obtained is indeed lower by an amount ΔS which agrees with the above estimate. Observe that the entropy which remains in the nucleonic system first rises quickly with energy but it flattens out at $E_{LAB} < 1$ GeV/n and remains nearly constant at $S/A \approx 3$ for $E_{LAB} \geq 1$ GeV/n. It is this remaining entropy $(S/A)^{n+p}$ which one can hope to determine from the experimental fragment yield data. The determination of the total hadronic entropy in the moment of highest compression requires the additional information on how much entropy has been carried of by e.g. pions. Hence a simultaneous measurement of total pion yields and spectra would be necessary before this goal can be accomplished. We will now turn to the connection between the entropy and the fragment yields in terms of the quantum statistical model (QSM).

5. Nuclear Fragmentation in the Quantum Statistical Model

The quantum statistical model of nuclear fragmentation is based on the model presented in ref. 2. A similar, but classical model has been developed independently by Randrup, Koonin and Fai[20]. Entropy creation and - determination have not been considered by that group.

In these statistical models it is assumed that thermal and chemical equilibrium are established during the expansion of the system. By then the (fast) pions have been emitted[9,10]. If the expansion is isentropic, then the temperature and density have dropped drastically from the high initial values. Therefore, the high temperatures which reflect the pion yields should be accompanied by much smaller temperatures which characterize the fragment yields. At a later time also the chemical abundance and the momentum distribution of each species of fragment freezes out[2,9,18,20]. After this freeze out the fragment yields change again due to the subsequent decay of instable states. We include ≈ 100 stable and β-active nuclei up to mass number 130 and ≈ 500 instable light nuclei with $A < 20$. The yield of each species is determined from it's chemical potential μ_i, its statistical weight g_i and the temperature via nonrelativistic Bose -

$$n_i = \frac{g_i}{e^{m_i c^2/T} - 1} + 2\pi\, g_i V \left[\frac{2m_i T}{h^2}\right]^{3/2} \int_0^\infty \frac{\sqrt{x}\, dx}{e^{x-\mu_i/T} - 1} \qquad (12)$$

or Fermi-distributions

$$n_i = 2\pi\, g_i\, V \left[\frac{2m_i T}{h^2}\right]^{3/2} \int_0^\infty \frac{\sqrt{x}\, dx}{e^{x-\mu_i/T}+1} \tag{13}$$

where m_i is the mass of species i and V is the available volume (see below). The chemical potential of a cluster in equilibrium is given by the chemical potentials of its constituents and its binding energy E_i[2,16]

$$\mu_i = Z_i\, \mu_P + N_i\, \mu_N + E_i \tag{14}$$

with

$E_i = Z_i\, m_P c^2 + N_i\, m_N c^2 - m_i c^2$

Z_i = Proton number of species i

N_i = Neutron number of species i.

We consider nucleons as hard spheres of fixed volume in the present context. Therefore we calculate the total volume V_T as the sum of the available and the excluded volume

$$V_T = V + V_{excl} = V + A/\rho_0 \tag{15}$$

where

A = Total number of nucleons

which leads to the expression

$$\rho = \frac{A}{V_T} = \frac{\rho_{pp}}{1+\rho_{pp}/\rho_o} \tag{16}$$

Here $\rho_{pp} = \rho_{pointparticle} = A/V$. The density ρ is connec-ted with the volume V, which appears in equations (12), (13), (15). This connection is not unambigous[20,21], the differences between the distinct approaches are small at low densities ρ_{pp} and rise at higher densities. However, neither the relative fragment yields nor the calculated entropy per nucleon are modified by the inclusion of the excluded volume - this rather amounts to a shift in the density-scale.

The actual calculation consists - at a given temperature - of a search for the chemical potentials of protons and neutrons, which yield the desired N/Z ratio and density. The entropy is then determined by:

$$S = \sum_i \frac{P_i V + U_i - \mu_i n_i}{T} = \sum_i \left(\frac{5}{3} U_i - \mu_i n_i\right) \frac{1}{T} \qquad (17)$$

where U_i is the thermal energy of species i.

The experimental information needed for this calculation was extracted from the tables of Ajzenberg-Selove[22]. Here we find the statistical weights, the binding and excitation energy of each fragment as well as the various sequential decay channels used after break-up in the evaporation calculation.

To determine which specific level of a daughter nucleus is populated by a decay process, we derive the transition probability to this level for each orbital angular momentum of the emitted particle. The barrier penetrability factor is calculated using the WKB-approximation.

$$P_{\ell,E} = \begin{cases} \sqrt{E} & \text{no barrier} \\ \sqrt{E}\,\exp\{2[k\cdot R\cdot x - \eta(\frac{\pi}{2} + \arcsin(\frac{\eta - kR}{n^2+(\ell+1/2)^2})) \\ -(\ell+1/2)\log\frac{x\cdot(\ell+1/2)+\eta+(\ell+1/2)^2/k^2R^2}{\sqrt{\eta^2+(\ell+1/2)^2}}]\} \end{cases} \quad (18)$$

with

R : $(1.25\,A^{1/3}+1.3)$fm (potential Radius)

E : transition energy

η : $Z_1 Z_2 \frac{e^2}{\hbar c}\sqrt{\frac{mc^2}{2E}}$

k : $\sqrt{2\mu c^2 E/\hbar c}$

x : $\left[\frac{2\eta}{kR} + \frac{(\ell+1/2)^2}{k^2R^2} - 1\right]^{1/2}$

The phase space factor for a transition with a fixed ℓ - value is given by a sum over all possibilities to couple ℓ and the spin of the emitted particle to a total spin j, which is compatible with the spins of parent and daughter nucleus[23].

Possible ℓ-values are given by triangle rules involving the spins of parent, daughter and emitted particle. Summation over all ℓ-values then yields the relative probability of this particular level, compared to other possible levels in the daughter nucleus. γ-instable state always decay into the groundstate.

6. Thermodynamic Properties of the Fragment Mixture in the Quantum Statistical Model

Fig. 4a shows the curves of constant entropy per baryon in the

density - temperature plane as obtained from the present quantum statistical model.

Note the remarkable difference to the simple $T \sim \rho^{2/3}$ dependence of an isentropic (S/A = const) Fermi gas of nucleons, which would be recovered if the fragment formation were neglected.

Fig. 4b shows the isothermals in the entropy - density plane. Observe that the entropy varies only slightly for small temperatures, say T = 5 MeV, over a broad range of densities; the analogous result is observed in Fig. 4a, were for $S/A \approx 0.5$ $T \approx 2$ MeV for nearly all densities between 0.05 and 0.9 ρ_0.

Fig. 5 shows curves of constant density in the entropy - temperature plane. Observe the fast increase of the temperature with density: eg. at $S/A \approx 3$, $T \approx 10$ MeV for $\rho/\rho_0 = 0.1$ but $T \approx 90$ Mev for $\rho/\rho_0 = 0.80$.

For an ideal gas, the thermal energy and the temperature are related by $E_T = 3/2\ T$, independent of density. Fig. 6 shows E_T vs. T for ρ/ρ_0 = 0.1, 0.33 and 0.8. A strong density dependence is observed. However, E_T is the thermal energy per nucleon, while the ideal gas formula relates to the thermal energy per particle (i.e. per fragment). Fig. 7 shows the thermal energy per fragment vs. the temperature - indeed, there is only a small density dependence observable, which is due to the quantum statistics.

The point is that the quantum effects are still substantial in the single channels, in particular in the neutron channel. They become particularly strong if the number of available fragment states is reduced to include fewer species: then the quantum concentration will finally reduce to that of a pure nucleon gas, and the $\rho^{2/3}$- dependence of E_T (S/A = const) is recovered.

In the mixture of fragments there are about as many fermions present as there are bosons, so the average kinetic energy is weighted with quantum distribution functions where the + and − signs occur approximately equally often. Thus averaged thermodynamic quantities look like they belong to a classical system. However, even at rather high entropies, $S/A \simeq 4$, the effects of the quantum statistics on averaged observables is about 10% – for details see chapter 9.

7. Entropy Measurements via "S"= $3.95 - \ln\tilde{R}_{dp}$?

The problem of how to measure the value of the entropy per nucleon S/A produced in heavy ion reactions was first tackled by Siemens and Kapusta[24]. They claimed that from a measurement of the ratio of the deuteron yield to the proton yield, $R_{dp} =: d/p$, the entropy can be determined via the simple formula:

$$S/A = 3.95 - \ln R_{dp} \tag{19}$$

Their treatment was subsequently extended[25] to include tritium, ^{3}He and α-particles by defining the ratio d-like- to- p-like

$$\tilde{R}_{dp} =: \frac{d + \frac{3}{2}(t + {}^3He) + 3\,{}^4He}{p + d + t + ({}^3He + {}^4He)} \tag{20}$$

It was claimed[25] that by inserting $\tilde{R}$ instead of R into eq. 19, the effects of the formation of clusters other than the deuteron are readily included, and the modified eq. 19 can then be used to extract the entropy from data.

However, for this simple formula to be valid one must assume[24-26] that protons and neutrons are <u>much</u> more abundand in the chemical equilibrium stage than all the different cluster species together, an approximation which is not supported by recent data[1]. Only under this assumption is it possible to derive eq. 19. Furthermore, this approach stops at the α-particle, excludes instable fragments and sets

$$\mu_i = (Z_i + N_i)\, \mu_N \,. \tag{21}$$

where μ_N is the nucleon chemical potential, i. e. the binding- and excitation energies of the fragments are neglected. The formula does not account for quantum statistical corrections[26] and the finite volumes of the produced fragments.

It was pointed out[2,18] that the inclusion of heavier and instable clusters and their binding and excitation energies change the entropy values substantially and that the decay of particle instable complex fragments (d^*, He^*, Li^* etc.) alters the values of R_{dp} and $\tilde{R}_{dp}$ drastically[2,18]: decay protons (and neutrons) are abundantly produced in an evaporation stage subsequent to the thermal and chemical break-up. An entropy determination via the simple formula, eq. 19, has been demonstrated[2,18] to yield erroneous results. The entropy determination rather requires the numerical evaluation of the relation $S/A(\tilde{R}_{dp})$, e. g. via a quantum statistical model of fragment formation, which includes the decay of instable fragments[2].

We will here demonstrate explicitely that the simple formula for $S/A(\tilde{R}_{dp})$, eqs. 19, 20, can only be used with reasonable (10%) accuracy if the entropy <u>exceeds</u> $S/A \approx 5$. Such high entropy values are not expected in the mixed gas of nuclear fragments, however (see Fig. 3).

The experimental data indicate entropy values S/A = 2–4 (see below and refs. 1–4). Figs. 8 and 9 show the entropy values as derived from the calculated fragment yields via the simple formulae, eqs. (19,20), vs. the actual entropy value obtained from the correct thermodynamical relation, eq. 17. If we include only protons, neutrons and deuterons into our calculation (Fig. 8), the old d/p- formula[24] is a good approximation. However, already the inclusion of fragments up to the α - particle changes the picture completely (Fig. 9); the d/p formula is totally wrong at small entropies, it even exhibits a minimum at $S/A \approx 2.5$. Also the improvements[25,26] neglect the decay of particle instable states and the stronly enhanced fragment yields, and therefore overestimate drastically the correct entropy value at low entropies. They coincide with the correct result only for $S/A > 5$. Also, we must point out that the entropy values extracted from eq. 20 cannot drop below $S/A \simeq 3.5$, since by the definition of $\tilde{R}_{dp}$ we get for $S/A \to 0$

$$\tilde{R}_{dp}(S/A \to 0) \to \frac{3\ {}^4He}{2\ {}^4He} = 1.5 \longrightarrow S/A \gtrsim 3.95 - \ln 1.5 \qquad (22)$$

This is the origin of the contradictory results obtained by the authors of ref. 1 from their 'asymptotic' data, when using either the simple analysis proposed in refs. 25, 26, which yields $S/A \simeq 4.2$, or using on the other hand the present QSM, which yields $S/A \simeq 2.5$.

8. Distortion of Fragment Yields due to Feeding from Instable Fragments

One of the reasons for this complete failure of the simple

entropy formula is the distortion of the yields of the fragments formed due to the feeding from particle instable complex fragments: Figs. 10 - 14 show the ratios of proton-, deuteron-, triton-, α-, and ^{7}Li-yields before - and after the decay of the instable states has taken place. Observe that distortions of factors 11 (for protons) and 19 (for alphas) are reached at entropies $S/A \simeq 1.5 - 2$. Even the deuteron yields suffer distortions of 50% to more than a factor of two in this entropy range. Observe also that the distortions of p and d are modest (< 10%) at high entropies, $S/A > 5$, where the heavier fragments (in particular the α's!) still show substantial distortions. Also note that the distortions are less pronounced for smaller break-up densities.

9. The Nonanalytic Relation of Entropy vs. $\tilde{R}_{dp}$.

The results presented in the previous two sections are very discouraging - as they stand - for anybody who is interested in measuring the entropy created in heavy ion collisions.

However, it has been pointed out already several years ago[2,18] that the entropy can be determined from the observed d/p - ratios - although the effects of the complex fragments and decay of particle instable resonances destroy the simple analytical relation between S and R_{dp} (or $\tilde{R}_{dp}$, for this matter). The solution to this paradoxical statement is that a careful investigation of all the above mentioned effects - like implementation of quantum statistics of complex fragments, and treatment of the decay of instable resonances - results in a nicely behaving functional dependence of $\tilde{R}_{dp}$ (and other ratios of particle yields, see below) on the entropy. It is important to point

out that these effects result in <u>some</u> (small) dependence of the function $\tilde{R}_{dp}(S/A)$ on the break-up density.

However, this dependence is rather moderate and allows for an entropy determination with a systematic error - resulting from this density dependence - of less than a half a unit in entropy. This is clearly demonstrated in Fig. 15 which shows the ratio d-like- to-p-like, $\tilde{R}_{dp}$, versus the thermodynamic entropy, S/A, after the instable clusters have decayed. The solid, dashed and dotted lines are for $\rho/\rho_o = 0.1$, 0.33 and 0.8, respectively. This corresponds to a variation of the point particle density by a factor of 40! Also shown is the analytical result "S"/A = 3.95 - ln $\tilde{R}_{dp}$ (full dots). It is evident that this relation can be applied with reasonable accuracy only for S/A > 5. Observe that the quantum statistical model result approaches $\tilde{R}_{dp} = 1.5$ for $S/A \rightarrow 0$, as it should because at low entropies the α's are the dominant light fragments and $\tilde{R}_{dp} \rightarrow \frac{3\alpha}{2\alpha}$. Applying the analytical formula, eqs. 19,20, would yield "S"/A($S/A \rightarrow 0$) $\approx$ 3.5 - it can never yield an entropy below this value, just because of it's analytical form.

The importance of the decay of instable fragments is observed by comparing Fig. 15 to Fig. 16, which displays the same results but <u>before</u> the fragments have decayed: At entropies S/A $\simeq$ 1-3 we observe a $\approx$ 20% higher $\tilde{R}_{dp}$ than after the decay. At lower entropies, it is clear that the definition of $\tilde{R}_{dp}$ yields the same answer and at higher entropies there are only few unstable fragments produced, most of the system's baryon number resides in free protons and neutrons.

Another important question for the reliability in applying the curves shown here to deduce the entropy from data is: to what extend does this function $\tilde{R}_{dp}(S/A)$ depend on how many different excited and

ground state isotopes are implemented into the analysis? This is displayed in Fig. 17: The solid line is the result with all the ≈ 600 nuclides included, the dashed line is only including particles up to α's. Note that there is only a ≃ 10% effect. This is in spite of the fact that the more massive fragments, A > 4, completely dominate the system at S/A < 2.5 (see Fig. 53). Again this is a consequence of the analytical behaviour of R_{dp} as S/A goes to zero.

Another source of uncertainty which can be studied in the present approach is the dependence of $\tilde{R}_{dp}$ on the total charge - to mass ratio of the system under consideration: Fig. 18 shows $\tilde{R}_{dp}$ for the symmetric system Ca + Ca. Observe a systematic downward shift of $\tilde{R}_{dp}$ with a rather substantial (≈ 20%) deviation from the previous Nb + Nb results in particular at modest entropies, S/A ≈ 2. Therefore, in comparing to data one always should perform a calculation for the appropriate Z/A ratio - again, the simple analytical formula has been derived for symmetric systems with the assumption $\mu_p = \mu_n$, which is not fullfilled for asymmetric systems. Fig. 19 shows the predicition for the system Au + Au which is presently being analyzed by the experimentalists.

We have furthermore tested the importance of using quantum statistics rather than classical statistics. We find that for averaged quantities like R_{dp} the effects of quantum statistics are typically on the order of 10 % at entropies > 2, e.g. at $\tilde{R}_{dp}$ = 0.5 the entropy is about 0.4 units lower than in the corresponding classical calculation.

The final check on the sensitivity of the curve $\tilde{R}_{dp}$(S/A) on the physics input in the framework of the statistical model is the assumption that a <u>grand</u>canonical ensemble is appropriate to describe systems which consist of, say, 50 or 100 particles only. Our rational in using this model here is that the uncertainty in a typical

observable, e.g. the energy, is given by $\Delta E/E \simeq f^{-1/2}$, where f = 6 A is the number of degrees of freedom and therefore $\Delta E/E$ is of the order of 5% for A = 50. To quantify this statement we compare in Fig. 20 the resulting $\tilde{R}_{dp}$ for the system Nb + Nb at maximum multiplicity, A = 186 in the present QSM at constant temperature, T = 70 MeV, with the classical microcanonical approximation of Randrup and Fai[27]. We find an excellent agreement between our results and the microcanonical calculations for large particle numbers $A \geq 100$. Even for A = 20, deviations are on the order of ≃ 10% only and for A = 10 they are only ≃ 20%. Therefore, the effects of quantum statistics and of a microcanonical treatment are of similar importance at low multiplicities. Both effects go also into the same direction: they both lower the entropy values at a given R_{dp} as compared to the classical grandcanonical results. The quantum corrections become increasingly important at lower temperatures; the systematics of $\tilde{R}_{dp}(S/A)$ is shown in Fig. 21 for various isotherms between T = 5 and 90 MeV, where ρ/ρ_o varies for each curve between 0.05 and 0.8. Observe that for small temperatures, T = 5 MeV, there is little variation in $\tilde{R}_{dp}$, while S/A varies from ≈ o.8 to 2.3. This is a consequence of the slow variation of S/A with T at 5 MeV, which is exhibited very clearly in Figs. 4a and b. This has the very uncomfortable consequence that the entropy determination at S/A < 2 must rely on a different method than the $\tilde{R}_{dp}$ - idea discussed in this chapter. These other methods exist, however, and are discussed extensively below.

In a series of recent papers[28] it was claimed that the classical microcanonical approach[27] predicts a strong dependence of R_{dp} (at S/A=const) on the density, in stark contrast to the published results[1,2,18] obtained with the present approach. It was further

reported that it is not possible to extract the entropy values from the d/p ratios. Rather one would find a strong correlation between $\tilde{R}_{dp}$ and the thermal energy of the system, independent of the break-up density. Recent checks[29] have revealed a coding error in the computer programs used in ref. 28. The revised code now reproduces our longstanding predictions[2,18].

Fig. 22 shows the dependence of $\tilde{R}_{dp}$ on the thermal energy in the present quantum statistical approach: Observe the very strong dependence of $\tilde{R}_{dp}(E_T)$ on the break up density. Fig. 23 shows the dependence of $\tilde{R}_{dp}$ on the density at a given constant entropy. Observe the above noted near constancy of $\tilde{R}_{dp}$. A moderate uncertainty of ≈ 0.3 units in entropy remains, however, at $S \simeq 2$-3. This reflects the unknown break-up density.

10. Multiplicity Dependence of the Entropy from 4π Data on $\tilde{R}_{dp}$

With the apparent insensivity of our above presented curves $\tilde{R}_{dp}(S/A)$ to the details of the method at hand we now proceed to use Fig. 15 to determine the entropy from recent multiplicity selected measurements[1] of $\tilde{R}_{dp}$ in the GSI - LBL Plastic Ball 4π electronic spectrometer system. The experimentalists have observed a very rapid increase of $\tilde{R}_{dp}$ with the multiplicity N_p, going from 0 at $N_p = 0$ to $\tilde{R}_{dp} \simeq 0.7$ at maximum observed multiplicity[1], $N_p \simeq 80$ (see Fig. 24). Fig. 25 shows the dependence of the entropy on the participant multiplicity as extracted from the data[1] of Fig. 24 via the calculated relation $\tilde{R}_{dp}$ (S/A). The entropy values extracted from the data are for Nb + Nb at 400 MeV/n (solid line) and 650 MeV/n (dashed line) bombarding energy, respectively. Observe the drop from $S/A \simeq 5$ at

small multiplicity (large impact parameter), where the grand canonical approach overestimates the entropy by $\approx$ 10%, to S/A $\simeq$ 3.5 at multiplicity $\simeq$ 80. Note also the systematic $\simeq$ 0.2 unit higher multiplicity in the 650 MeV/n data. The experimenters used the present quantum statistical model to estimate the entropy at an extrapolated "asymptotic" (i. e. infinite) multiplicity. They then obtain $(S/A)^{\infty} \simeq$ 2.5, values which are in striking contrast to the values $(S/A)^{\infty} \approx 4.2$ obtained from the asymptotic R_{dp} values using the method of ref. 26[1]. In view of the above sections, this discrepancy is not surprising - it is due to the neglect of (stable and instable) fragments with A > 4 in ref. 26.

Fig. 26 shows the entropies as extracted from the data via $\tilde{R}_{dp}$ (S/A) for high multiplicity selected Nb + Nb[1], La + La[30] (in ref. 30, both groups report $\tilde{R}_{dp} \simeq 0.68$ at E_{LAB} = 0.8 GeV/n) and for the system Ca + Ca at 400 MeV/n and 1.05 GeV/n[1]. Also shown are the entropy values extracted from high multiplicity biased inclusive mass distributions of intermediate mass fragments, A > 4, from Ar + Au collisions at much lower energies, 40 - 140 MeV/n, which had been analyzed before[3].

11. Multiplicity Dependence of X/p - Extraction of the Breakup Temperature and Entropy

By using $\tilde{R}_{dp}$ to measure S/A one looses the information about the various distinct fragment species which are emitted. They can serve as independent observables to determine the entropy from experiment, as pointed out earlier[2]. Fig. 27-32 show the dependence of X/p on the entropy for the systems Ca + Ca (right handside) and Nb + Nb (left).

Here X stands for d, t, ^{3}He, ^{7}Li, ^{12}C, respectively. The dashed and dotted curves give the ratios after decay for the respective break up densities.

It should be pointed out that the final ratios are again nearly independent of the break-up density chosen, and that for A(X) < 4, the X/p(S/A) curves exhibit sharp maxima with X/p < 1 at S/A ≃ 2, while the ratio X/p increases monotonically with decreasing S/A for α and ^{12}C. That means that the present approach predicts d/p, t/p and ^{3}He/p ratios are always less than 1 while the α yield should exceed the proton yield for S/A ≈ 2. For smaller S/A values we predict a decrease of d/p, t/p, ^{3}He/p and a monotoneous increase of α/p.

The presently available Plastic-Ball data correspond, even at the highest multiplicities (Nb(400 MeV/n) + Nb: $N_p^{max} \approx 80$), still to too high an entropy to check this prediction experimentally.

The data for the heavy Au + Au system at lower energies are presently being analysed. We will have to wait for these data to see whether the low entropy S/A < 2 necessary to check this prediction can be reached at the highest possible multiplicity and the lowest available energy (i.e. Au (150 MeV/n) + Au).

Figs. 33 and 34 show the multiplicity dependence of the various X/p ratios for Ca + Ca and Nb + Nb collisions. Also shown is a 3 parameter (ρ^∞,λ,S^∞) least mean square fit of the quantum statistical model results to these data, as well as the predicted yields of complex fragments: Here ρ^∞ and S^∞ are the density and entropy at infinite multiplicity and λ is the mean free path.

$$V^{eff}(N_p) = \frac{N_p A}{\rho^\infty Z}\left[1+\lambda\left[\frac{4\pi}{3}\frac{Z}{A}\frac{\rho^\infty}{N_p}\right]^{1/3}\right]^3 \qquad (23)$$

is the available effective volume of the participants, which takes into account Kapusta's suggestion[26] of the additional "surface volume" due to the mean free path effects discussed in the previous section. N_p, i.e the number of bound and unbound protons (p-like multiplicity), is taken from experiment, as well as the Z/A of the incident system.

The fits are quite satisfactory, considering that only 3 parameters are adjusted to fit simultaneously the varying steepness of the curves and the absolute as well as the relative yields of the different fragments in one particular plot. The best χ^2-values have been achieved consistently with $\rho^\infty = 0.8\ \rho_o$. Values of $\lambda = 5 - 7$ fm come out in the four fits, the asymptotic entropy values come out $S^\infty =$ 1.57 and 1.53, respectively for the Nb and Ca collisions at 400 MeV/n, i.e. the extrapolation to infinite multiplicity converges. S^∞ increases to 1.7 and 1.8 when going to the higher energies, 650 and 1050 MeV/n, respectively.

The break-up temperatures (assumed to be independent of multiplicity), which correspond to these entropy values are T = 12, 16 and 20 MeV for the 400, 650 and 1050 MeV/n Ca and Nb data, respectively. These values are much smaller (a factor 1/3) than the temperatures extracted from pion yields at the same energies[8]. This result can be understood if the pions are created in the early, hot stage of the collision, while the fragments are formed after an isentropic expansion of the system at small densities where the temperature is low. This would imply that in the late stage of the reaction a large fraction ($\simeq$ 80%) of the available center of mass energy resides in (possibly isotropic) flow.

The multiplicity dependence of the entropy per nucleon S/A (not

S^{∞}) as calculated for the 400 MeV/n Nb data is shown in Fig. 35. It coincides with the values deduced in Fig. 25 from $\tilde{R}_{dp}$. It will be interesting to see if the predicted rather substantial yields of complex fragments (Z > 3) can be observed experimentally at the rather high bombarding energies at high multiplicities. The measurement of ratios of particle instable to stable complex fragments could then provide an additional consistency check on the temperature- (and entropy) values obtained here - the difficulties associated with such temperature measurements are discussed extensively in the next section. The degree of uncertainty in the extrapolation to complex fragments is obvious if we compare Figs. 33 and 34 with Fig. 36 and 37 which show the prediction of X/p for all species and multiplicities, but using $S(N_p)$ from the fits to the $\tilde{R}_{dp}$ values (Fig. 25). Observe that with this latter method ^{6}Li and heavier fragments are predicted to be more abundant than with the χ^2-fit with 3 free parameters.

The actual measurement of the complex fragments and their unstable states will allow for additional constraints on the above thermodynamic parameters and this can yield a further refined entropy determination.

The presently obtained values of S/A are compared in Fig. 38 to the entropy calculated in the fluid dynamical model with the equations of state which fit the pion data. It is obvious therefore to note here that the apparently completely different experiments are all intermoven und that we will need precise measurements of all the available observables to zoom in on the properties of excited nuclear matter.

We have now extensively discussed $\tilde{R}_{dp}$ and X/p as measures of the entropy. These quantities are useful for determining large entropies

S/A > 2.

Below we pesent other observables which offer excellent entropy determination capabilities both at low (S/A < 2) and at high entropy values. These novel observables have not been discussed to date. They offer other intriguing views of various aspects of multifragmentation. Before we discuss these novel observables, let us discuss the possibilities of measuring temperatures and entropies from ratios of γ - instable, particle instable and stable complex fragments.

12. Distortion of Temperature Measurements due to Instable Complex Fragments

Recently, experimental efforts have been made[5,6,7] to determine the break-up temperature directly from ratios of excited states to ground states in Lithium and Beryllium nuclei at bombarding energies around 50 MeV/nucleon. A surprising difference was found: γ-instable systems like $^7Be^*$(478 keV) / ^7Be(gs) give T ≈ 0.5 MeV, particle instable systems like $^5Li^*$(16.66 MeV) / ^5Li(gs) yield T ≈ 5 MeV, if the simple Boltzmann - Ansatz proportional to $\exp(-\Delta E/T)$ is used for the yield ratio. Fig. 39 shows that the reason for these paradoxical results is the different amount of feeding for these channels by the sequential decay[2]: in the case of ^7Be (lower left hand frame), drastic feeding (mainly to the ground state) from heavier particle- instable fragments sets in as early as at T ≈ 2 MeV. For T > 3 MeV, a ratio of ≈ 0.2 is obtained, independent of the actual temperature. Hence these ratios are not useful for a temperature measurement.

On the other hand, some ratios of particle-instable states in the weakly bound ^5Li- and ^6Li- nuclei (upper frames) show only a moderate

distortion by the sequential decay as long as $T < 10$ MeV. Therefore the Boltzmann - Ansatz might be a useful approximation here. Temperatures of $T \approx 5$ MeV can be estimated from some of the measured ratios in Ar + Au collisions at 60 MeV/nucleon[7].

These values are much lower than the corresponding slopes of the energy spectra of the particles, which yield $T = 10 - 20$ MeV. These low values fit, however, in the above discussed systematics of the 'too small' temperatures, $T = 12 - 20$ MeV, obtained from the Plastic Ball data at Bevalac energies (see chapter 11).

However, observe the lower right hand side of Fig. 39: Even though the ratio of two high-lying particle instable states of ^{8}Be is considered, we do observe a strong distortion due to feeding from other states which had been overlooked before[7]. Therefore, one must be very careful in using this idea to measure the temperature.

Fig. 40 shows the tremendeous distortions to be expected in ratios of γ-instable - to groundstate yields of $^{6,7}Li$ and ^{8}Li - fragments. Here it is predominantly the feeding to the groundstate which hurts the possibility of measuring the temperature. Some of these states seem to be, however, interesting condidates for possible future entropy measurements; the feeding has the effect of resulting in a rather nice one - to - one relation between ratios of ^{6}Li and ^{7}Li lowlying states - to - groundstates and the entropy, see Fig. 41: These states may be useful for entropy measurements for $S/A > 2$.

13. Mass Yield Curves and Entropy Measuremts

Let us now study how the composition of our system changes with the excitation energy and entropy. Fig. 42 shows the mass yields, Y(A)

for the system Ca + Ca at a density of $\rho/\rho_0 = 0.33$ and for T = 15, 5 and 2 MeV. Observe that at each mass intervall we have plotted two bars which indicate the yields before and after the evaporation stage. At T = 15 MeV we observe a smooth exponential fall-off ot the mass yield Y(A). However, at T = 5 MeV the mass yield is nearly constant - that means that in the 30 - 60 MeV/n region, where T ≃ 5 MeV has probably been observed (as discussed in the previous section) there are about the same amount of <u>light</u> fragments as there are fragments of <u>higher</u> mass. In particular it shows that there are by far more nucleons bound in fragments (remember, A • Y(A) would give the contribution for each complex fragment to the total nucleon number!) then there are free nucleons (see also Fig. 53).

At T = 2 MeV, Y(A) is actually increasing with A, and one can very clearly observe the effects of nuclear binding - shell effects result in peaks in Y(A) at A = 4, 8, 12, 16 and 20. However, also within one isotope chain one can observe the effects of the excitation energy: Fig. 43 shows the yield of carbon isotopes for T = 6.5, 13 and 47 MeV when the total entropy of the system is constraint to S/A = 2.5. Observe that the total yields drop by about an order of magnitude, respectively, when the temperature is increased, but further more the distribution is skewed towards smaller mass numbers: this shows that the binding and symmetry energy effects loose their importance at T is increased, and that the system tries to avoid large masses.

Fig. 44 shows now a most interesting property of the mass distributions, namely that the slope parameter of the fall-off of Y(A) is approximately exponential and connected with the total entropy per baryon in the system[2-4]: The entropy has been fixed at S/A = 2.5, but

the ρ - T values have been varied over a large range. Fig. 45 shows a polynomial- and an exponential fit to the calculated mass distribution. Note that the polynomial fit does not give a good description of Y(A), while the exponential fit is quite reasonable. See ref. 4 for a detailed discussion of the power law fits which have occured in the literature.

Fig. 46 shows the dependence of the slope parameter of the mass distribution Y(A) on the entropy S/A for three different densities. Observe the nearly linear dependence of the slope parameter on S/A. Note also that there is an uncertainty of about $\Delta S \simeq \pm 0.5$ in the absolute value of S/A if the slope parameter is known. This reflects the finite density dependence of Y(A) at a given entropy value, in analogy to the above observed dependence of $\tilde{R}_{dp}$ (S/A) on the density. However, all the other available methods of determing the entropy show this uncertainty due to the density dependence at a given entropy.

We have used the present quantum statistical model to extract entropy values from the measured high multiplicity yields of complex fragments[3,4]. Figs. 47 a,b,c show our fits to the observed isotopic distributions for the system Ar + Au at 42, 92 and 137 MeV/n, respectively; the measurements extend to A = 14, a large variety of isotopes of He, Li, Be and B has been observed. We fitted in a χ^2 - fit all observed isotopes with A > 4 simultaneously, from this fit we obtain entropy values S/A $\approx$ 1.5 - 2. This entropy is close to the entropy of the nuclear Fermi gas at the "flash point", i.e. where nuclei become unbound[4] (E^* ~ 16 MeV, T ~ 8 MeV). These S/A - values are shown in Fig. 26 as a function of the bombarding energy.

14. Yields of Isobaric nuclei as Measure of the Entropy

Fig. 48 a,b shows the dependence of the n/p ratio for Au + Au at two different densities before and after the decay of instable fragments. Note that the decay does not distort the n/p ratio much, although the separate yields are strongly affected. Hence the n/p ratio would be a nice independent measure of the entropy for $S/A < 2$. The same holds for the $t/^3He$ ratios shown in Fig. 49. Observe the strong increase of $t/^3He$ below $S/A \simeq 2$.

These curves are in sharp contrast to the n/p- and $t/^3He$-ratios obtained for the charge symmetric system Ca + Ca (see Figs. 50 and 51). Both ratios show a sharp decline to values less than one at $S/A < 2$. This reflects the importance of the binding energies at low entropies: The most deeply bound nuclei have $N > Z$, so the neutrons in the charge symmetric system are eaten up by heavy nuclei.

Observe that for the Ca- case, the asymptotic ($S/A > 5$) n/p ratio is 1, while it approaches $n/p = (N/Z)$ of Au in the previous case. This prediction could be tested experimentally.

15. The Composition of the Fragment Conclomerate - The Average Fragment Mass as a Measure of the Entropy

As we have seen in Chapter 13, there is a rather strong correlation between the mass yield curve and the entropy. Physically this reflects the definition of the entropy: The entropy is a measure of the degree of disorder - if there are a few heavy fragments in the system then we observe a state of higher order than if there are many

independently moving light fragments. This leads us right away to two promising canditates for observables useful for entropy measurements: the mean multiplicity of charged particles in the system (divided by the total number of charges (protons) in the system) and the average mass of the emitted fragment. These quantities may be easier to measure in actual experiments than a complete isotope distribution on an event-by-event basis.

Fig. 52 a, b and c show the dependence of the yields of various fragments from neutrons to ^{6}Li on the total entropy of the system. Observe that for the system Au + Au, the neutrons are the most abundant species at any entropy. Their yield is also mostly affected by the quantum effects, since their density is the highest. Note that the protons, on the other hand, get eaten up by the fragments and for S/A < 2, the α, d, and t yields are <u>higher</u> than the proton yields! Also note that there is not only a n/p ratio substantially different from 1, but also t/^{3}He $\neq$ 1, as one would expect because of the neutron excess in the Au + Au system.

Figs. 53 a, b show the contribution of fragments with A = 1, A = 2–4, and A > 4, respectively, to the total number of bound and unbound nucleons in the system as a function of the total entropy per nucleon. a) shows the primordial distribution, b) is after decay. Observe that at S/A > 2, the majority of the nucleons resides in light complex fragments, A = 2–4. For S/A < 2 the intermediate mass fragments dominate the system. Only for S/A > 4.5 are the <u>free</u> nucleons the dominant channel. <u>This</u> is the origin of the failure of the simple "S"/A formula proposed in refs. 24 – 26.

The relative importance of the various components in the system to the entropy is most clearly displayed by a look at the different

contributions of nucleons, stable- and instable nuclei to the total entropy in the system shown in Fig. 54a-d, again for the Au + Au and Ca + Ca system and at two different densities.

The instable fragments by far dominate the entropy for S/A < 3. Even at S/A = 4 there is only a 50 % contribution of the nucleons to the total entropy. Only at entropy values below S/A = 0.5 can the stable nuclei be dominant.

The importance of the massive fragments for the composition at entropies below S/A = 4 is also evident from Fig. 55 a,b, which shows for Ca + Ca the average nucleon number <A> per fragment as a function of entropy for two different densities, ρ/ρ_o = 0.1 and 0.8, before and after decay, respectively. Note the downwards shift in <A> of about 2 mass units as a consequence of the decay of instable fragments. Observe that a complete event measurement of <A> would be very worth while, because <A> allows for a rather accurate (better than 20 %) entropy determination in the region S/A < 2.5, where most of the other proposed observables are rather insensitive to S/A.

16. Charge Particle Multiplicity as an Entropy Measure

An even narrower determination of S/A would be enabled, however, by a simple measurement of the total multiplicity of charged fragments.

Figs. 56a, b show the total charged particle multiplicity M_c as a function of total entropy for a central collision of Au + Au, i.e. with a total number of participant protons N_p= 158. The difference between M_c and N_p has been pointed out in ref. 1. Observe that M_c is approaching N_p at high entropies, but below S/A ≈ 3 there is a nearly

linear drop of M_c with S/A, while N_p = 158 stays constant. At S/A = 2, $M_c \approx 1/2\ N_p$ and $M_c \rightarrow 1$ as S/A → 0. This again reflects the physical meaning of the entropy: It is highest where the degree of disorder is largest, i.e. when the system is maximally dissociated.

We find that the multiplicity of charges is increased by about 20 at S/A = 2 as a result of the decay of particle instable states. The near independence of M_c on S/A again suggests to use M_c/N_p as a measure of the total entropy of the system at S/A < 4 with a rather modest uncertainty in the entropy at a given M_c/N_p of $\pm$ 0.3 units.

17. Multiplicity of Intermediate Mass (A > 4) Fragments

The multiplicity of charged fragments with mass A > 4 is shown in Fig. 57 for the system Ca + Ca and for ρ/ρ_0= 0.1 and 0.5 before and after the decay of the instable resonances. We would like to point out that in the primordial distribution there are 7 - 8 fragments with A > 4 at S/A ≈ 2. With ⟨A⟩ ≈ 6 this translates into ≈ 40 - 50 nucleons out of the total of A = 80 being bound in complex fragments! This is changed dramatically as a result of the decay of instable fragments: The multiplicity now has dropped to 2-3. At higher S/A-values the relative drop in M_c (A > 4) in even larger. Note also the value M_c (A > 4) → 3.3 for S/A → 0. This is the result of a truncated basis of instable fragments: The maximum mass fragment included into this calculation has A = 25. Therefore the system of 80 nucleons must settle into 3 separate fragments. This artifact does of course not occur if our normal input table with A^{max} = 130 is used. This can clearly been seen in Fig. 58a,b, which show M_c (A > 4) vs. S/A for the central Au + Au (N_p = 158) collision discussed in the previous

section.

We must emphazise here that multifragmentation events with up to M_c (A > 4) = 35 charged complex fragments are predicted by the present model. However, again this maximum value drops, by about a factor of two, to $M_c \approx 20$ after the decay of instable fragments has occured.

This effect should be observed experimentally as a maximum in the excitation function M_c (A > 4) vs. E_{LAB} of the number of midrapidity fragments with A > 4 in central collisions of massive nuclei. From our extraction of entropy values from experimental d/p ratios presented above we conclude that this maximum should be located at E_{LAB} = 50 - 200 MeV/nucleon; again, this prediction should be verifiable experimentally.

18. Summary and Conclusions

We have presented the QSM of nuclear multifragmentation. It was emphazised that stable and instable medium mass fragments play an important role in determining T and S/A: They alter the relation $S/A(R_{dp})$ dramatically and distort via feeding simple temperature measurements. However, these fragments allow by their very abundance for a variety of new, alternative methods to determine S/A from data on multifragmentation (ratios of complex fragment yields, mass yield curves, and charged particle multiplicities). Entropy values deduced from 4π Plastic Ball data exhibit a strong multiplicity dependence. For large multiplicities the entropy residing in nuclear fragments appears to be independent of the bombarding energy and low in absolute value, $S/A \simeq 3.5$. The absolute values are close to the S/A values calculated with the fluid dynamical model if nuclear equations of

state are employed which correctly reproduce the observed pion multiplicities.

The corresponding breakup temperatures of the fragment conglomerate are T = 12, 16, and 20 MeV at E_{Lab} = 400, 650, and 1050 MeV/n, respectively. These values are much smaller (a factor 1/3) than the temperatures extracted from pion yields. This result can be understood only if the pions are created in the early, hot stage of the collision, while the fragments are formed after an isentropic expansion of the system at small densities where the temperature is low. This would imply that in the late stage of the reaction a large fraction (≃ 80%) of the available center of mass energy resides in (possibly isotropic) flow.

It seems therefore tractable to extract the nuclear equation of state from a simultaneous analysis of fragment- and pion data, and flow experiments via a comparison with more detailed three- plus one-dimensional dynamical model calculations.

Acknowledgements:

Stimulating discussions with Prof. W. Greiner, J. Maruhn, and members of the experimental groups ref. 1,3-7 are greatfully acknowledged.

References

1. K.G.R. Doss, H.A. Gustafsson, H.H. Gutbrod, B. Kolb, H. Löhner, B. Ludewigt, A.M. Poskanzer, T. Renner, H. Riedesel, H.G. Ritter, A. Warwick and H. Wieman, Phys. Rev. C32 116 (1985).
2. H. Stöcker, G. Buchwald, G. Graebner, P. Subramanian, J.A. Maruhn, W. Greiner, B.V. Jacak and G.D. Westfall, Nucl.Phys. A400 63c (1983);
   D. Hahn, H. Stöcker, Proc. Int. Workshop XIV on Gross Properties of Nuclei and Nuclear Excitations, Hirschegg, Austria 1986, H. Feldmeier (ed) p. 90.
3. B.V. Jacak, G.D. Westfall, C.K. Gelbke, L.H. Harwood, W.G. Lynch, D.K. Scott, H. Stöcker, M.B. Tsang, and T.I.M.Symons, Phys. Rev. Lett 51 1846 (1983);
   B.V. Jacak, thesis, Michigan State University 1984;
4. B.V. Jacak, H. Stöcker, G.D. Westfall, Phys. Rev. C29, 1744 (1984);
   G.D. Westfall et al., ibido C29, 861 (1984)
5. D.J. Morissey, W. Benenson, E. Kashy, B. Sherrill, A.D. Panagiotou, R.A. Blue, R.M. Ronninge, I. van der Plicht, and H. Utsunomiya, Phys. Lett. 148B 423 (1984);
6. D.J. Morissey, W. Benenson, E. Kashy, C. Bloch, M. Lowe, R.A. Blue, R.M. Ronningen, B. Sherill, H. Utsunomiya, and I. Kelson, Phys. Rev. C32 877 (1985);
   D.J. Morissey, C. Bloch, W. Benenson, E. Kashy, R.A. Blue, R.M. Ronningen, R. Aryaeinejad, Phys. C34, 761 (1986).
7. J. Pochodzalla et al., Phys. Rev. Lett. 55 177 (1985)
   J. Pochodzalla et al., Phys. Rev. B161 275 (1985)

H.M. Xu, D.J. Fields, W.G. Lynch, M.B. Tsang, C.K. Gelbke, D. Hahn, M.R. Maier, D.J. Morrissey, J. Pochodzalla, H. Stöcker, D.G. Sarantites, L.G. Sobotka, M.L. Halbert, D.C. Henseley, MSU-preprint CL 560 (1986).

8. D. Hahn, H. Stöcker, Nucl. Phys. A452 , 723 (1986);

9. For recent reviews see e.g.
H. Stöcker, W. Greiner, Phys. Reports 137 (1986) 277
J.J. Molitoris, D. Hahn, and H. Stöcker,
Prog. Part. Nucl. Phys. 15 (1986) 239;

10. H. Stöcker, W. Greiner, W. Scheid, Z.Physik A286, 121 (1978);

11. J.W. Harris, R. Stock, R. Bock, R. Brockmann, A. Sandoval, H. Stroebele, G. Odyniec, H.G. Pugh, L.S. Schröeder, R.E. Renfordt, D. Schall, D. Bangert, W. Rauch, and K.L. Wolf, Phys.Lett. 153B, 377 (1985);M. Sano, M. Guylassy, M. Wakai and Y. Kitazoe, Phys.Lett. 156B, 27 (1985);
R. Stock, Phys. Reports 135, 259 (1986).

12. J. Cugnon, D. Kinet, J. Vandermeulen, Nucl.Phys. A379, 553(1982);
J. Cugnon, T. Mituzani, J. Vandermeulen, Nucl.Phys. A352, 505 (1983);
M. Cahay, J. Cugnon, J. Vandermeulen, Nucl.Phys. A411, 524(1983);

13. R. Stock, R. Bock, R. Brockmann, J.W. Harris, A. Sandoval, H. Stroebele, K.E. Wolf, H.G. Pugh, L.S. Schroeder, M. Maier, R.E. Renfordt, A. Dacal, and M.E. Ortiz, Phys.Rev.Lett. 49, 1236 (1982);

14. Table of Particle Properties, Rev. Mod. Phys.56, 1984;

15. J. Boguta, Phys.Lett. 109B, 251 (1982);

16. U. Heinz, W. Greiner, and W. Scheid, J.Phys. G5, 1383 (1979);
L.D. Landau and E.M. Lifschitz, Statistische Physik, Akademie

Verlag Berlin, 1975;

17. A. Sandoval, R. Stock, H.E. Stelzer, R.E. Renfordt, J.W. Harris, J.P. Brannigan, J.V. Geaga, L.I. Rosenberg, L.S. Schroeder, and K.L. Wolf, Phys.Rev.Lett. 45, 874 (1986);

18. H. Stöcker, J.Phys.G Lett. 10, 111 (1984);
J. Gosset, J.I. Kapusta, G.D. Westfall, Phys. Rev. C18, 844 (1978).
A. Mekjian, Nucl.Phys. A312, 491 (1978);

19. H. Stöcker, A.A. Ogloblin and W. Greiner, Z.Physik A303, 259 (1981);
J. Kapusta, D. Strottmann, Phys.Rev. C23, 1282 (1981);
J. Kapusta, Nucl.Phys. A418, 573c (1984);

20. J. Randrup, S.E. Koonin, Nucl.Phys. A356, 223 (1981);
G. Fai and J. Randrup, Nucl. Phys. A381, 557 (1982);

21. F. Karsch and H. Satz, Phys.Rev. D21, 1168 (1980);

22. F. Ajzenberg-Selove, Nucl. Phys. A360, 1 (1981);
Nucl.Phys. A375, 1 (1982); Nucl. Phys. A392, 1 (1983);
Nucl.Phys. A415, 1 (1984); Nucl.Phys. A433, 1 (1985);

23. W. Hauser, H. Feshbach, Phys.Rev. 87, 366 (1952);

24. P. Siemens and J. Kapusta, Phys.Rev.Lett. 43, 1486 (1979);

25. G. Bertsch and J. Cugnon, Phys.Rev. C24, 2514 (1981);

26. S. das Gupta, B.K. Jennings and J. Kapusta, Phys.Rev. C26, 274 (1982);
J. Kapusta, Phys.Rev. C29, 1735 (1983);
L.P. Csernai, J.I. Kapusta, Phys. Reports 131, 223 (1986);

27. G. Fai and J. Randrup, Nucl.Phys. A404, 551 (1983);
J. Randrup, private communication;

28. L.P. Csernai, J.I. Kapusta, N.K. Glendenning and G. Fai, Proc.

Int. Workshop on Gross Properties of Nuclei and Nuclear Excitations XIV, Hirschegg, Austria, 1986, H. Feldmeier (ed.), P. 146;

L.P. Csernai, J.I. Kapusta, G. Fai, Evidence for Explosive Dynamics from Nucleosynthesis in Central Nb + Nb Collisions, University of Minnesota Supercomputer Institute preprint, UMSI 85/12 and

L.P. Csernai, G. Fai, UMSI 85/14;

29. L.P. Csernai, J.I. Kapusta, G. Fai, D. Hahn, J. Randrup, H. Stöcker, to be published;

30. A. Sandoval, private communication;

I. Tanihata, private communication.

Figure Captions

Fig. 1. Thermal energy per nucleon versus available center of mass energy in the 1 - dimensional shock calculation. The two best fitting equations of state[8] are used with K_l = 1400 MeV (solid line) and K_q = 800 MeV (dashed line). The dots and squares indicate the energies of the pion experiments.

Fig. 2. Dependence of the pion number per nucleon, π/A, on the thermal energy for two different densities in the shockzone, ρ_o (solid line) and 4 ρ_o (dashed line). The dots and diamonds mark the experimental points of refs. 11,13,17.

Fig. 3. The dependence of the entropy on the bombarding energy in the shock calculation. The two upper lines have been calculated with the linear equation of state (K_l = 1400 MeV, solid line) and the quadratic EOS (K_q = 800 MeV, dashed line) of ref. 8, respectively. The two lower lines labeled nucleons only have been calculated for pure nucleonic matter (i.e. without pions or resonances) at the densities and temperatures resulting from the shock calculation using the linear EOS (dotted) and the quadratic EOS (dashed), respectively. The full dots and the open diamonds indicate the energies of the pion measurements of ref. 17.

Fig. 4.a The path of the fragment conglomerate for isentropic (i.e. at a constant entropy per nucleon) expansion in the T-ρ plane. N is equal to Z here.

Fig. 4b. Isotherms in the entropy- density plane are shown for the

fragment conglomerate.

Fig. 5 Dependence of the temperature on the entropy per nucleon at constant densities in the QSM.

Fig. 6 Thermal energy per nucleon versus temperature for 3 different densities.

Fig. 7 Thermal energy per cluster versus the temperature for two densities, $\rho = 0.1\ \rho_o$ (solid line) and $\rho = 0.8\ \rho_o$ (dashed line).

Fig. 8. The entropy values derived from the calculated d and p yields via eq. 19 (solid line)[24], via eq. 20 (dotted-dashed line)[25] and via the formalism of Kapusta (dashed line)[26] against the thermodynamic entropy for N = Z at $\rho = 0.1\ \rho_o$. Only neutrons, protons and deuterons have been included into the chemical equilibrium calculation.

Fig. 9. Same as Fig. 8, but tritons, ^{3}He and α-particles are also included.

Fig. 10. Ratio of protons after the decay of instable fragments versus primordial protons for the neutron rich Au + Au system. Two break-up densities have been used, $\rho = 0.1\ \rho_o$ (solid line) and ρ=0.8 ρ_o (dashed line).

Fig. 11. Same as Fig. 10 for deuterons.

Fig. 12. Same as Fig. 10 for tritons

Fig. 13. Same as Fig. 10 for α-particles

Fig. 14. Same as Fig. 10 for ^{7}Li in the ground state.

Fig. 15. The relation between the entropy per nucleon and the d-like to p-like ratio (eq. 20) is shown for 3 different break-up densities ρ = 0.1, 0.33 and 0.8 ρ_o (the solid, dashed and dotted line), respectively. The full dots mark the dependence obtained by using eqs. 19, 20 directly. The ratio has been calculated after the decay of instable fragments for the Nb + Nb system.

Fig. 16. Same as Fig. 15, but d-like/p-like has been calculated before the decay of instable clusters.

Fig. 17. The solid line shows the same results as the solid one in Fig. 15, the dashed line has been calculated with the same parameters T, ρ, N/Z but with only protons, neutrons, deuterons, tritons, ^{3}He and α's present.

Fig. 18. Same as Fig. 15 for N = Z (Ca + Ca).

Fig. 19. Same as Fig. 15, but for the Au + Au system.

Fig. 20. Comparison of the present QSM (full curve) with the classical microcanonical approximation of Randrup and Fai[27] (dots). The calculations shown are for T = 70 MeV, but the agreement is also found at all other temperatures T > 10 MeV. We would like to thank J.

Randrup for providing his results.

Fig. 21. Same as Fig. 15, but the curves are for constant T, not for constant ρ. The density varies for each curve from 0.05 to 0.8 ρ_o.

Fig. 22. Thermal energy per nucleon versus the d-like/p-like ratio in the quantum-statistical model. The solid line shows the results for $\rho = 0.1\ \rho_o$, the dashed one for 0.8 ρ_o.

Fig. 23. Connection between d-like/p-like and the break-up density for constant entropy. The calculation has been done for the Au + Au system.

Fig. 24. The measured[1] ratio d-like to p-like as a function of the multiplicity N_p for Nb + Nb at 400 and 650 MeV/n bombarding energy. The curves are from fits to the coalescence model.[1]

Fig. 25. The multiplicity dependence of the entropy extracted from the d-like/p-like ratios of ref. 1 (Fig 24) for Nb + Nb collisions at 400 MeV (solid line) and 650 MeV (dashed line). A break-up density of 0.1 ρ_o has been assumed.

Fig. 26. Entropy values extracted from experiments via the quantum statistical model. Full dots are fits to mid-rapidity measurements[3,4] of heavy clusters, A > 4 in Ar + Au collisions, see Figs. 47 a-c and the text for details.

The other points have been fitted to d-like/p-like ratios at the highest measured multiplicity. Stars show the results for Nb + Nb at

400 and 650 MeV/n[1], diamonds are for Ca + Ca at 400 and 1050 MeV/n[1] and the open circle is for two independent new measurements of the system La + La at 800 MeV/n[30].

Also shown are the nucleonic entropy values calculated above (see Fig. 3) with the equations of state which reproduce the observed pion multiplicities.[8,11,13] See also Fig. 35.

Fig. 27. Deuteron to proton ratios for an asymmetric (left Figure) and a symmetric system versus the entropy *per* nucleon. The solid and dotted- dashed line show the primordial results for $\rho = 0.1\ \rho_0$ and $0.5\ \rho_0$ respectively; the dotted curve gives the ratio for $\rho=0.1\ \rho_0$, the dashed curve for $0.5\ \rho_0$, both after decay.

Fig. 28. Same as Fig. 27 for tritons to protons.

Fig. 29. Same as Fig. 27 for ^{3}He to protons.

Fig. 30. Same as Fig. 27 for α's to protons.

Fig. 31. Same as Fig. 27 for ^{7}Li in the groundstate to protons.

Fig. 32. Same as Fig. 27 for the ^{12}C groundstate to proton ratio.

Fig. 33. Experimental results[1] for the d/p (full dots), t/p (circles), ^{3}He/p (squares with diagonals) and α/p ratios (diamonds) versus multiplicity. Also shown are results of a least square fit based on eq. 23 for the ratios (in descending order of the curves): d/p, t/p, ^{3}He/p, α/p, ^{5}Li/p, ^{6}Li/p, ^{7}Li/p, ^{8}Li/p. The data were measured in Ca +

Ca collisions at 1050 MeV/nucleon.

Fig. 34a. Same as Fig. 33 for Nb + Nb at 400 MeV/nucleon.

Fig. 34b. Same as Fig. 33 for Nb + Nb at 650 MeV/nucleon.

Fig. 35. Multiplicity dependence of the entropy extracted from the least square fit to the four experimentally observed ratios X/p simultaneous for all multiplicities (see Fig. 34a). The multiplicity dependence of the fit is based on eq. 23.

Fig. 36a. The multiplicity dependence of all X/p ratios for the system Nb + Nb at 400 MeV/nucleon as predicted by the QSM when the fitted S/A ($\tilde{R}_{dp}$) of Fig. 25 are used as input. The experimental data[1] are the same as in Fig. 34a, circles stand for d/p, triangles for t/p, squares for ^{3}He/p and diamonds for α's. The curves show in descending order the calculated d/p, t/p, ^{3}He/p, α/p, ^{6}Li/p, ^{7}Li/p and ^{8}Li/p ratios.

Fig. 36b. Same as 36a for 650 MeV/nucleon bombarding energy.

Fig. 37. Same as Fig. 36 but for Ca + Ca at 1050 MeV/nucleon.

Fig. 38. The bombarding energy dependence of the entropy S/A. The curves are the same as in Fig. 7, derived from the hydrodynamical shock calculation. The full dots are fits to the d-like to p-like ratios as extrapolated to infinite multiplicity (ref. 1); the diamonds are the results of the least square fits to the 4 ratios d/p, t/p, ^{3}He/p and α/p simultaneously for all multiplicities (see Figs. 33, 34, 26). The error bars to the eight points due to uncertainties in the break up density are of the order of 0.75 units in entropy.

Fig. 39. Ratios of excited states to ground states (or other excited states in the upper right) for Ar + Au against the temperature for 3 break-up densities. Solid lines show the ratio in the case of a pure Boltzmann distribution, shaded areas show the experimental ratios (7).

Fig. 40. Same as Fig. 39.

Fig. 41. Three ratios of particle instable states to ground states versus the entropy/nucleon in the Ar + Au system. Three different break-up densities are used, 0.1 ρ_o (solid line) 0.5ρ_o (dashed line) and 0.8 ρ_o (dotted-dashed). Shaded areas show the experimental ratios.[7]

Fig. 42. Mass distributions for N = Z. Solid lines display primordial yields, dashed lines yields after decay. The break-up density is fixed at 0.33 ρ_o, the temperature is 2, 5 and 15 MeV, respectively.

Fig. 43. Distribution of Carbon isotopes in an N=Z system. As in Fig. 42, solid bars display primordial, dashed bars yields after decay. The entropy is held constant, S/A = 2.5.

Fig. 44. Same as Fig. 42, but S/A is constrained to 2.5 units, hence T and ρ change simultaneously.

Fig. 45. Mass distribution after decay in the N = Z system for 10 MeV temperature and ρ = 0.1 ρ_o. At A = 1, neutron and proton yields are shown separately. An exponential (solid line) and a polynomial

(dashed) have been fitted to these yields.

Fig. 46. Slope parameters from exponential fits $Y(A) \sim e^{-\sigma A}$ (see Fig. 41) to mass yields for a N=Z system. Three break-up densities $\rho = 0.1\ \rho_o$ (solid), $0.5\ \rho_o$ (dotted) and $0.8\ \rho_o$ (dashed) have been used.

Fig. 47a-c. Fit to the yields of heavy fragments (A > 4) up to nitrogen isotopes. The experimental points[3,4] (circles with bar) have been measured in Ar + Au collisions at 42 (a), 92 (b), and 137 MeV/nucleon (c). Results of the two parameter fit are the diamonds.

Fig. 48a. Ratio of neutrons to protons after decay of instable fragments for $\rho = 0.1\ \rho_o$ (solid line) and $\rho = 0.5\ \rho_o$ (dotted line).
Fig. 48b. Same as Fig. 48a before the sequential decay.

Fig. 49. Same as Fig. 48a for the tritium / ^{3}He ratio.

Fig. 50. Same as Fig. 48a for the N=Z system.

Fig. 51. Same as Fig. 49 for the N=Z system.

Fig. 52a. Yield of light, stable fragments after decay of instable clusters versus entropy for the neutron-rich Au + Au system, at a break-up density of $0.5\ \rho_o$.
Fig. 52b. Same as Fig. 52a for $\rho = 0.1\ \rho_o$.
Fig. 52c. Same as Fig. 52b for a N = Z system.

Fig. 53a. Contribution of the primordial yields of free nucleons

(solid), light complex fragments with A = 2 - 4 (dashed) and intermediate mass fragments with A > 4 (dotted) to the total number of nucleons in the system Au + Au at $\rho = 0.1\ \rho_0$.

Fig. 53b. Same as Fig. 53a, but after the decay of instable fragments.

Fig. 54a. The contributions of nucleons (solid line), stable clusters with A > 1 (dotted line) and instable clusters (dashed line) to the total entropy per nucleon versus the entropy itself. The calculations have been done for the Au + Au system at a break-up density $0.1\ \rho_0$.

Fig. 54b. Same as Fig. 54a for $\rho = 0.5\ \rho_0$.

Fig. 54c. Same as Fig. 54b for the N = Z system.

Fig. 54d. Same as Fig. 54b, but the contributions are normalised to one.

Fig. 55a. Average mass-number of clusters versus entropy for N=Z at a break-up density of $0.1\ \rho_0$ (solid line) and $0.8\ \rho_0$ (dashed line). The average is calculated before the decay of instable fragments.

Fig. 55b. Same as Fig. 55a but after the decay of instable fragments has taken place.

Fig. 56a. Entropy dependence of the total multiplicity for the Au + Au system before the decay of instable fragments. Values for two break-up densities, $0.1\ \rho_0$ and $0.5\ \rho_0$, are plottet.

Fig. 56b. Same as Fig. 56a after the decay of instable fragments.

Fig. 57. The entropy dependence of the primordial multiplicity of heavy fragments for two break-up densities, $\rho = 0.1\ \rho_0$ and $0.5\ \rho_0$ for the solid and dottet line, respectively. After the decay of instable

clusters, the dashed line depicts 0.1 ρ_o, the dotted-dashed 0.5 ρ_o. N is equal to Z.

Fig. 58a. Primordial multiplicity of heavy fragments versus entropy for ρ=0.1 ρ_o (solid line) and 0.5 ρ_o (dashed line) in the Au + Au system.

Fig. 58b. Same as Fig. 58a after the decay of instable fragments.

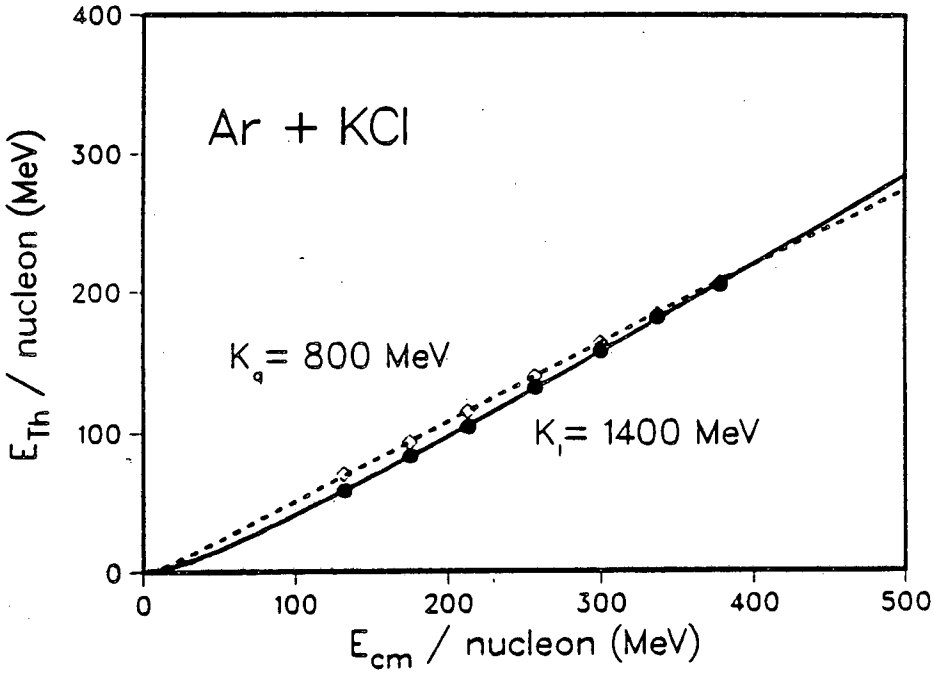

Figure 1

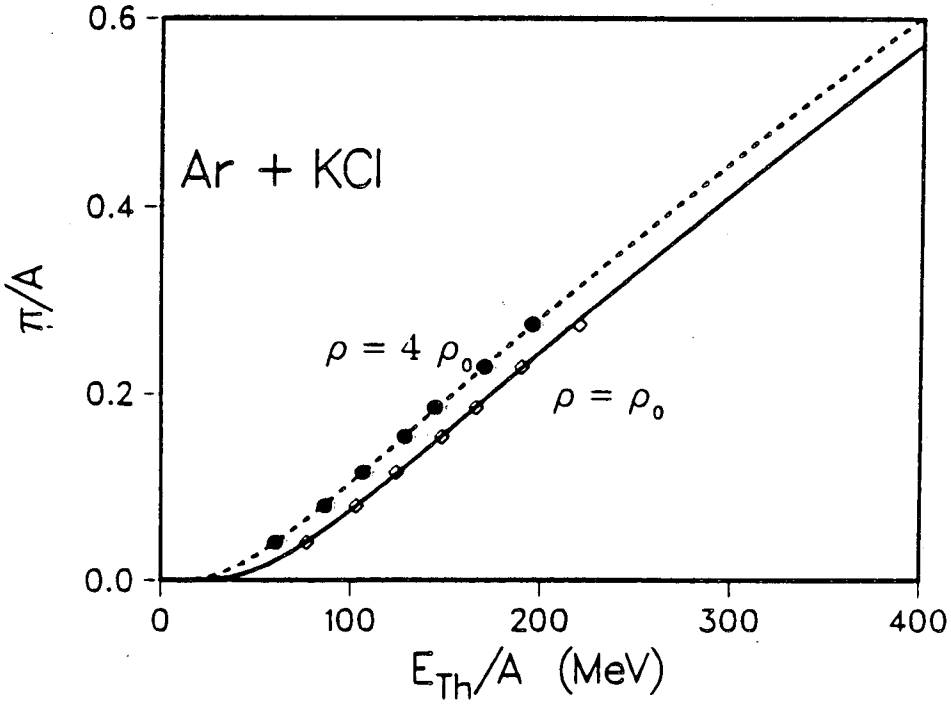

Figure 2

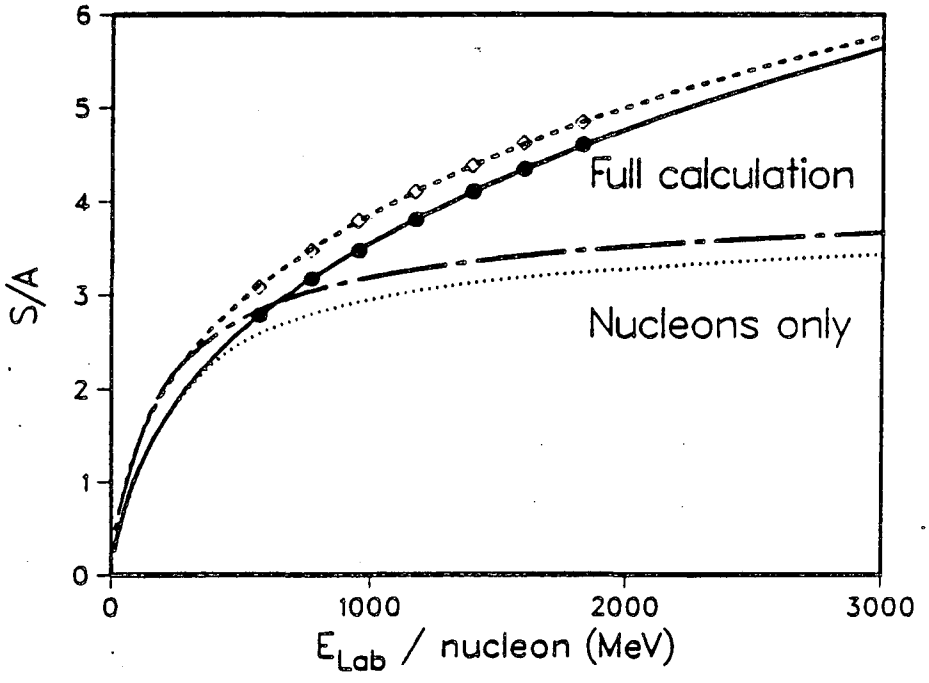
6
5
4
3
2
1
0
S/A
0
1000
2000
3000
E_Lab / nucleon (MeV)
Full calculation
Nucleons only

Figure 3

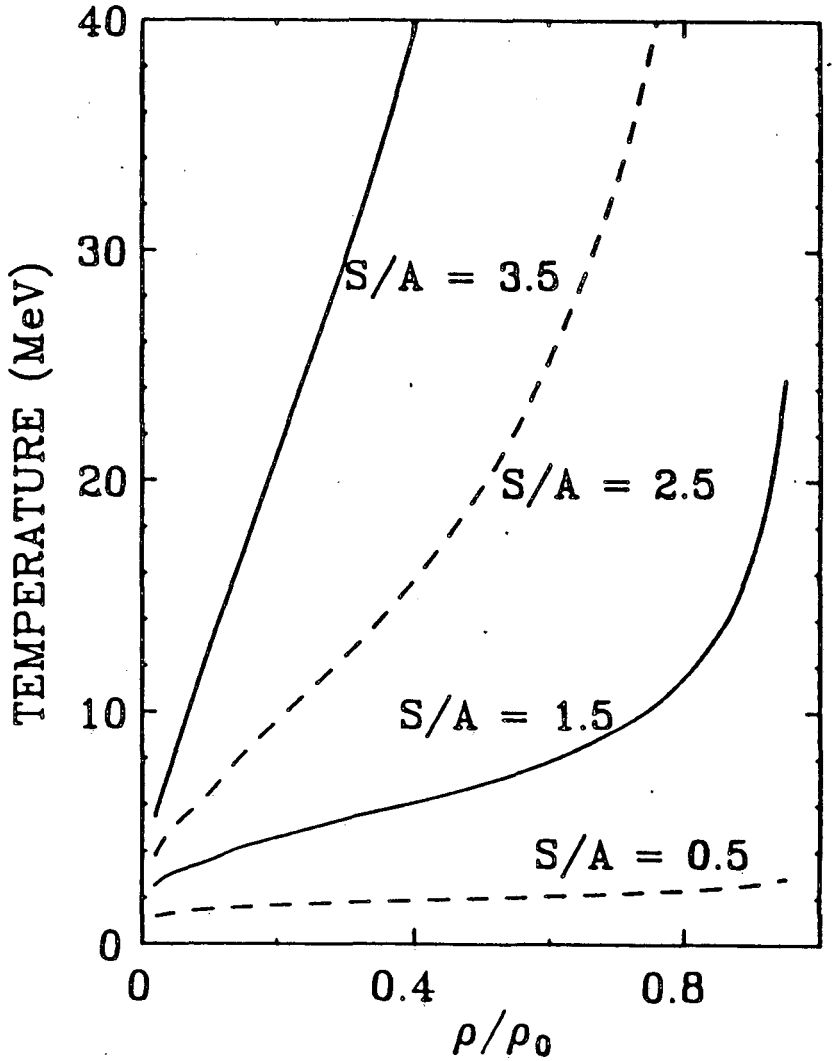

Figure 4a

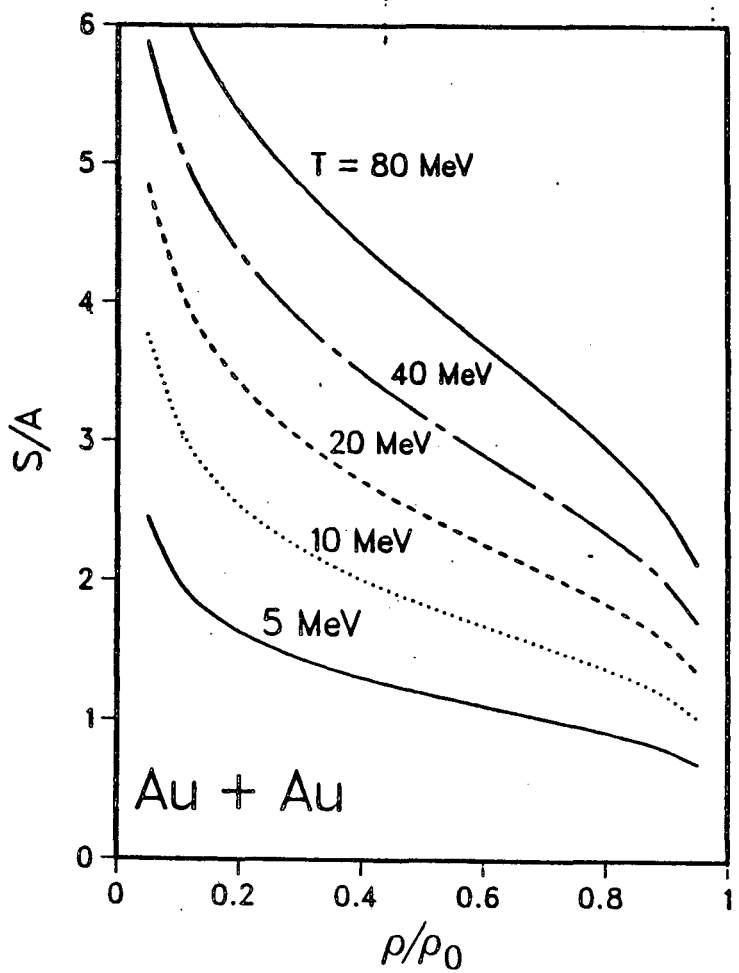

Figure 4b

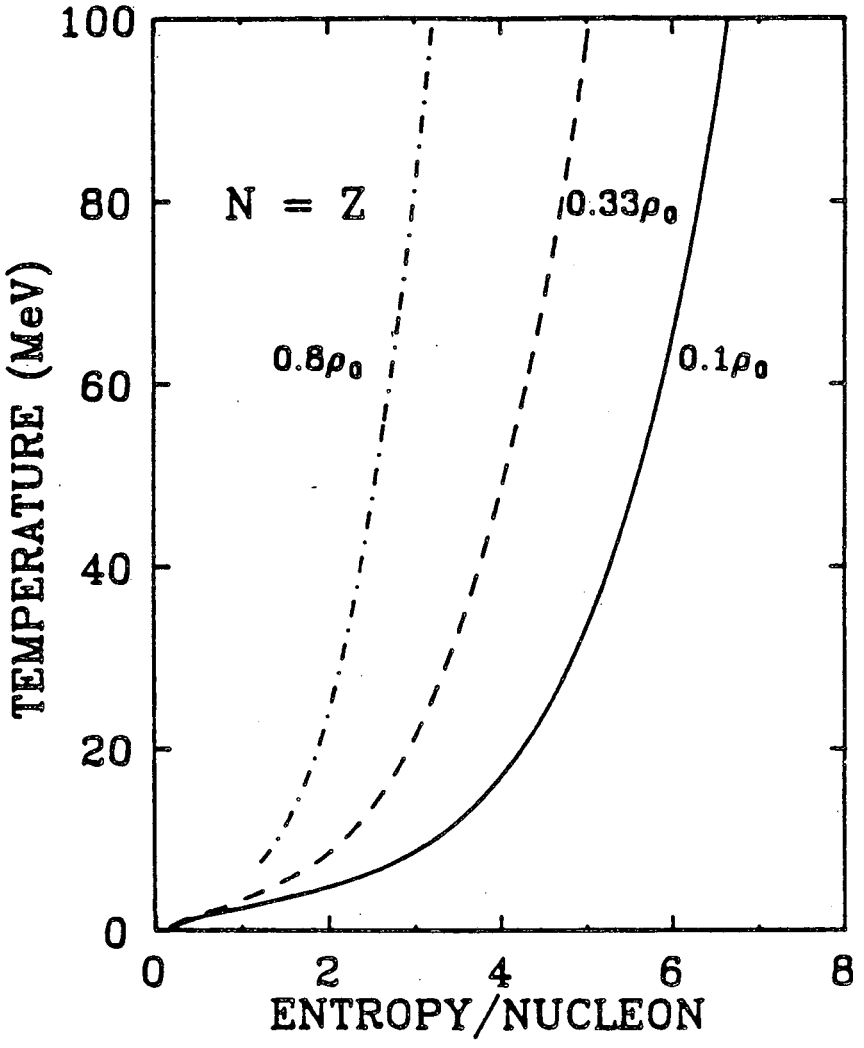

Figure 5

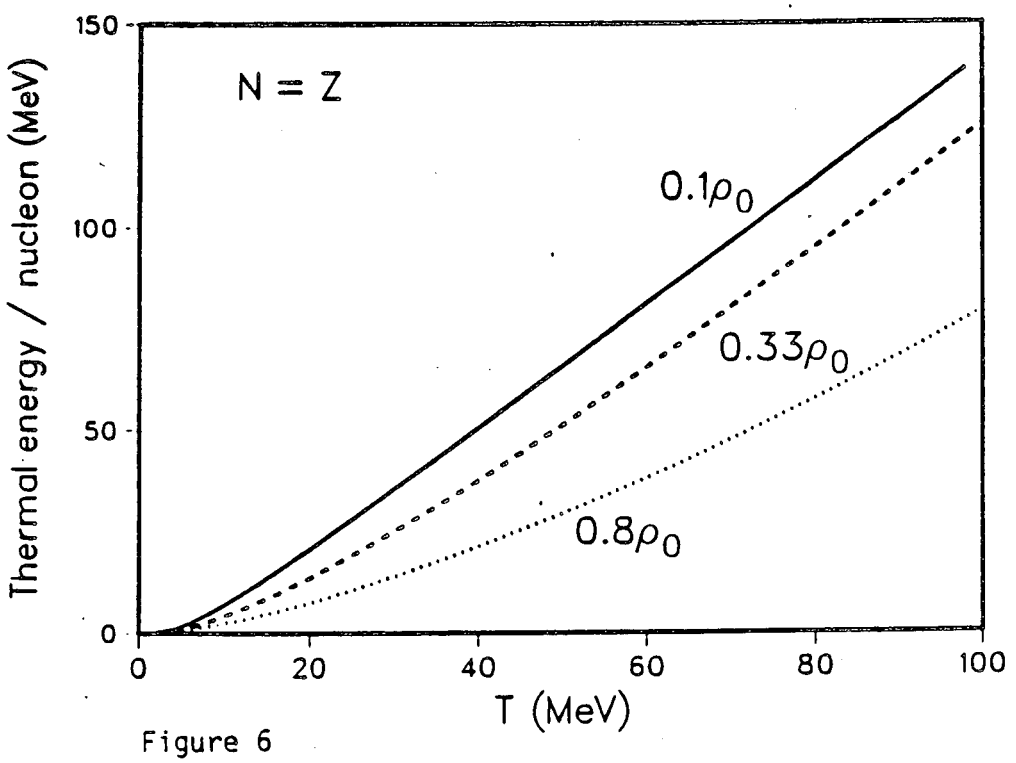

Figure 6

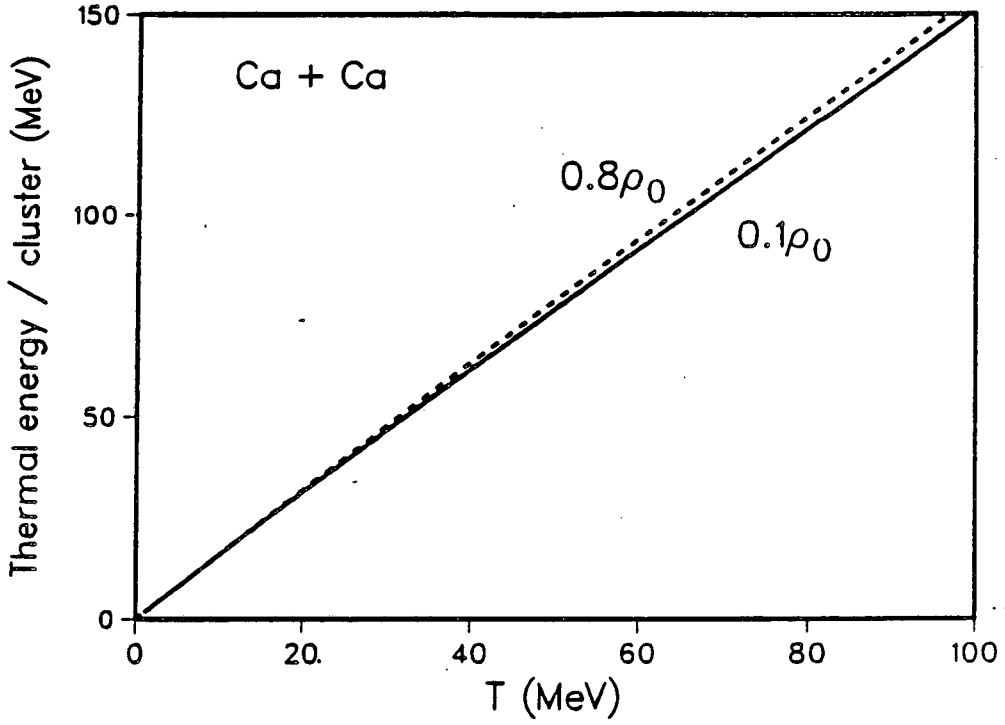

Figure 7

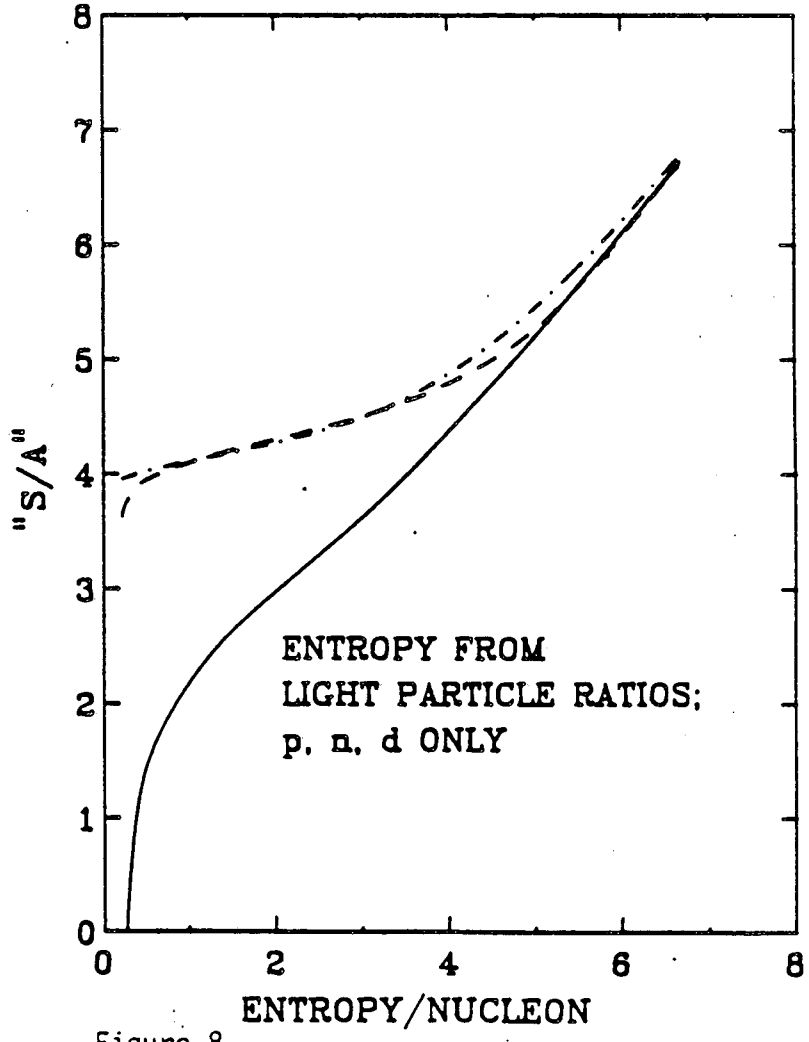

Figure 8

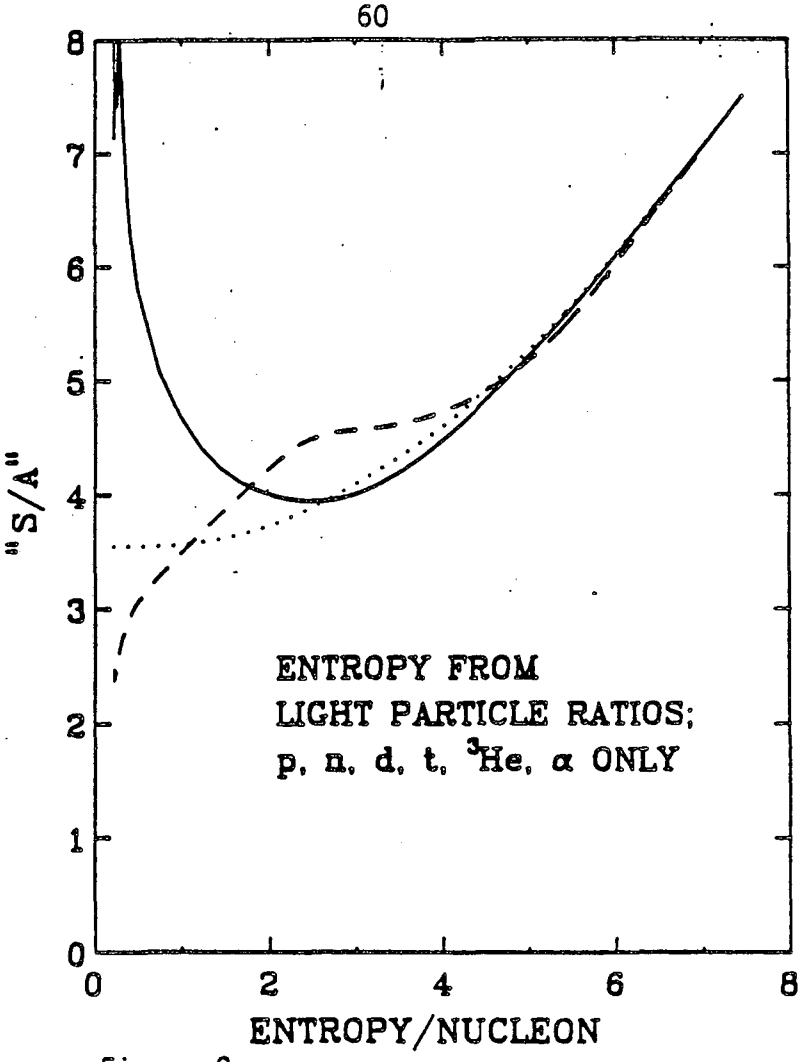

Figure 9

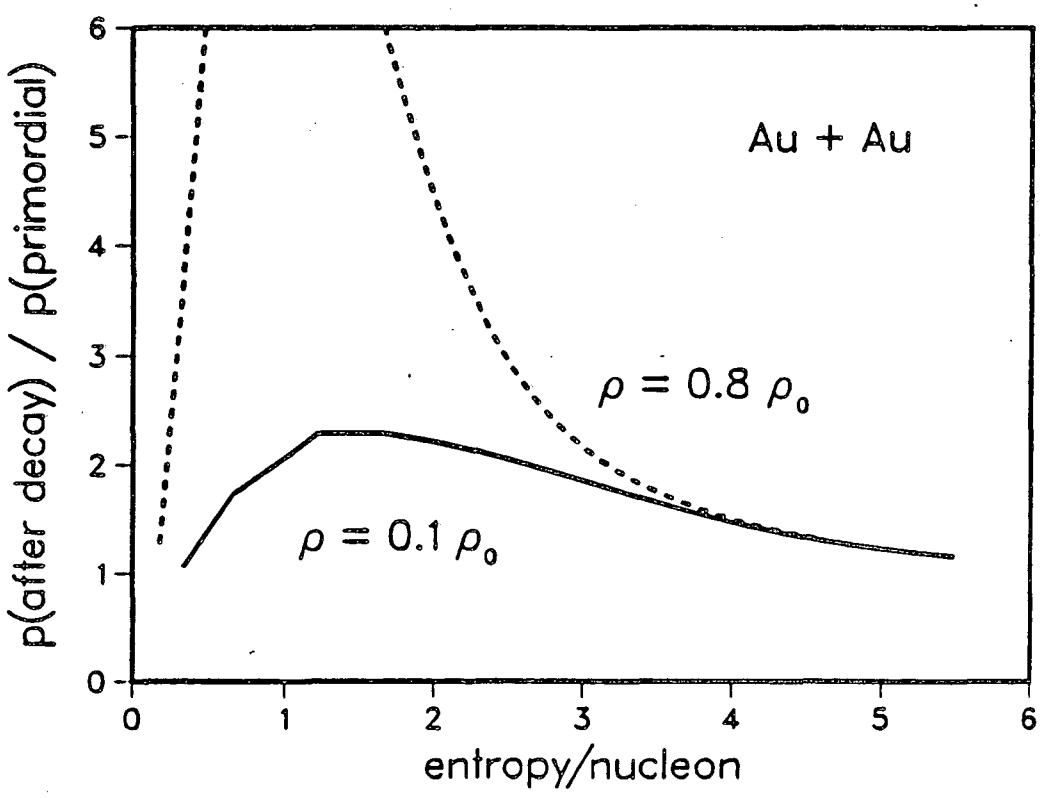

Figure 10

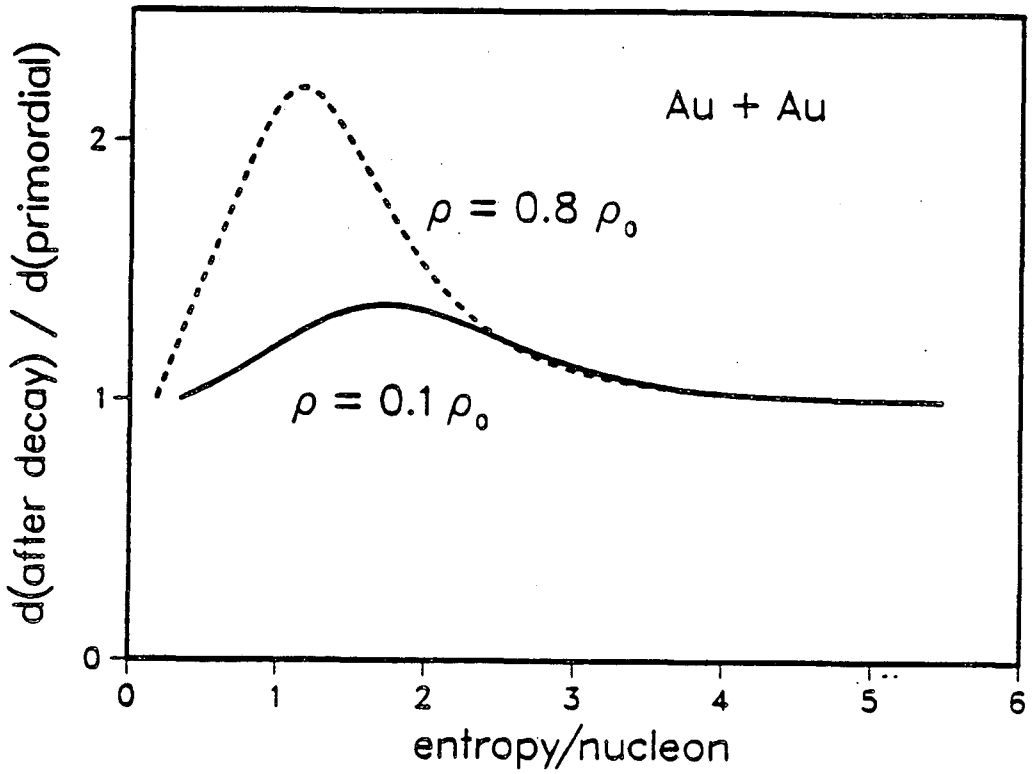

Figure 11

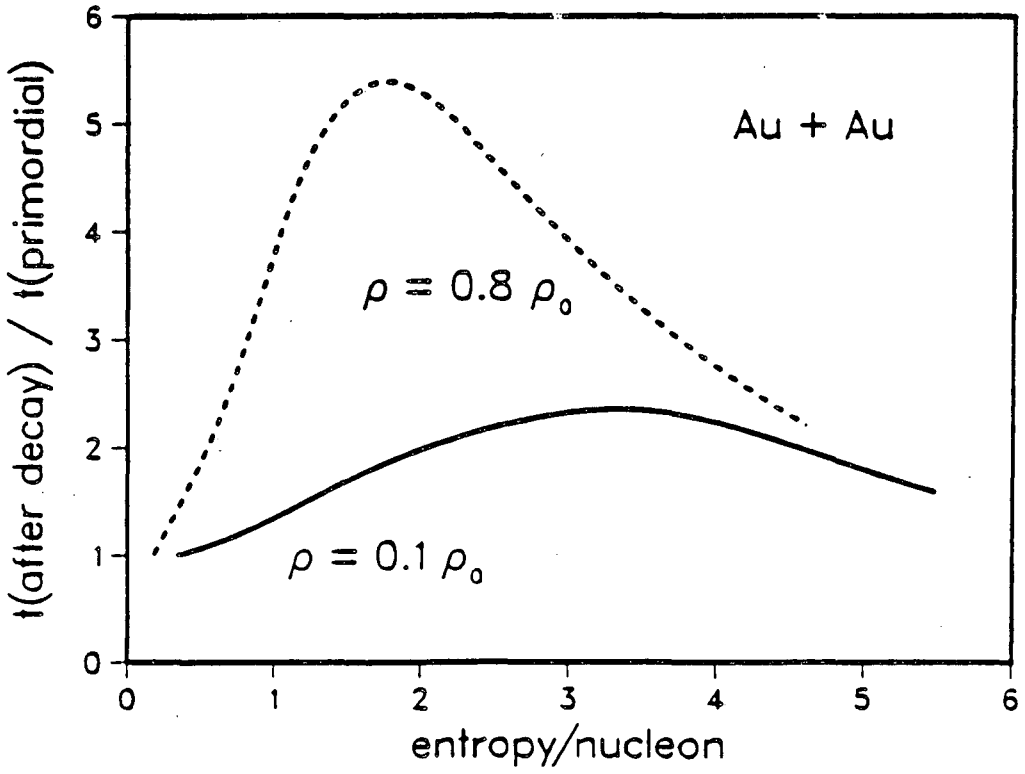

Figure 12

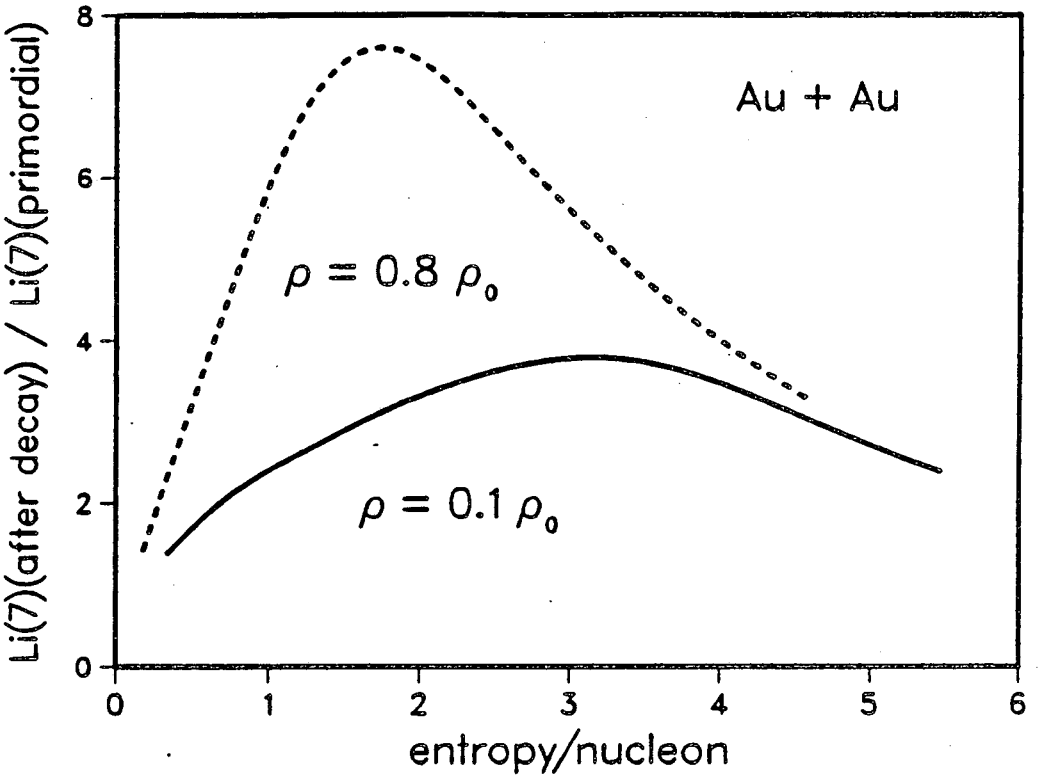

Figure 13

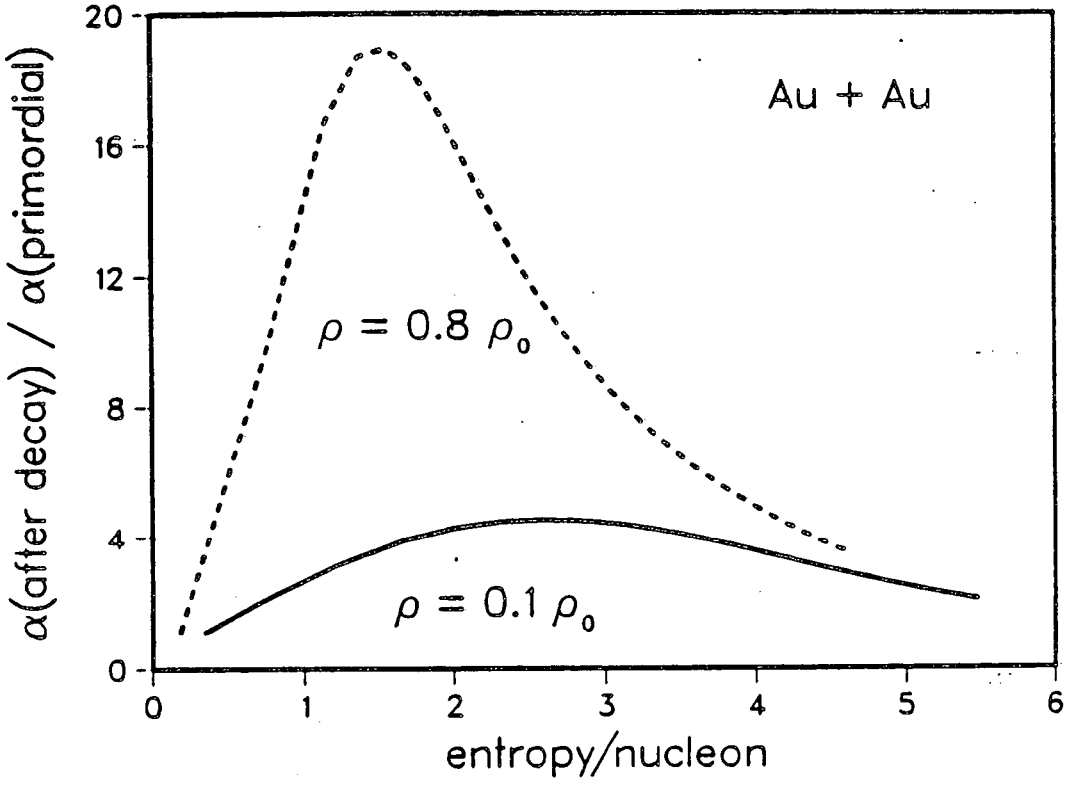

Figure 14

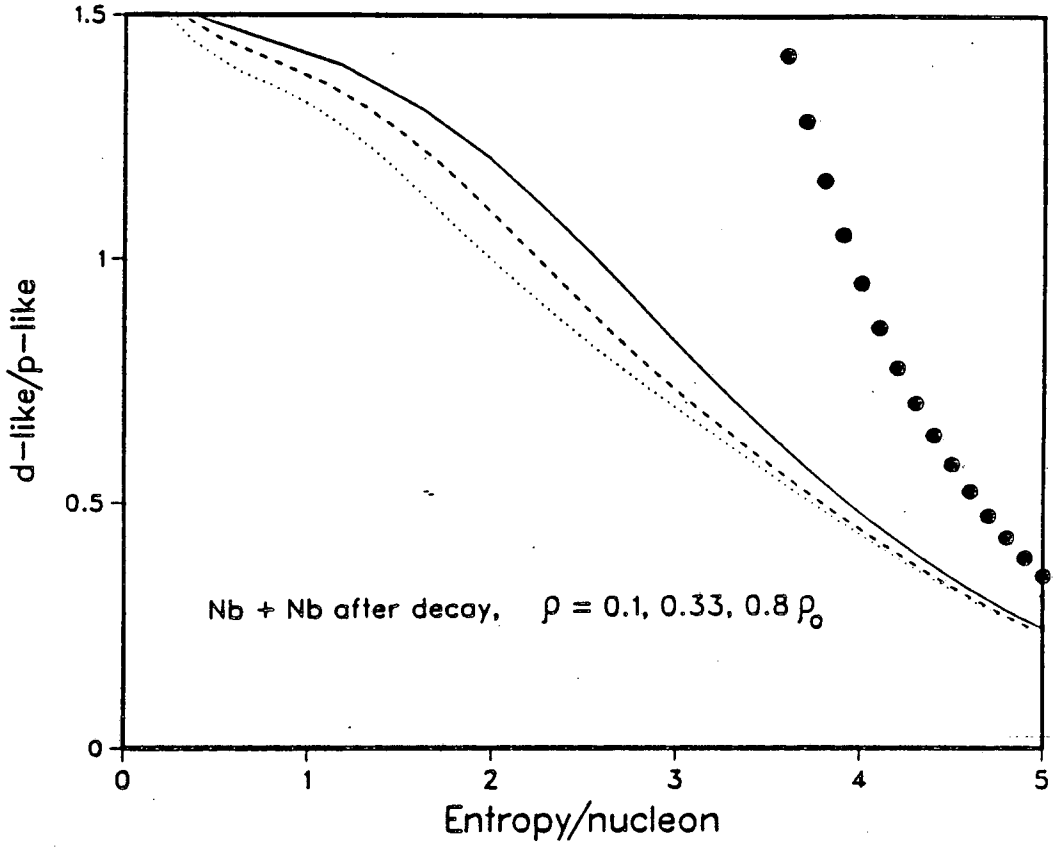

Figure 15

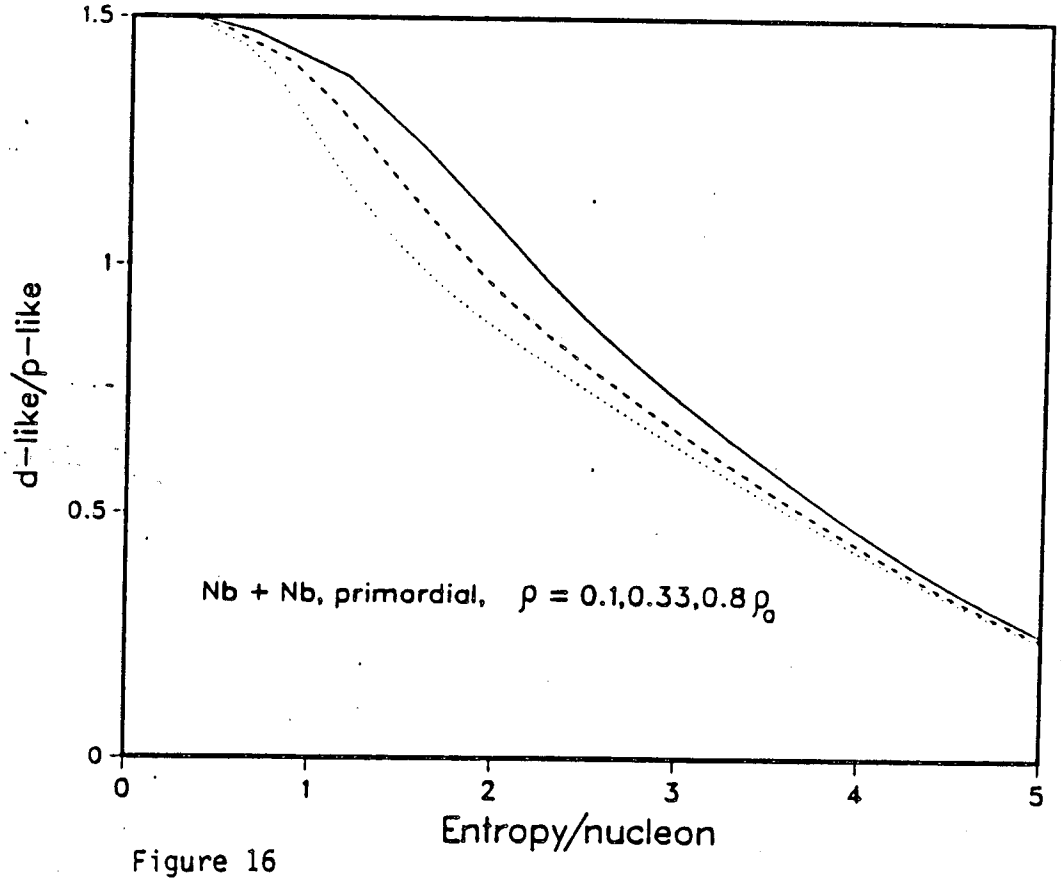

Figure 16

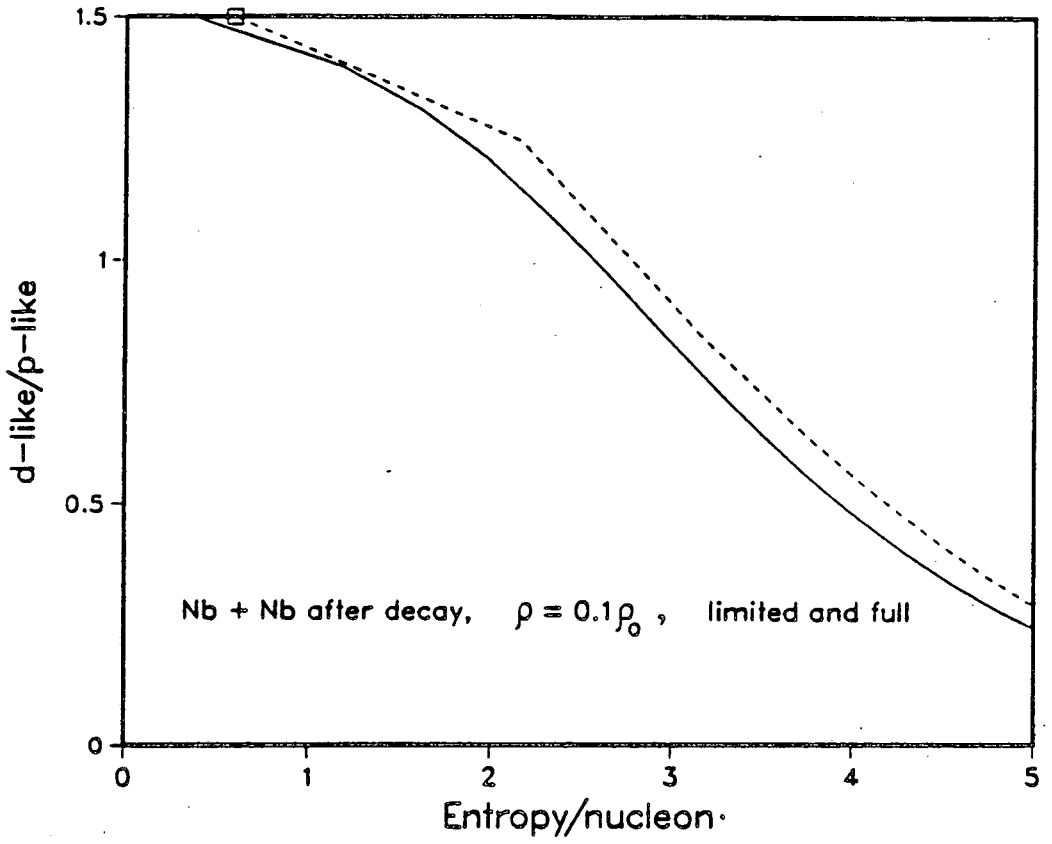

Figure 17

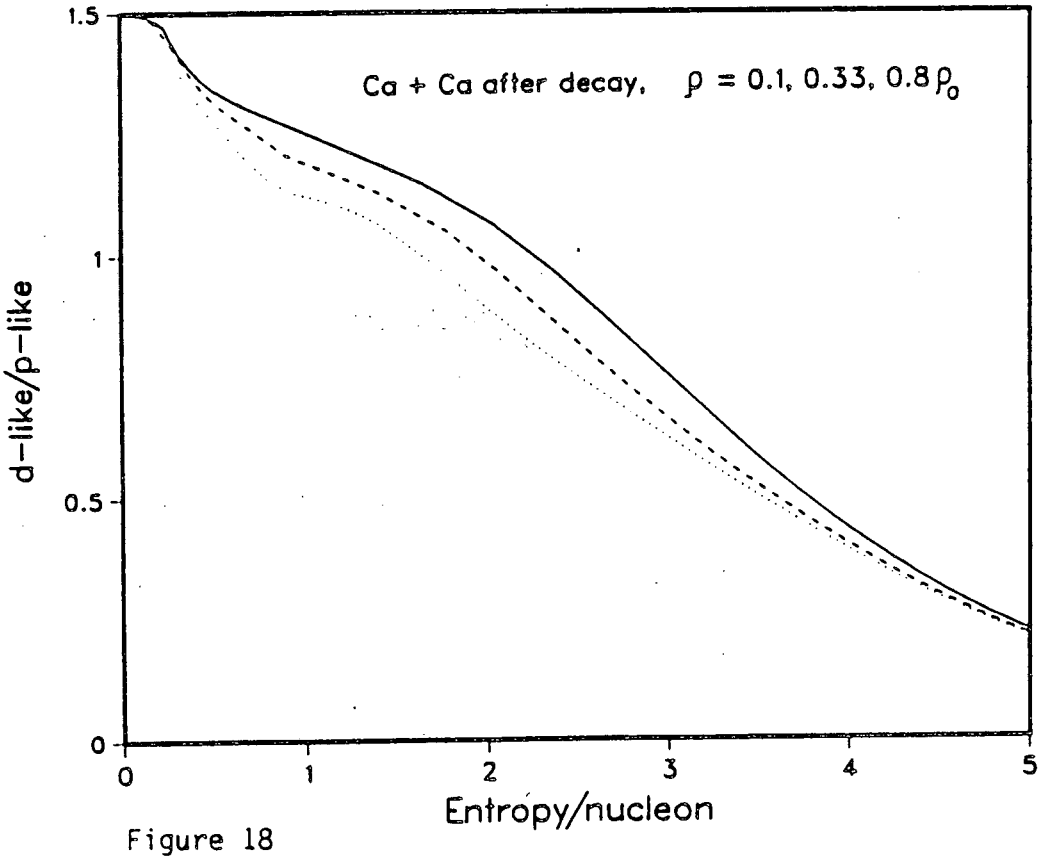

Figure 18

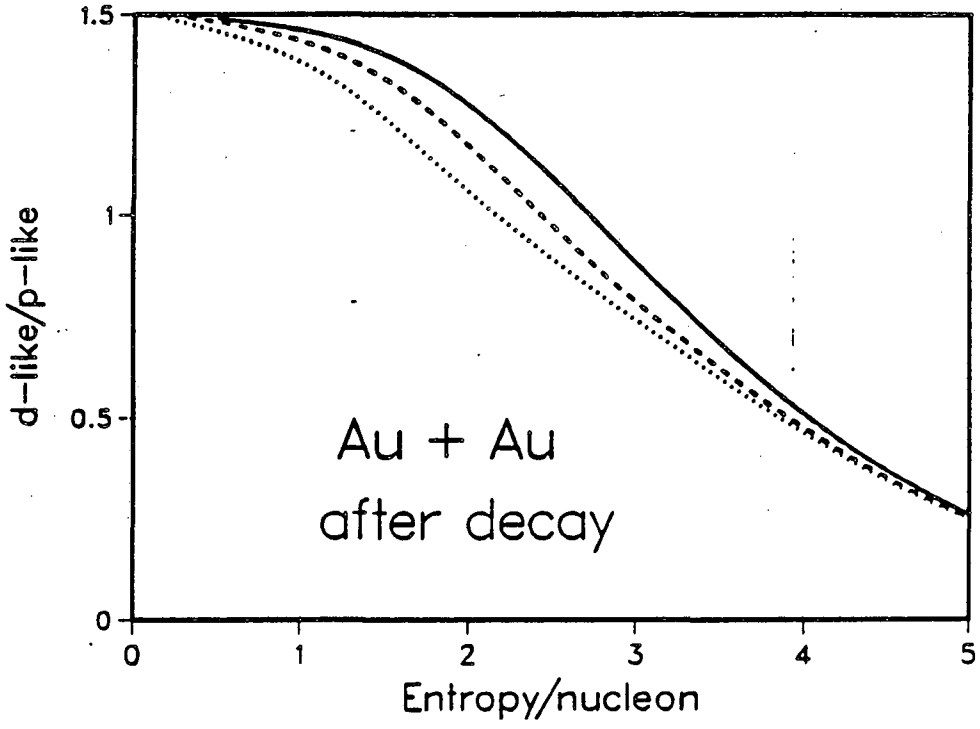
1.5
1
0.5
0
d-like/p-like
Au + Au
after decay
0
1
2
3
4
5
Entropy/nucleon

Figure 19

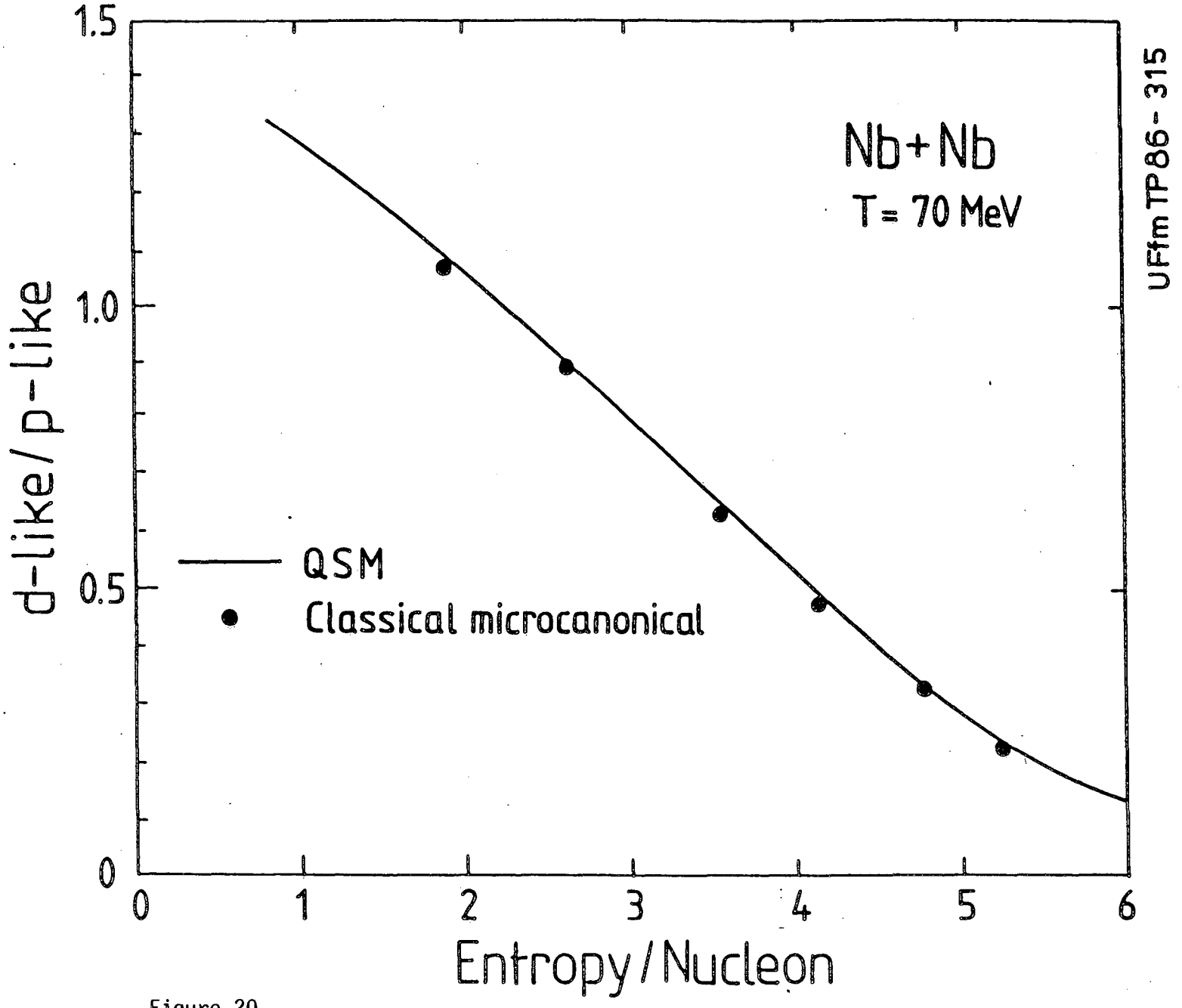
UFfm TP 86 - 315
Nb+Nb
T= 70 MeV
QSM
Classical microcanonical
d-like/p-like
Entropy/Nucleon
0
0.5
1.0
1.5
0
1
2
3
4
5
6

Figure 20

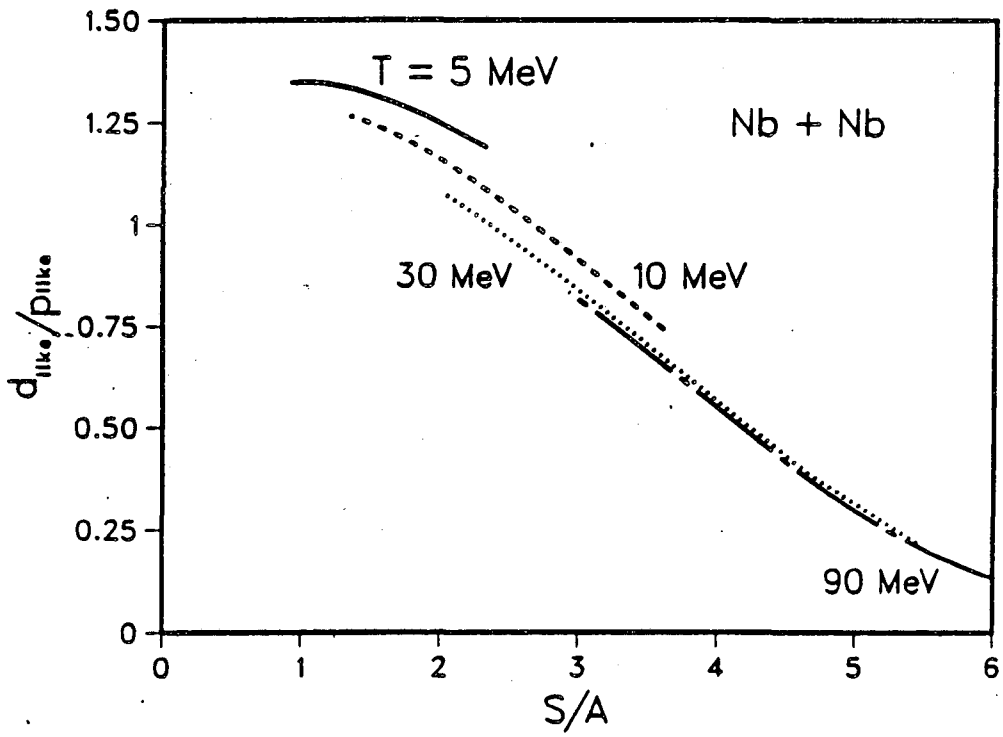
1.50
1.25
1
0.75
0.50
0.25
0
0
1
2
3
4
5
6
S/A
d_{like}/p_{like}
T = 5 MeV
Nb + Nb
30 MeV
10 MeV
90 MeV

Figure 21

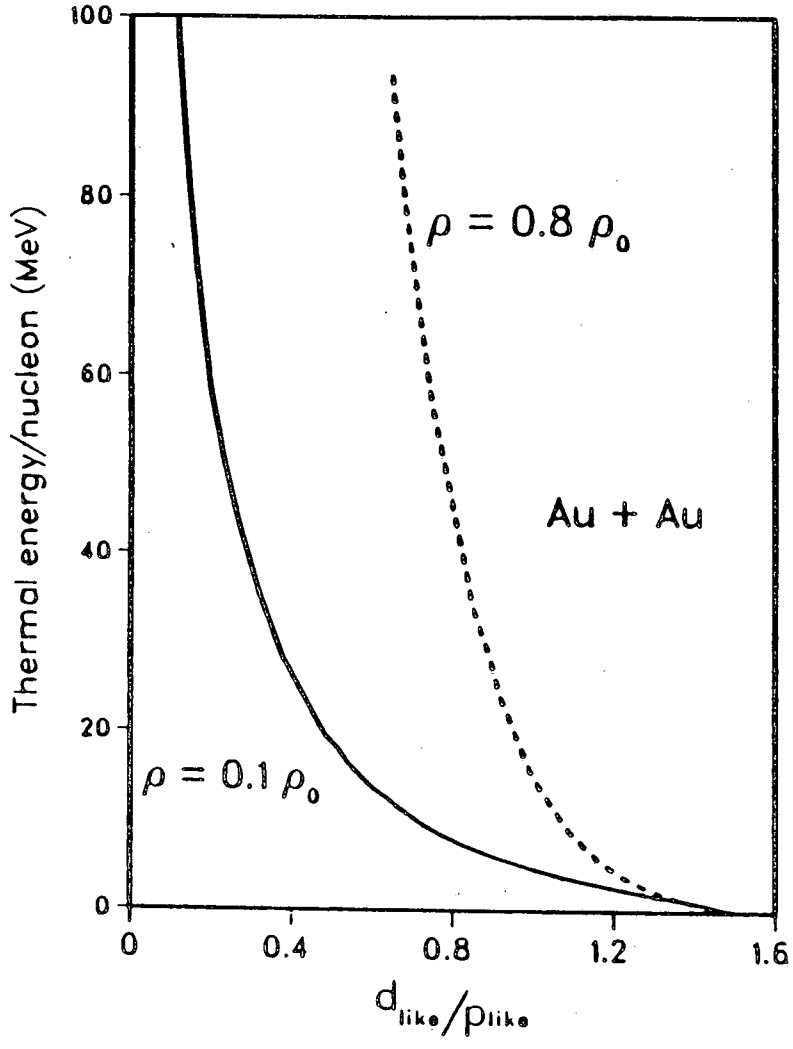

Figure 22

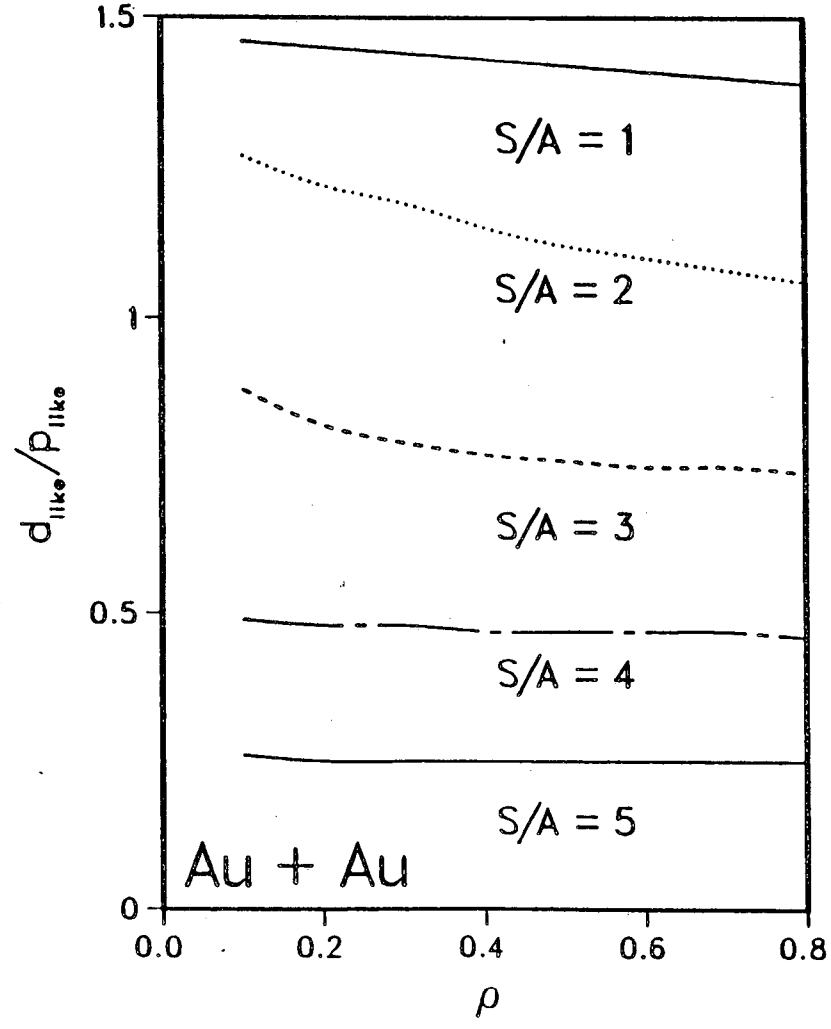

Figure 23

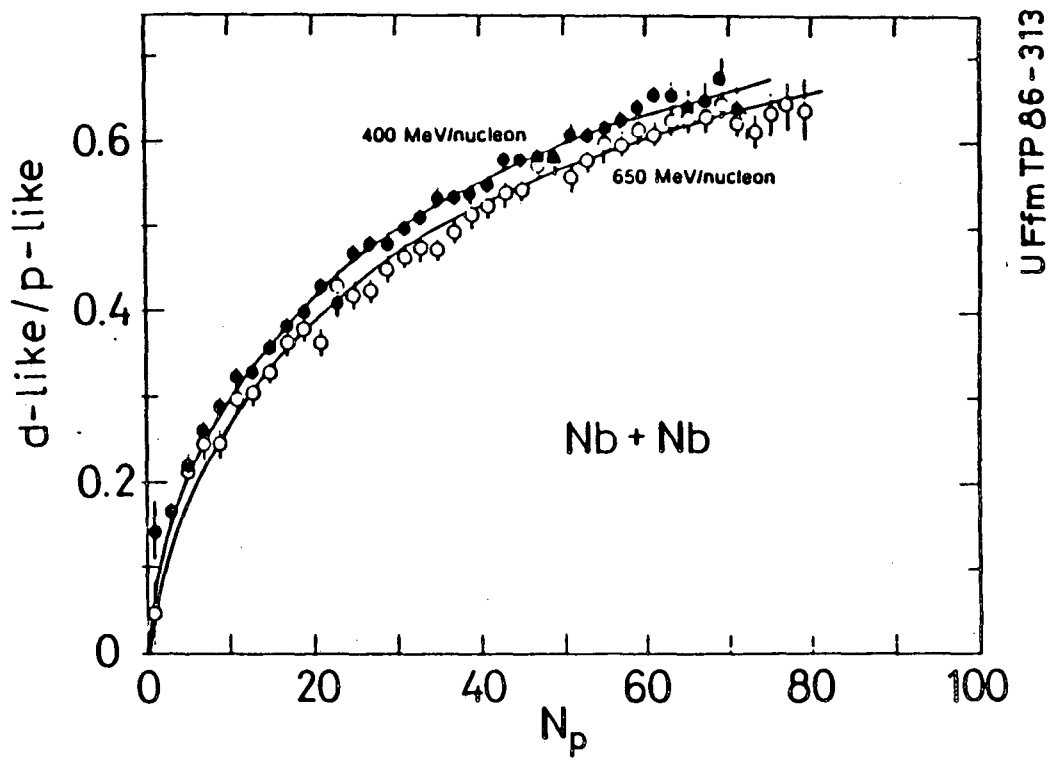

UFfm TP 86-313

Figure 24

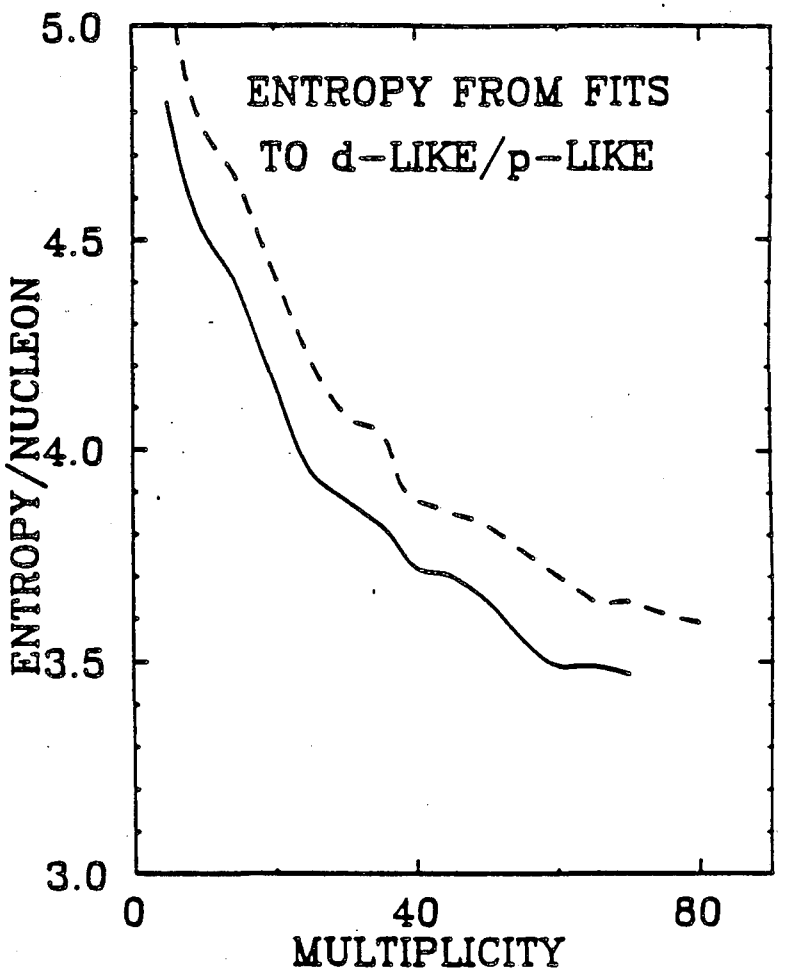
ENTROPY FROM FITS
TO d-LIKE/p-LIKE
5.0
4.5
4.0
3.5
3.0
ENTROPY/NUCLEON
0
40
80
MULTIPLICITY

Figure 25

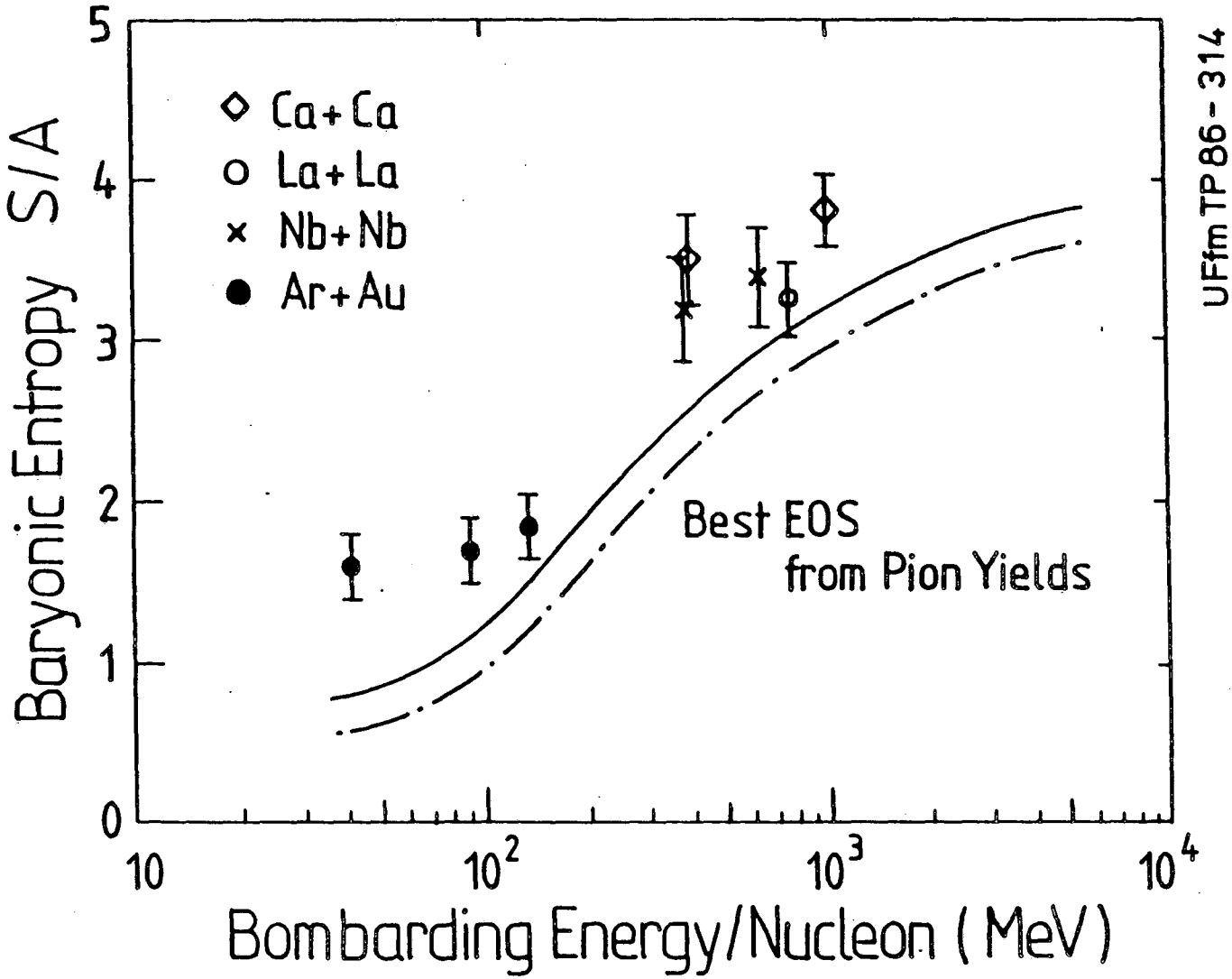
Baryonic Entropy S/A
Bombarding Energy/Nucleon (MeV)
Ca+Ca
La+La
Nb+Nb
Ar+Au
Best EOS
from Pion Yields
UFfm TP 86-314
0
1
2
3
4
5
10
10^2
10^3
10^4

Figure 26

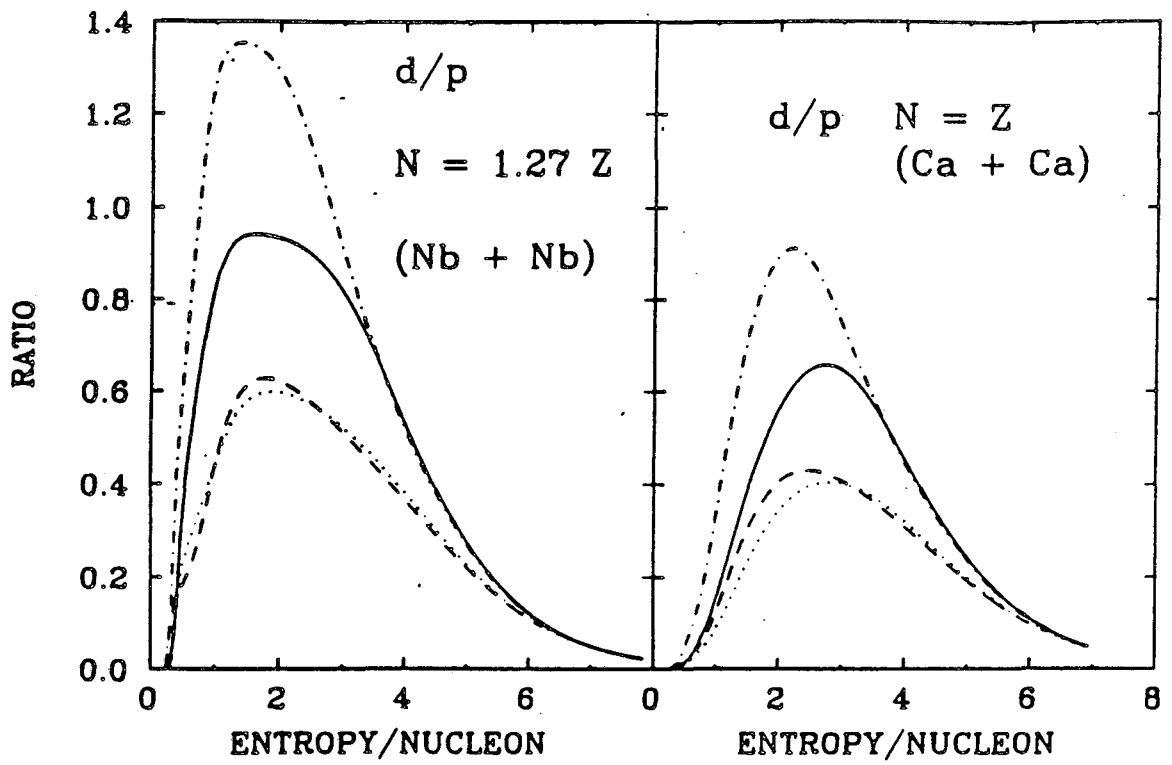
1.4
1.2
1.0
0.8
0.6
0.4
0.2
0.0
RATIO
d/p
N = 1.27 Z
(Nb + Nb)
d/p N = Z
(Ca + Ca)
0
2
4
6
0
2
4
6
8
ENTROPY/NUCLEON
ENTROPY/NUCLEON

Figure 27

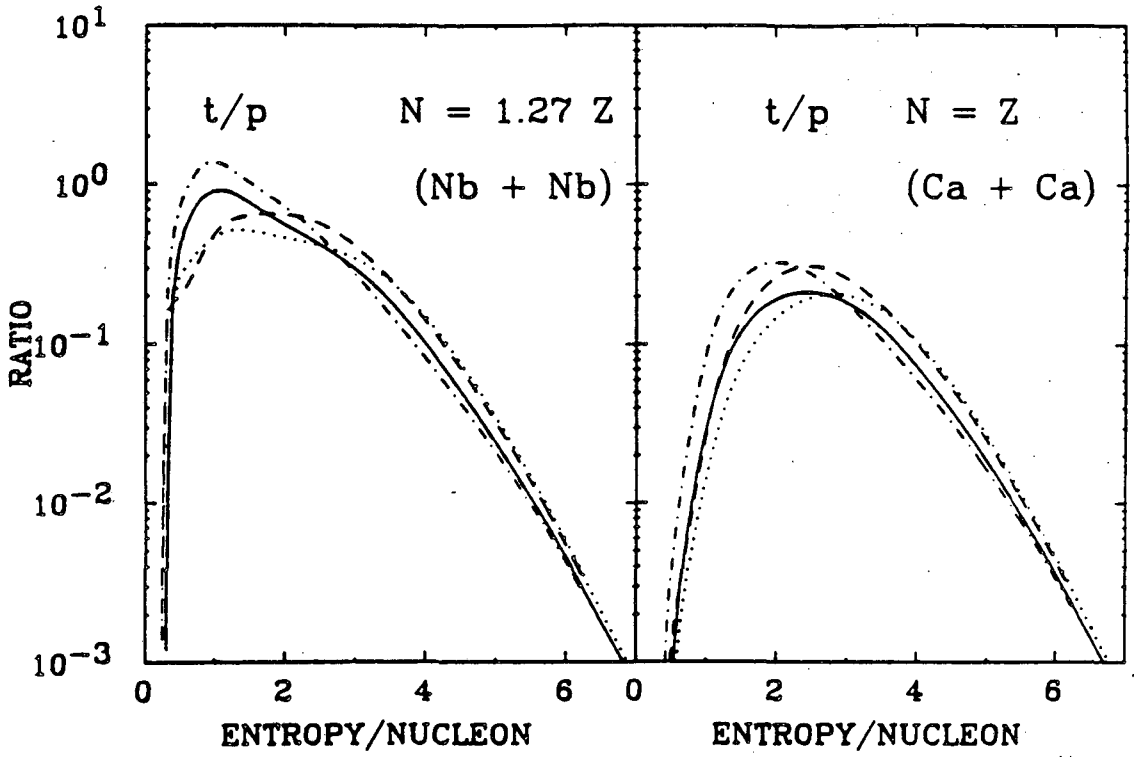

Figure 28

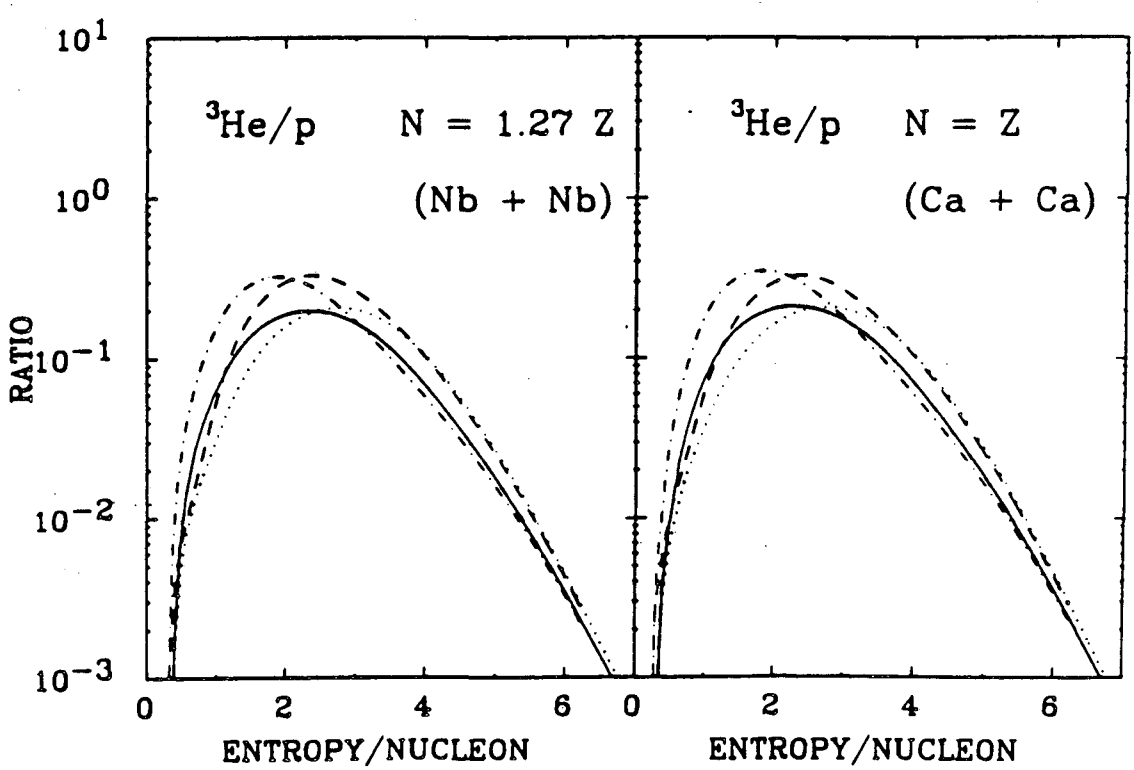

Figure 29

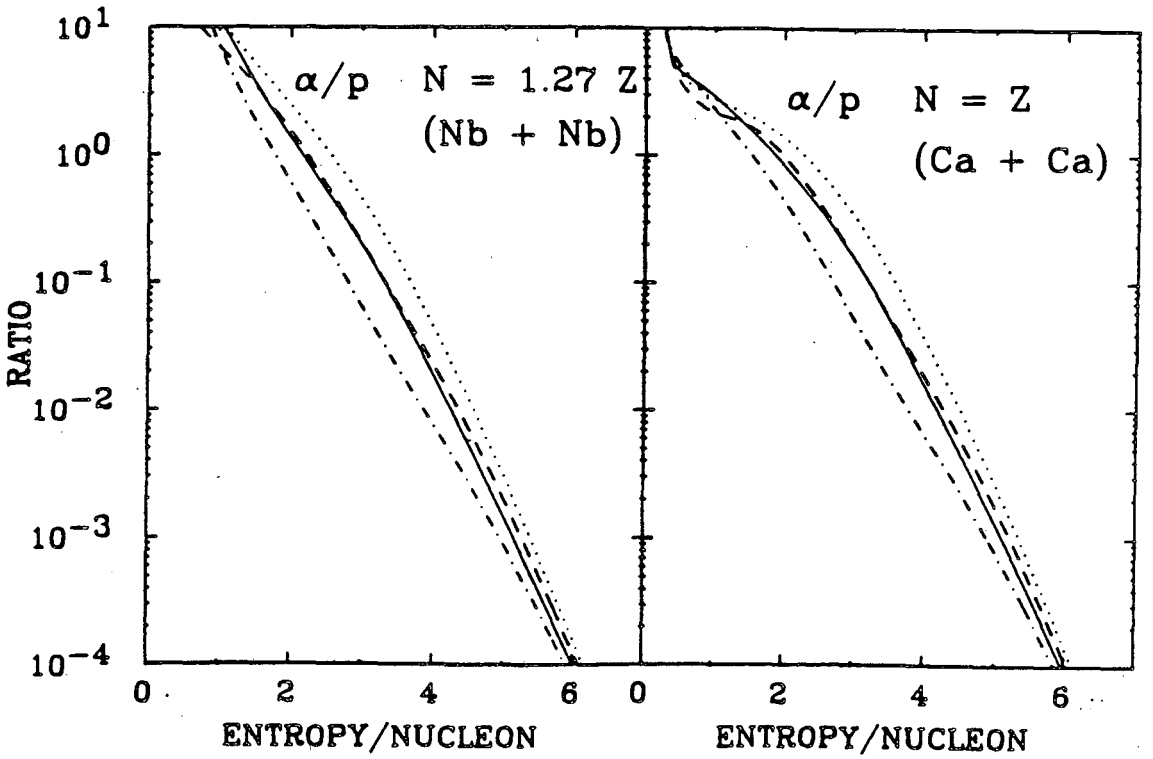

Figure 30

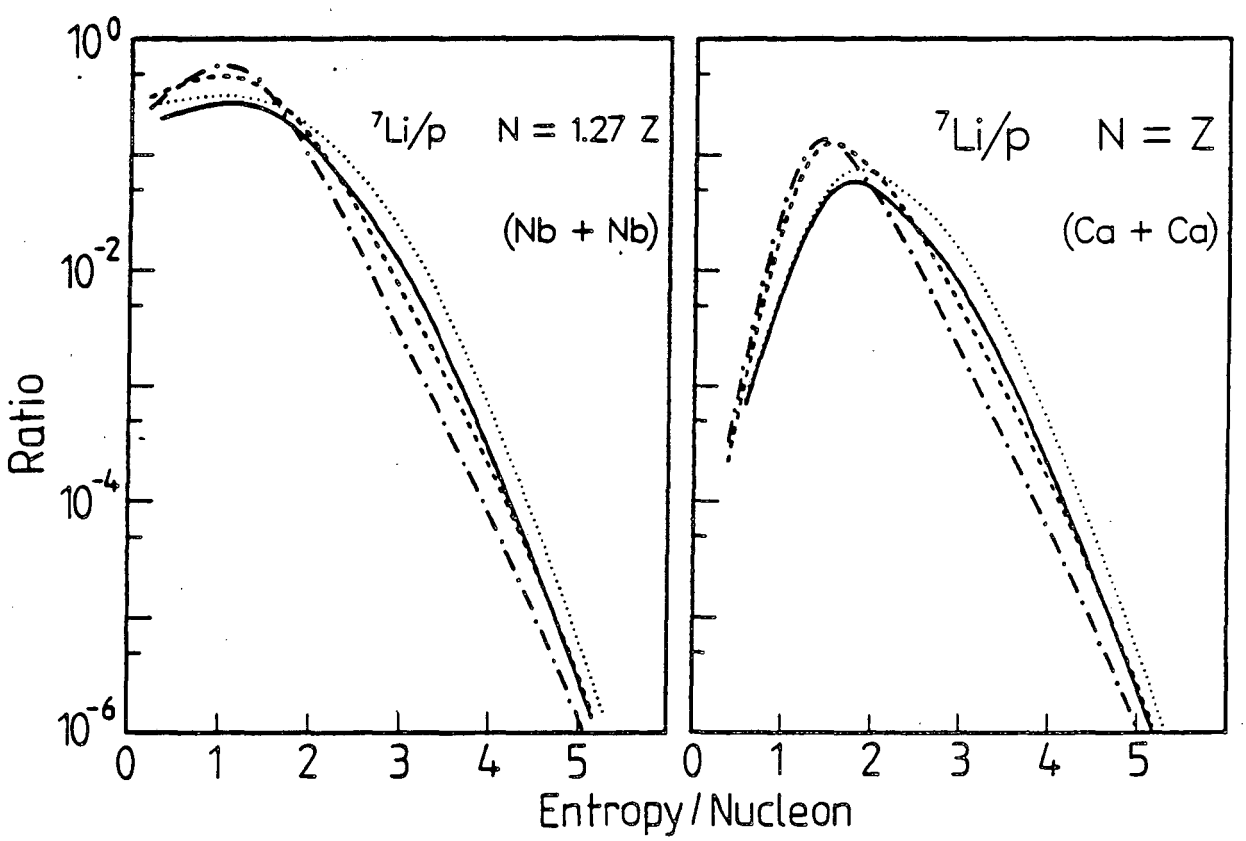

Figure 31

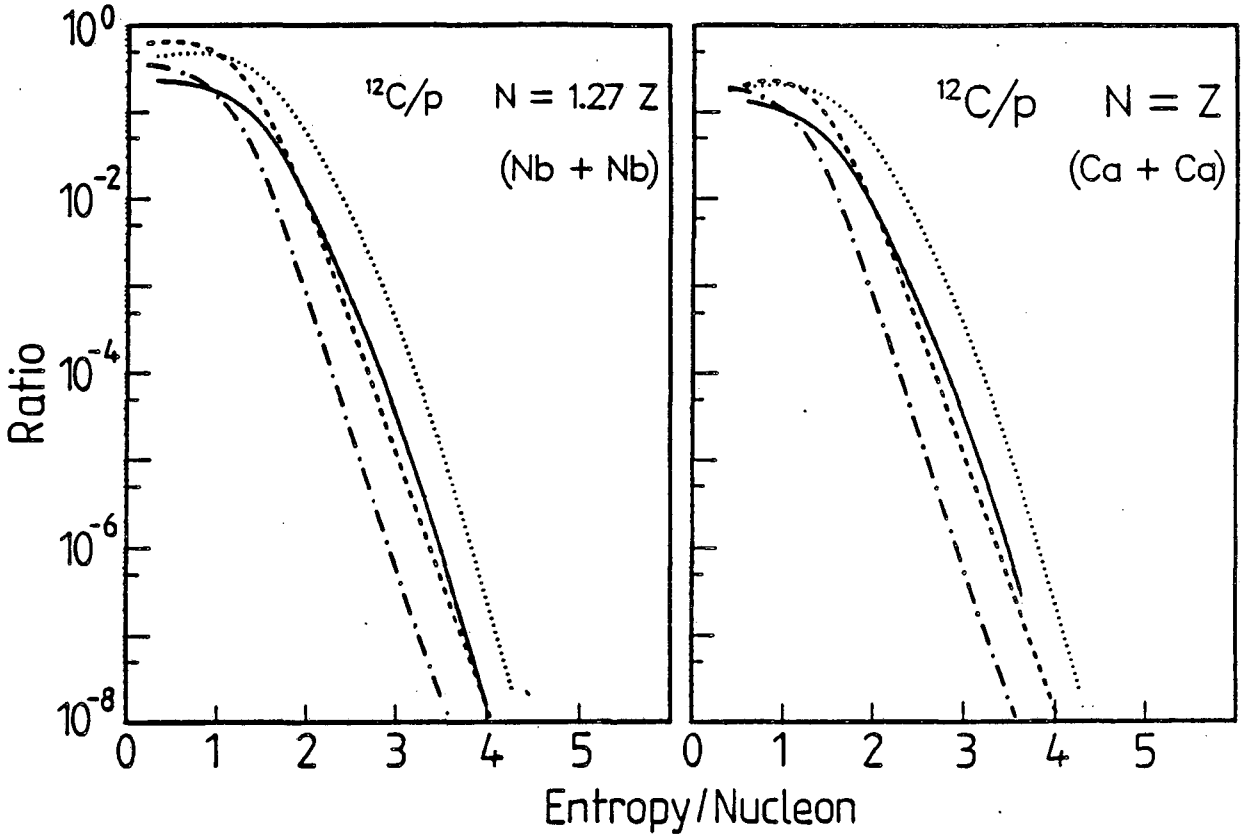

Figure 32

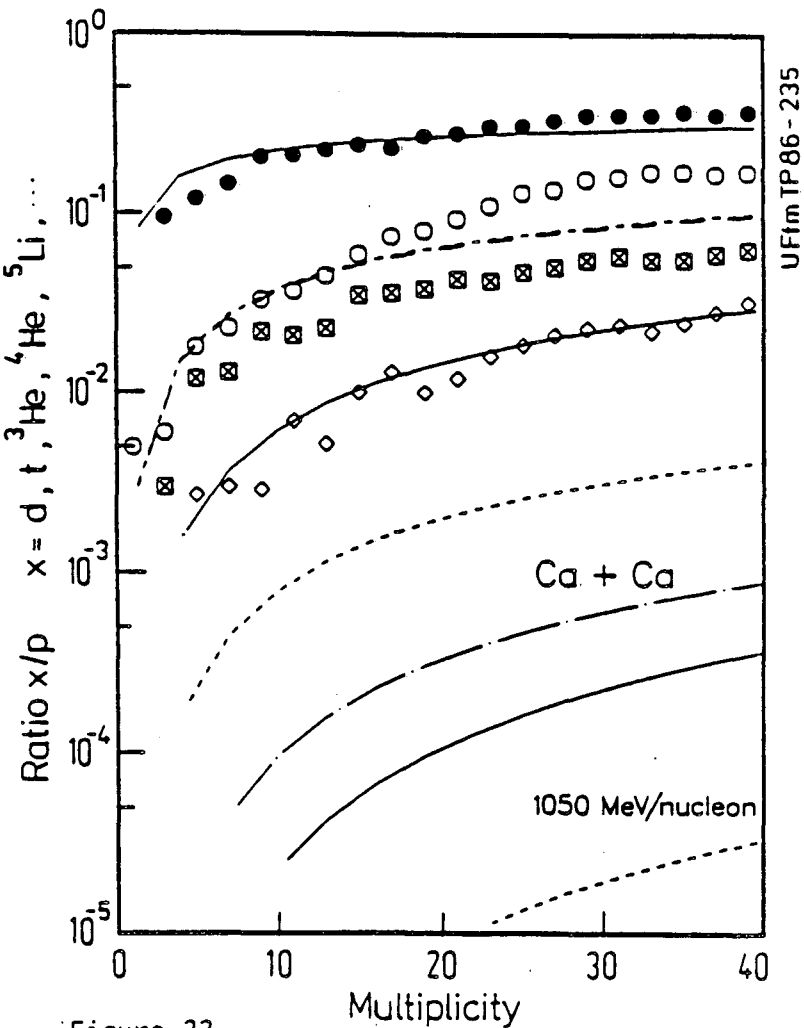

Figure 33

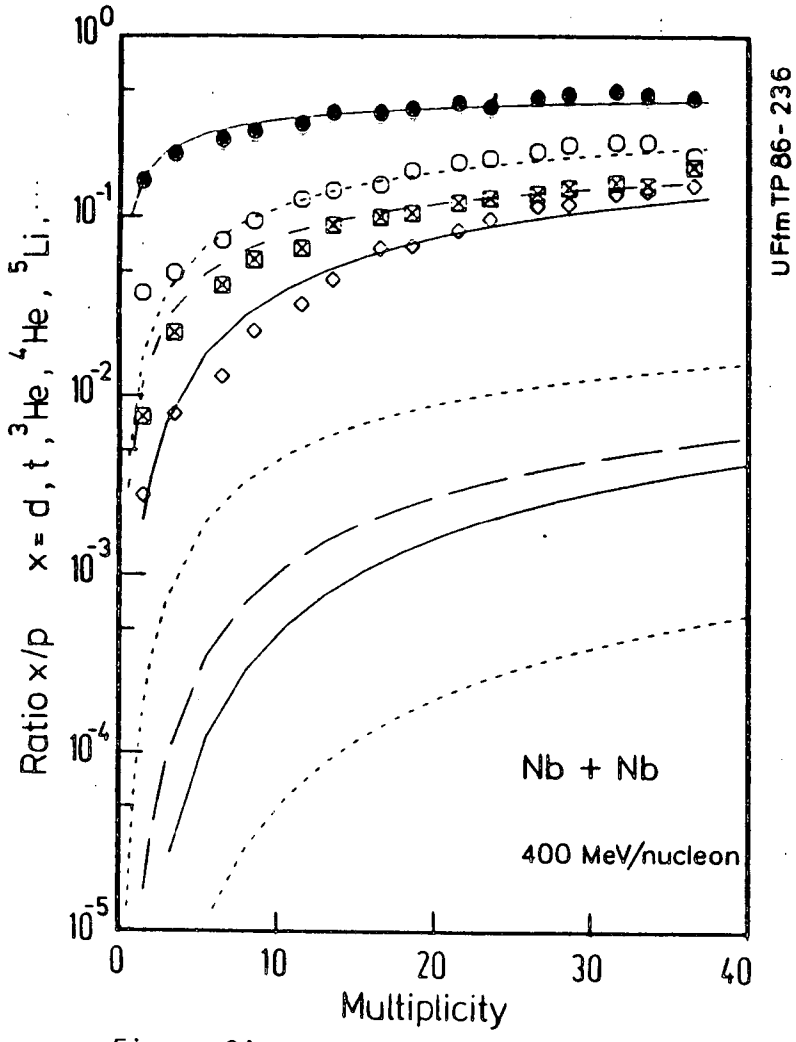

Figure 34a

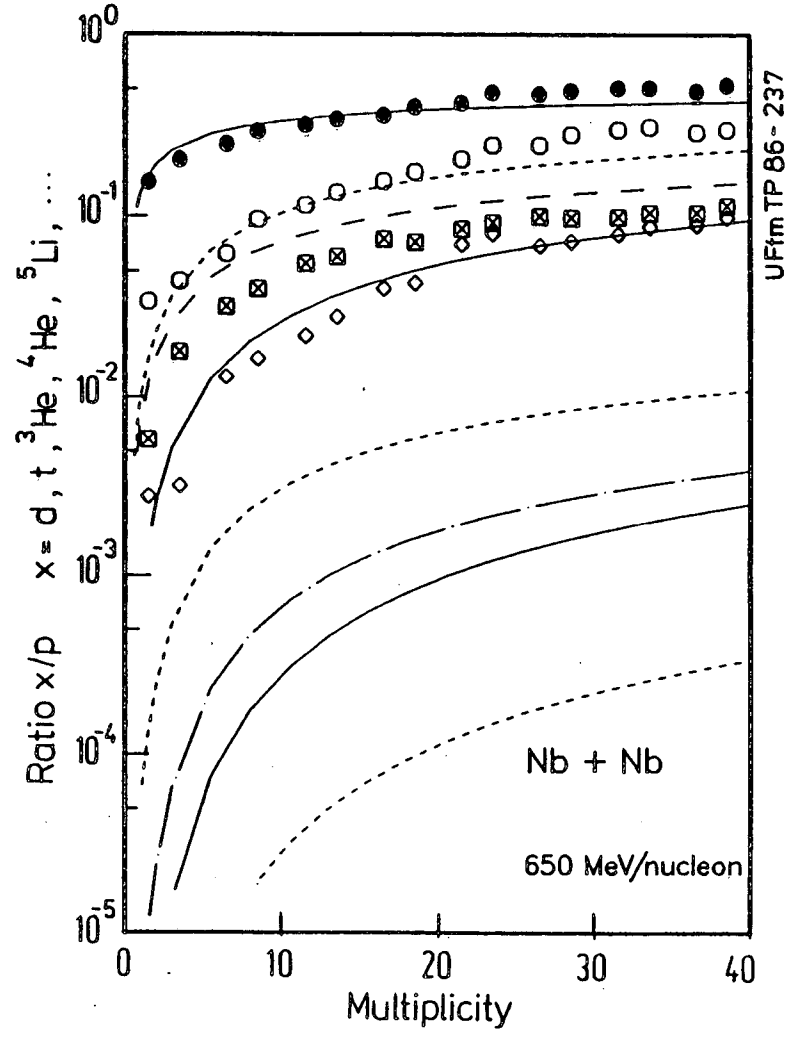

Figure 34b

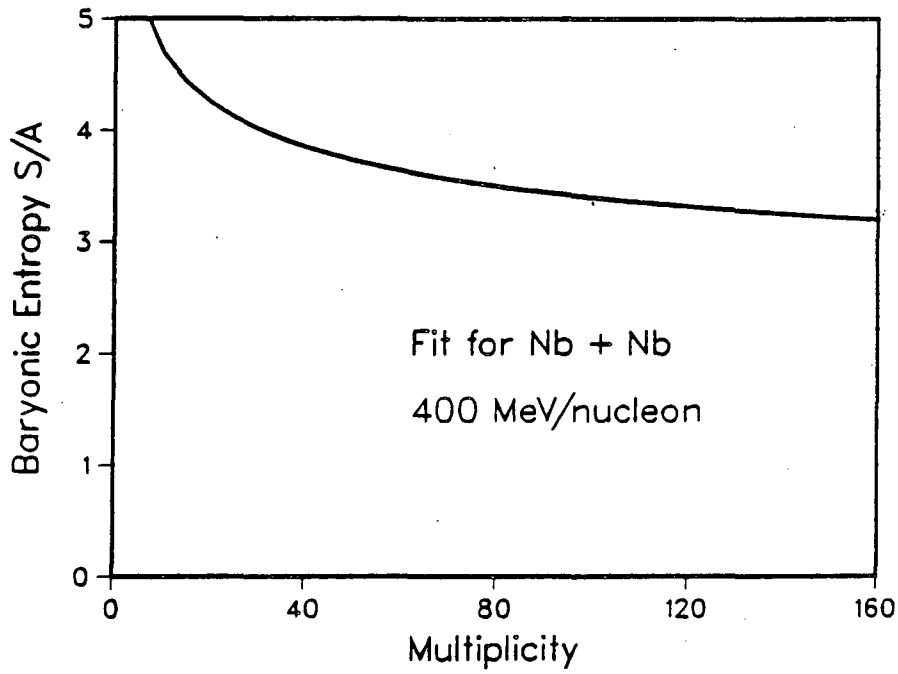
Baryonic Entropy S/A
5
4
3
2
1
0
0
40
80
120
160
Multiplicity
Fit for Nb + Nb
400 MeV/nucleon

Figure 35

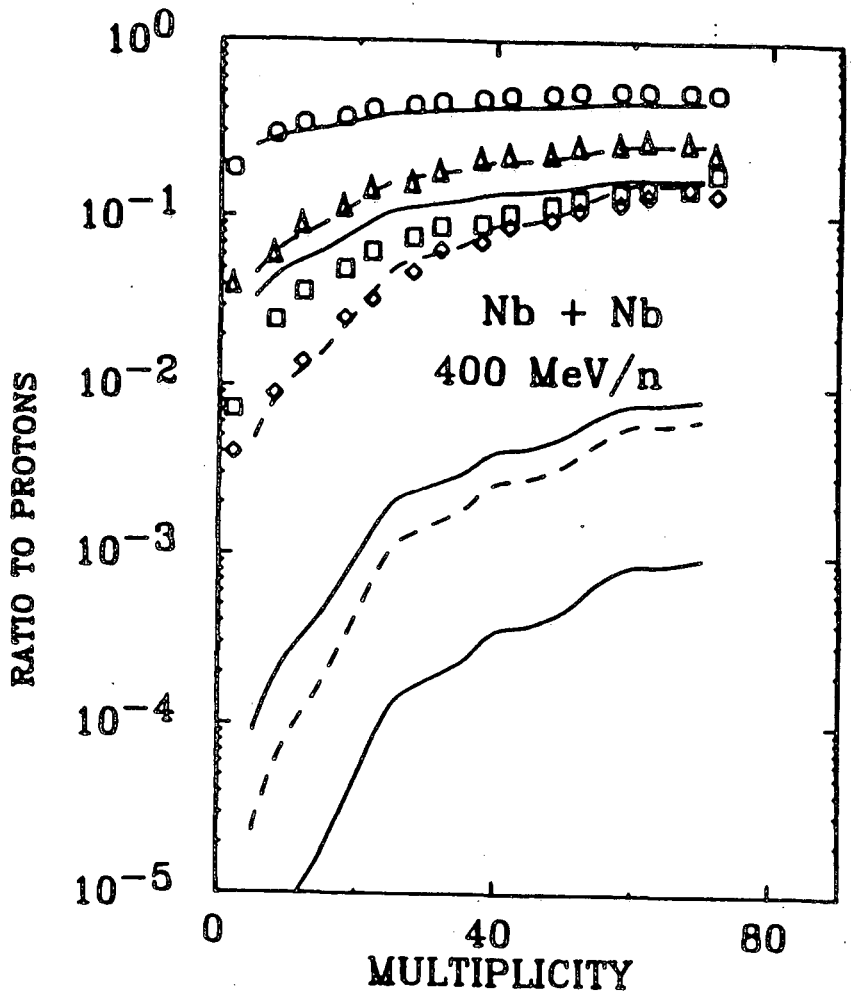

Figure 36a

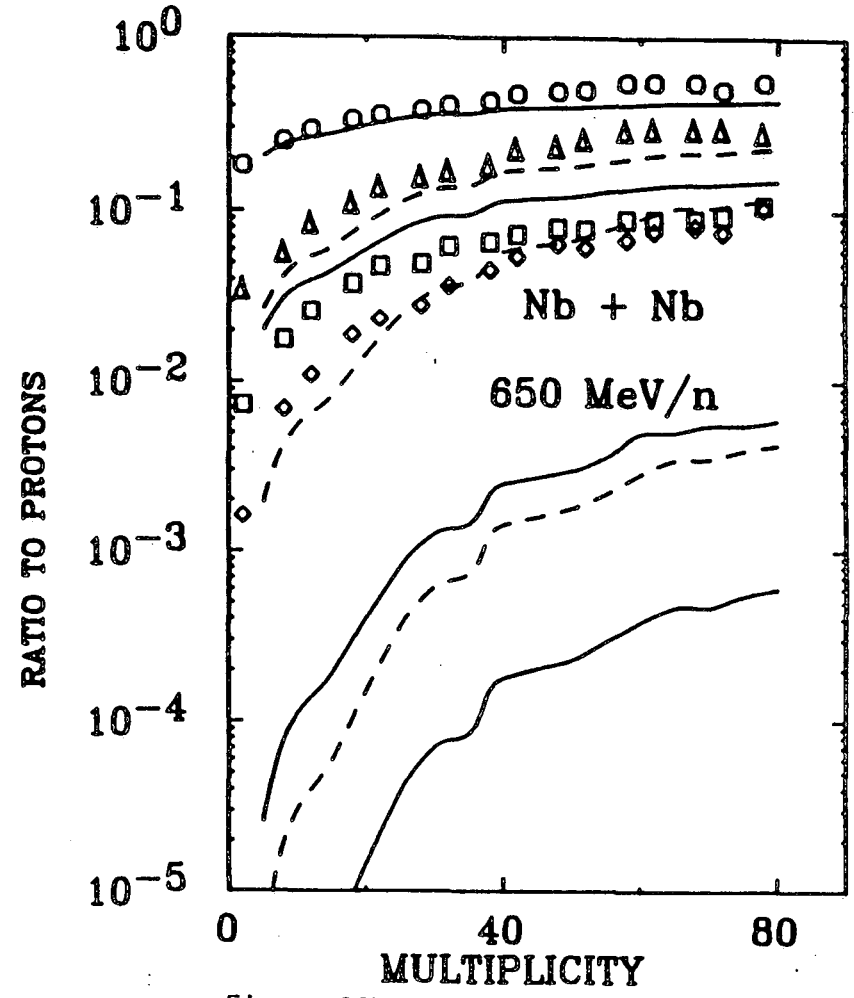

Figure 36b

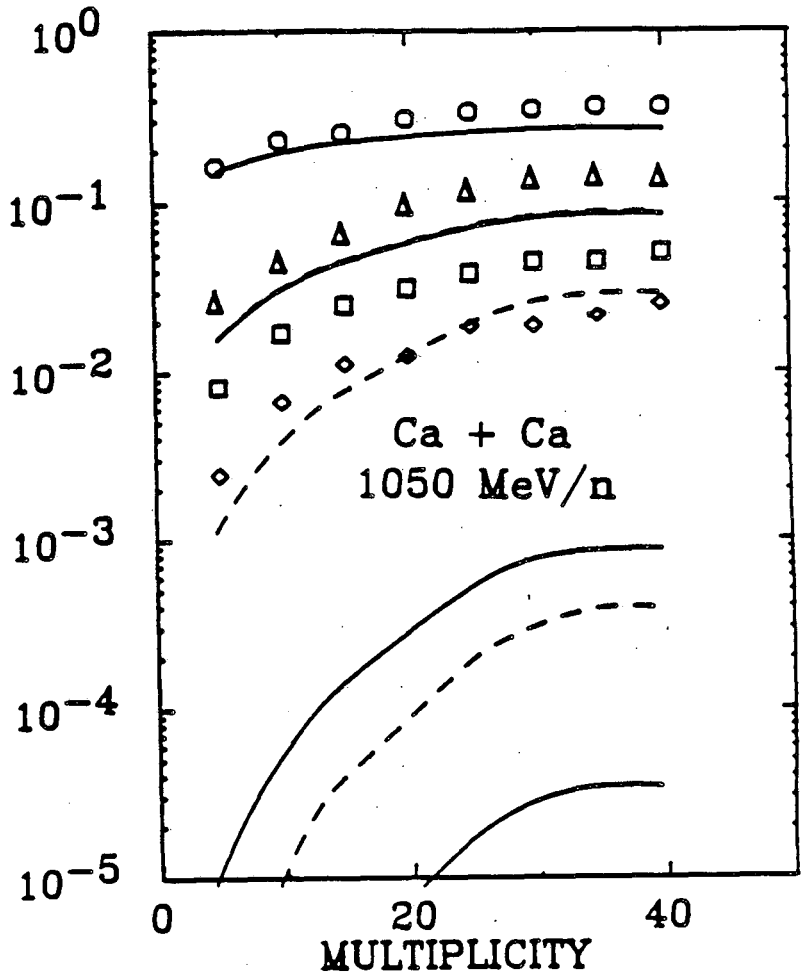

Figure 37

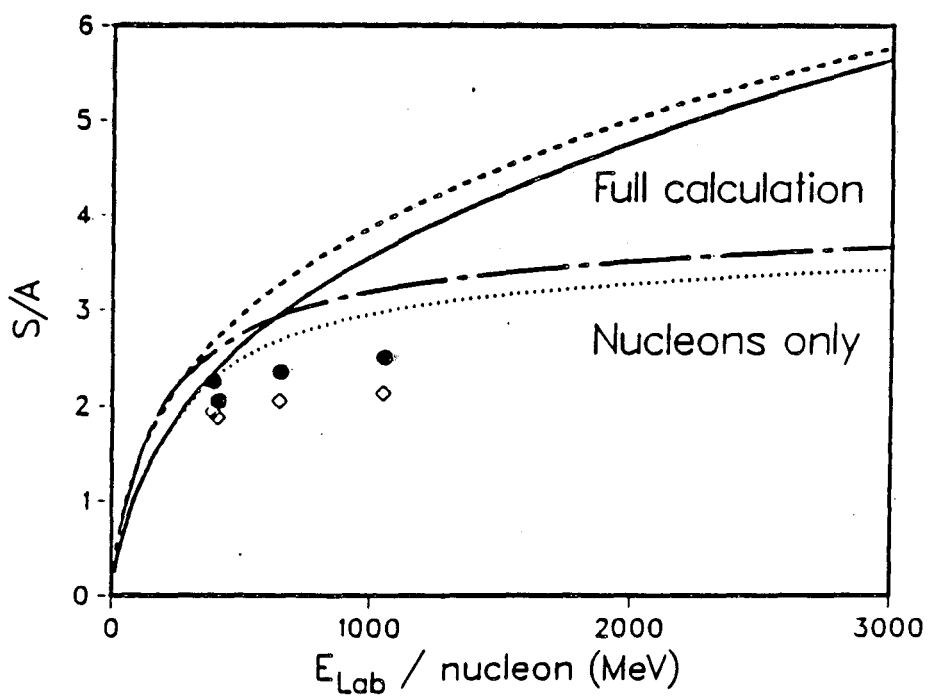

Figure 38

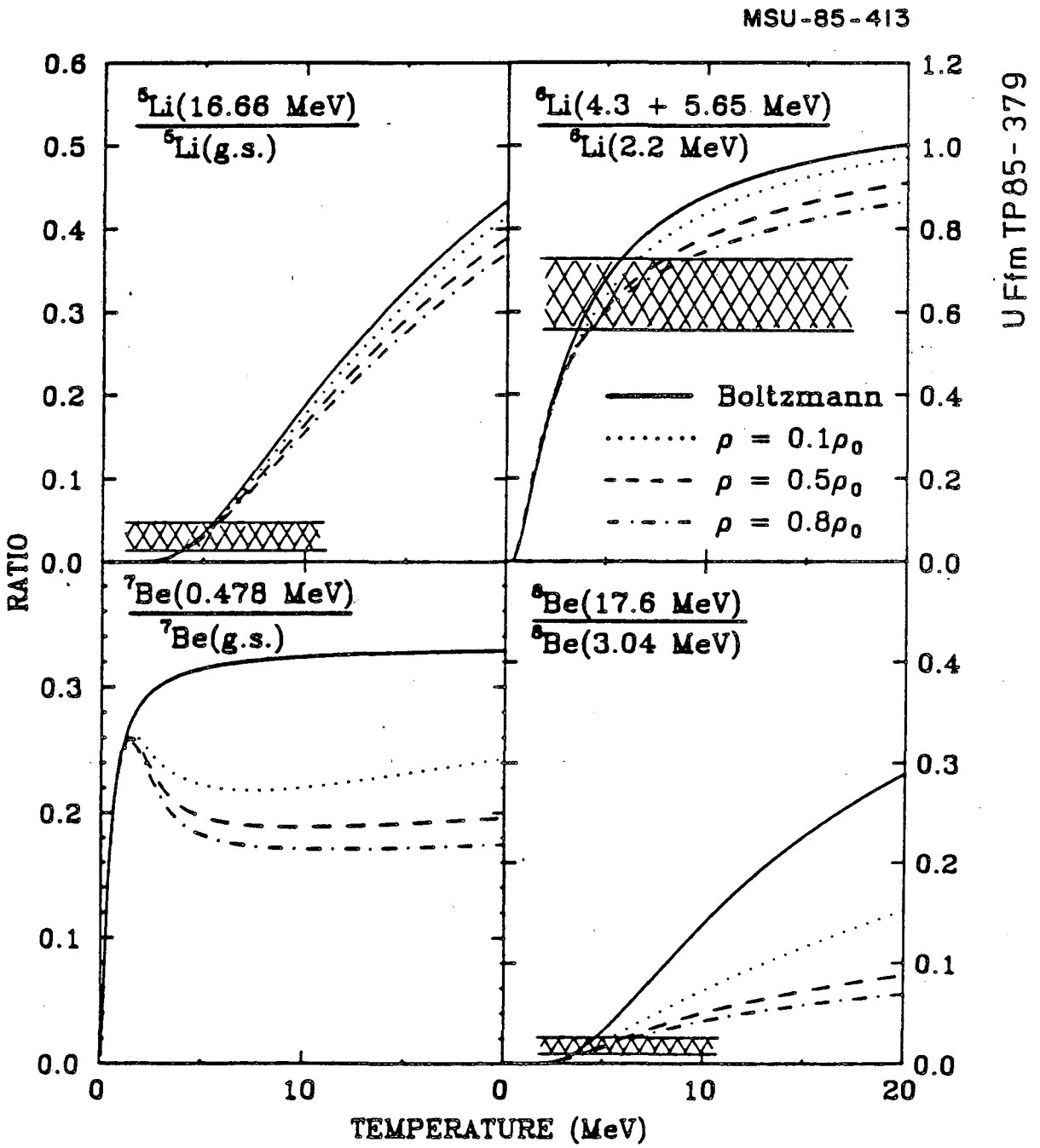
MSU-85-413
UFfm TP85-379
^{5}Li(16.66 MeV) / ^{5}Li(g.s.)
^{6}Li(4.3 + 5.65 MeV) / ^{6}Li(2.2 MeV)
^{7}Be(0.478 MeV) / ^{7}Be(g.s.)
^{8}Be(17.6 MeV) / ^{8}Be(3.04 MeV)
Boltzmann
$\rho = 0.1\rho_0$
$\rho = 0.5\rho_0$
$\rho = 0.8\rho_0$
RATIO
TEMPERATURE (MeV)
0.0
0.1
0.2
0.3
0.4
0.5
0.6
0.8
1.0
1.2
0
10
20

Figure 39

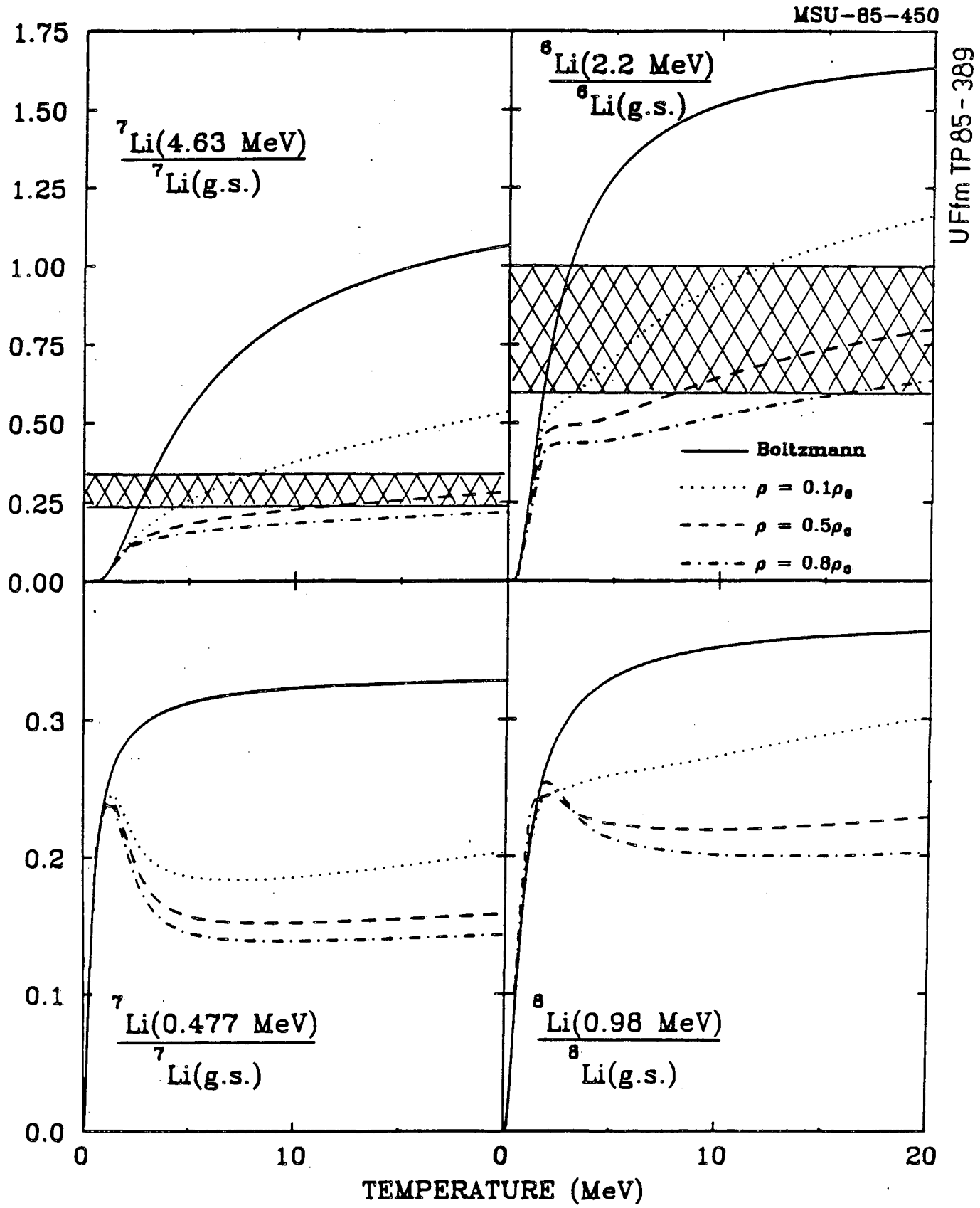
MSU-85-450
UFfm TP85-389
1.75
1.50
1.25
1.00
0.75
0.50
0.25
0.00
0.3
0.2
0.1
0.0
0
10
0
10
20
TEMPERATURE (MeV)
7Li(4.63 MeV) / 7Li(g.s.)
6Li(2.2 MeV) / 6Li(g.s.)
7Li(0.477 MeV) / 7Li(g.s.)
8Li(0.98 MeV) / 8Li(g.s.)
Boltzmann
ρ = 0.1ρ0
ρ = 0.5ρ0
ρ = 0.8ρ0

Figure 40

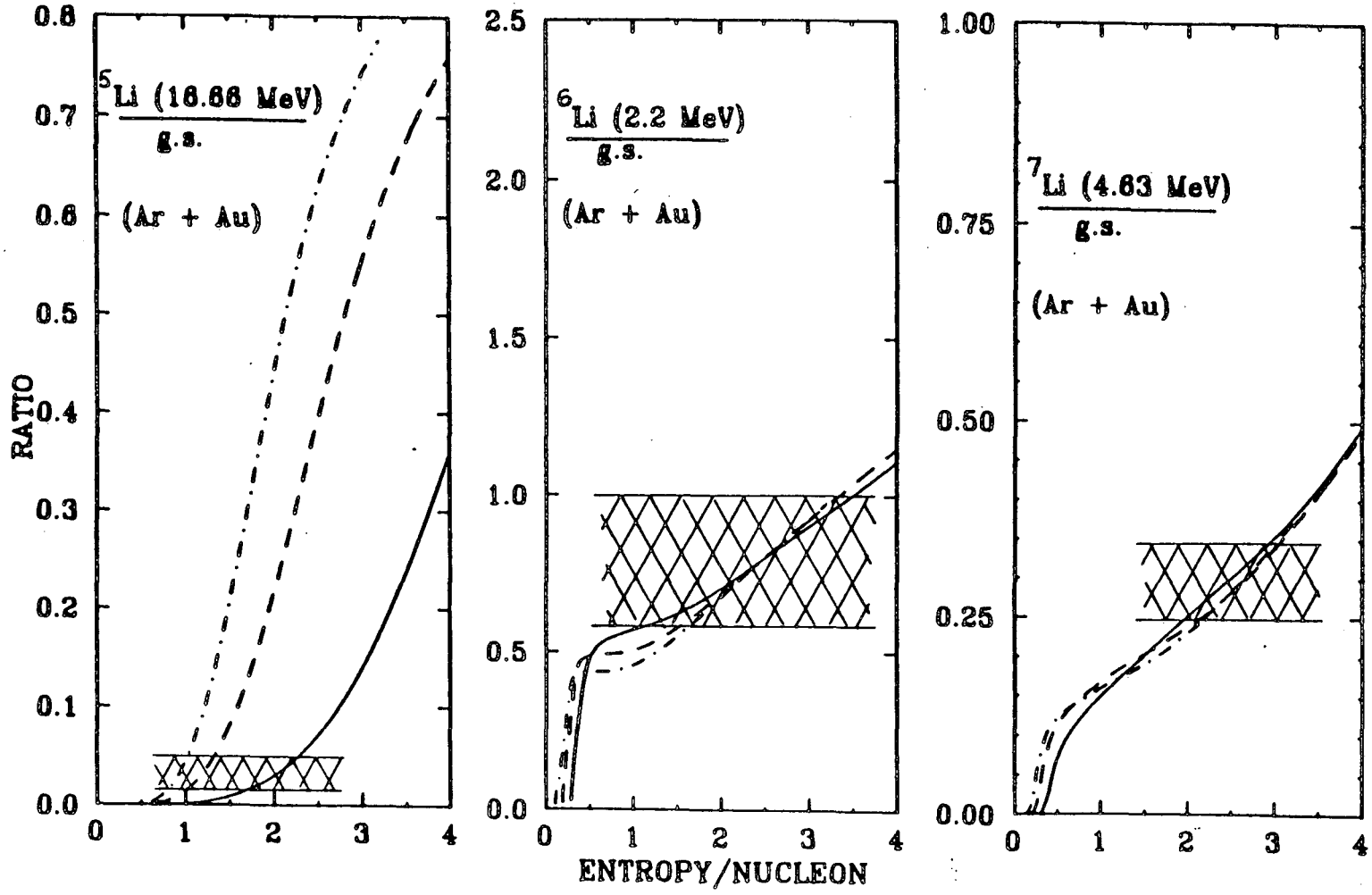
RATIO
^{5}Li (16.66 MeV)
g.s.
(Ar + Au)
^{6}Li (2.2 MeV)
g.s.
(Ar + Au)
^{7}Li (4.63 MeV)
g.s.
(Ar + Au)
ENTROPY/NUCLEON

Figure 41

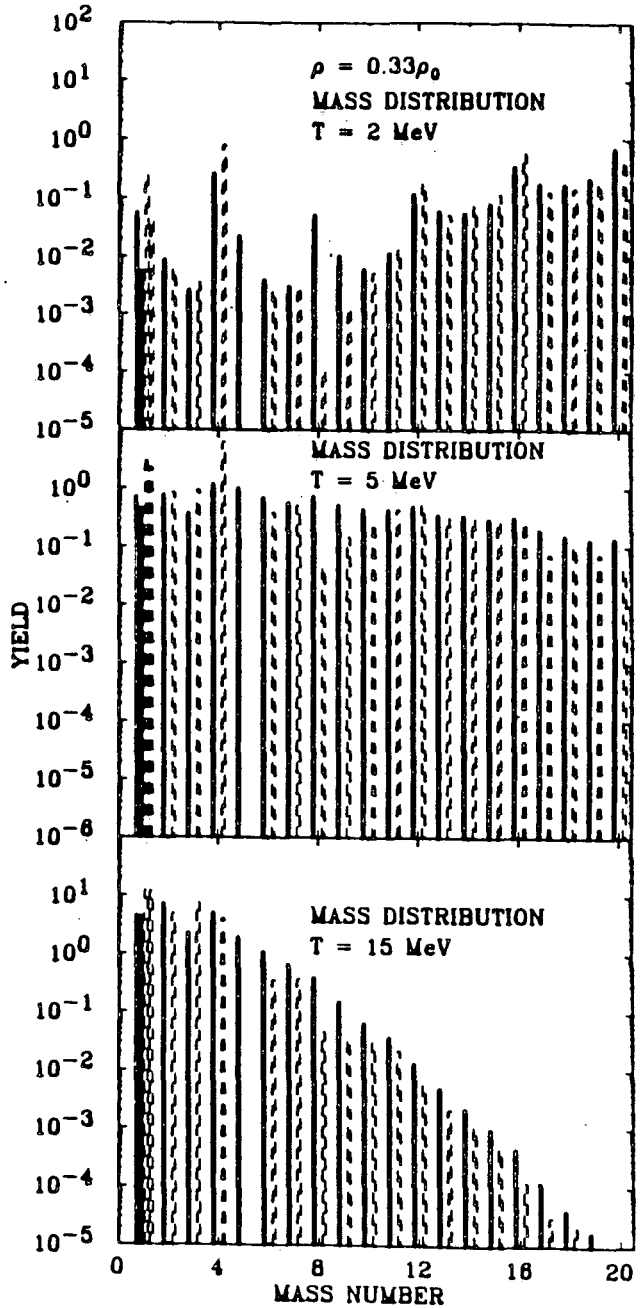

Figure 42

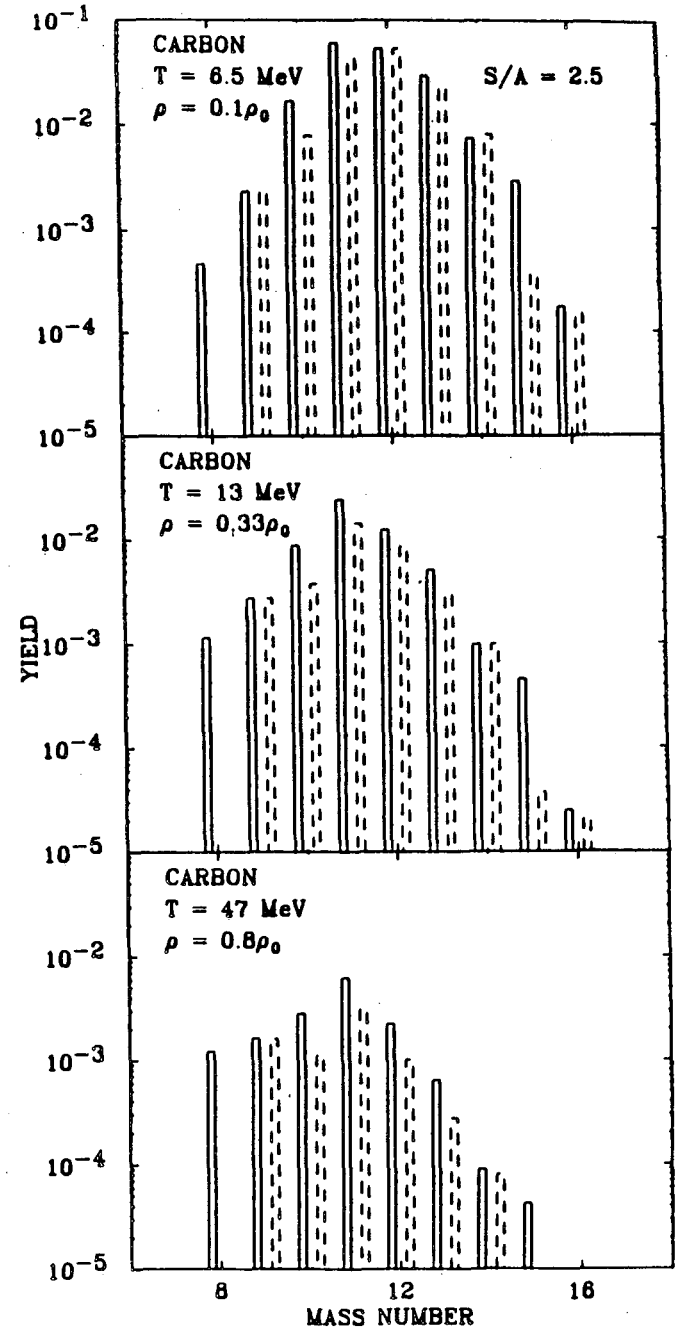

Figure 43

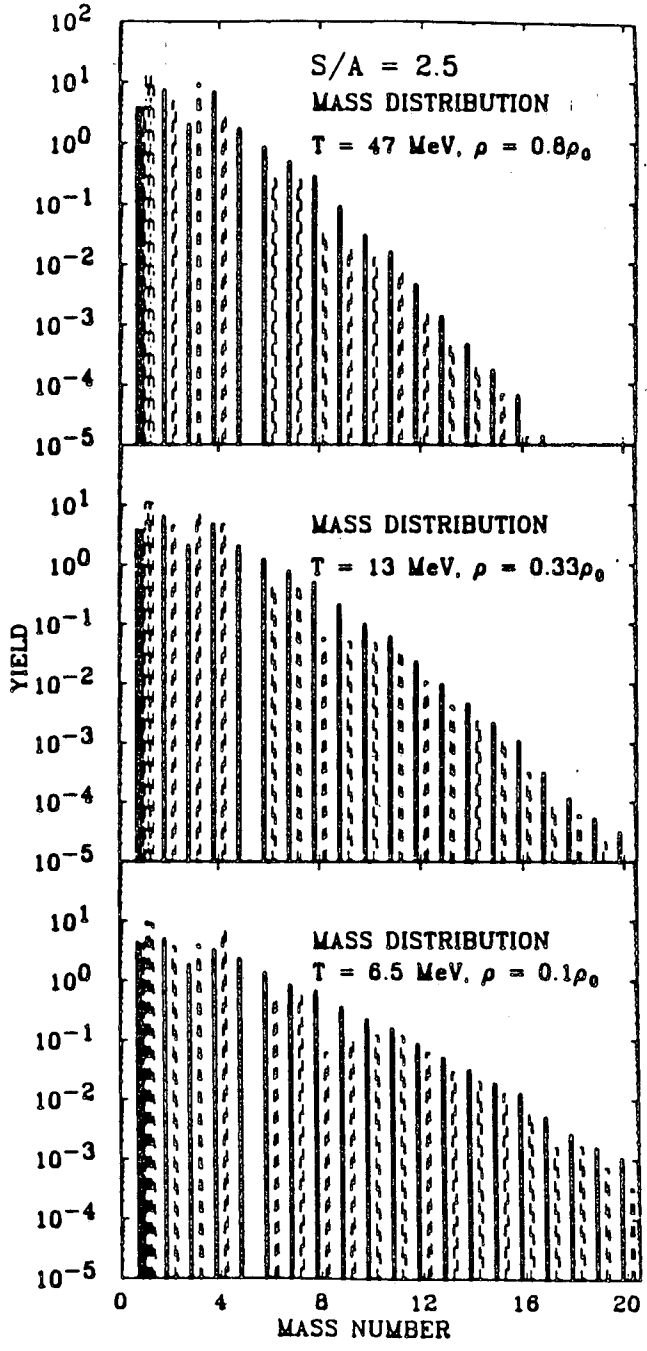

Figure 44

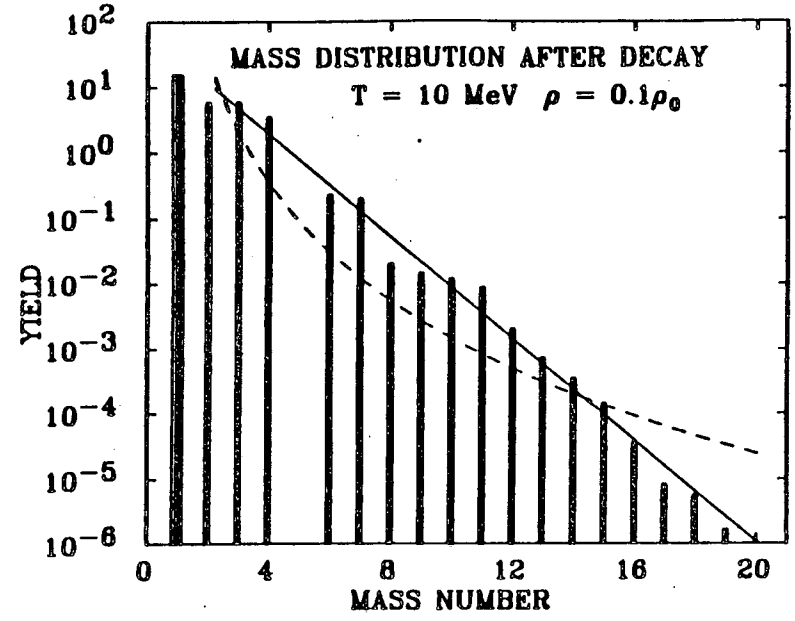

Figure 45

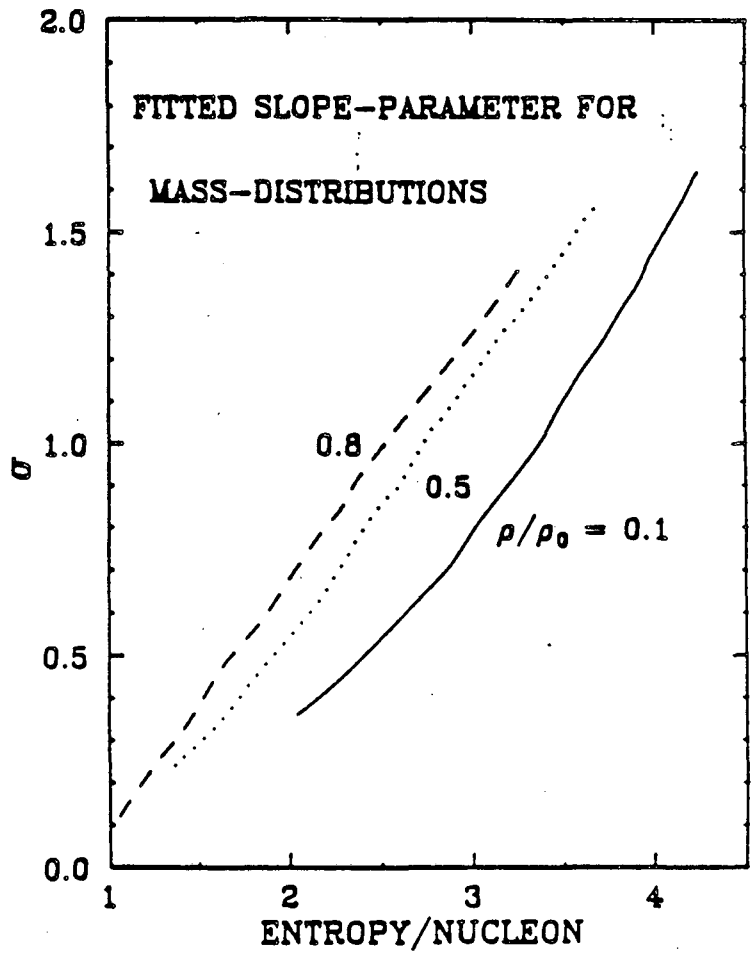
FITTED SLOPE-PARAMETER FOR
MASS-DISTRIBUTIONS
2.0
1.5
1.0
0.5
0.0
σ
0.8
0.5
ρ/ρ₀ = 0.1
1
2
3
4
ENTROPY/NUCLEON

Figure 46

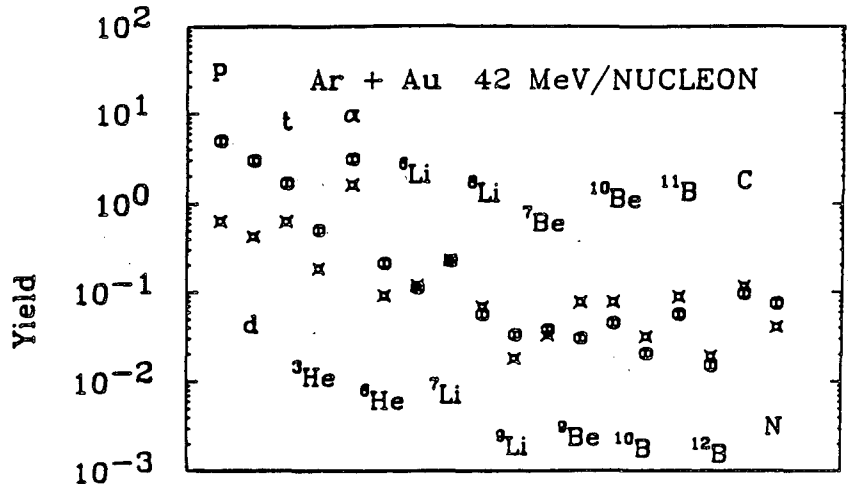

Figure 47a

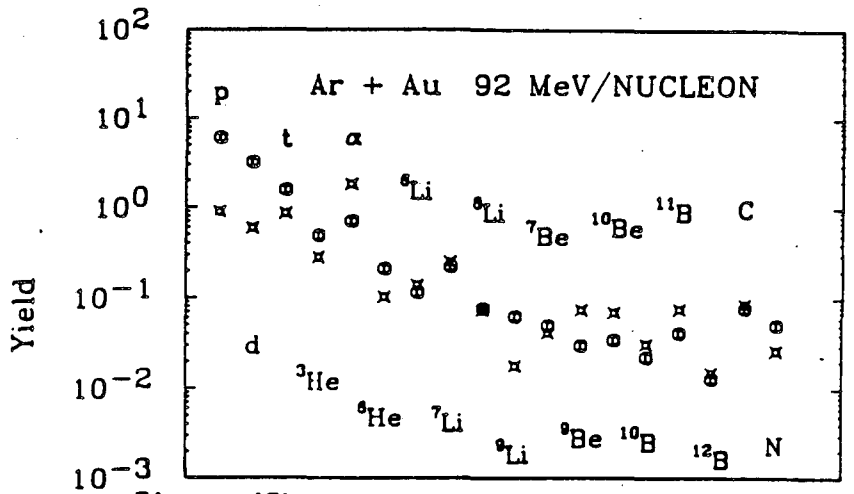

Figure 47b

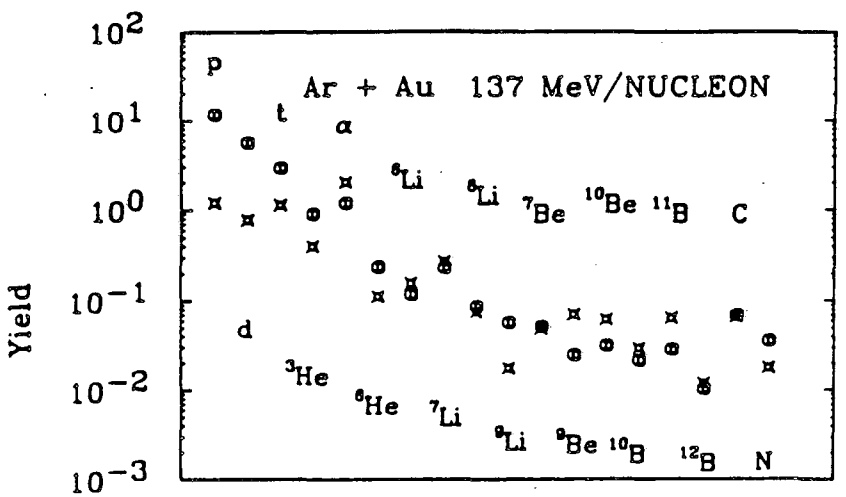

Figure 47c

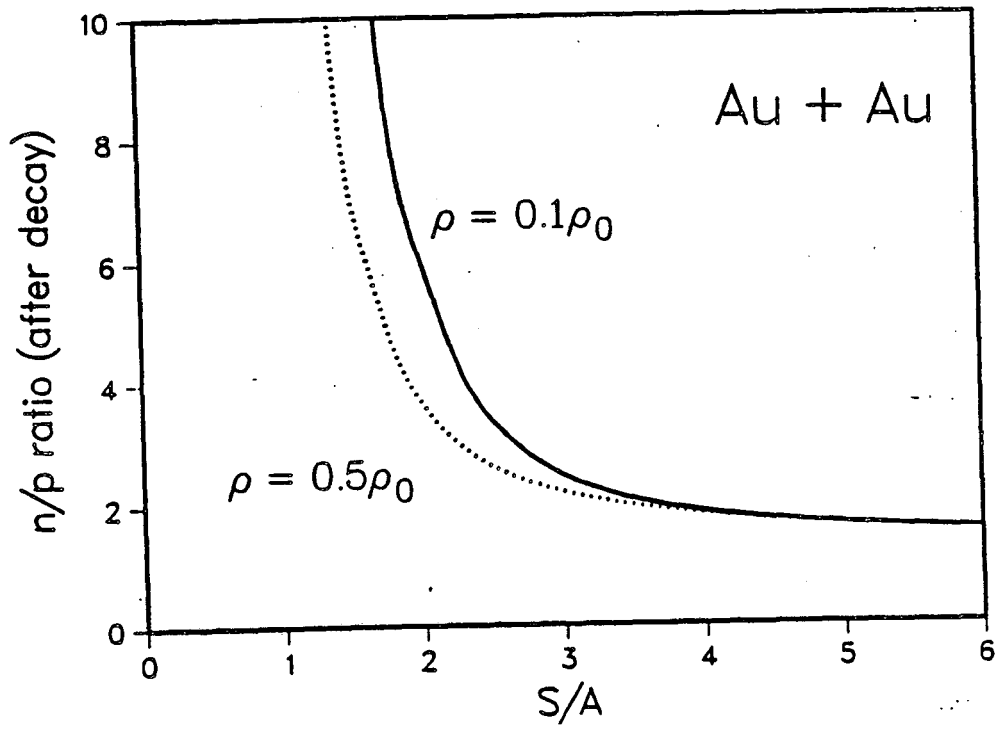

Figure 48a

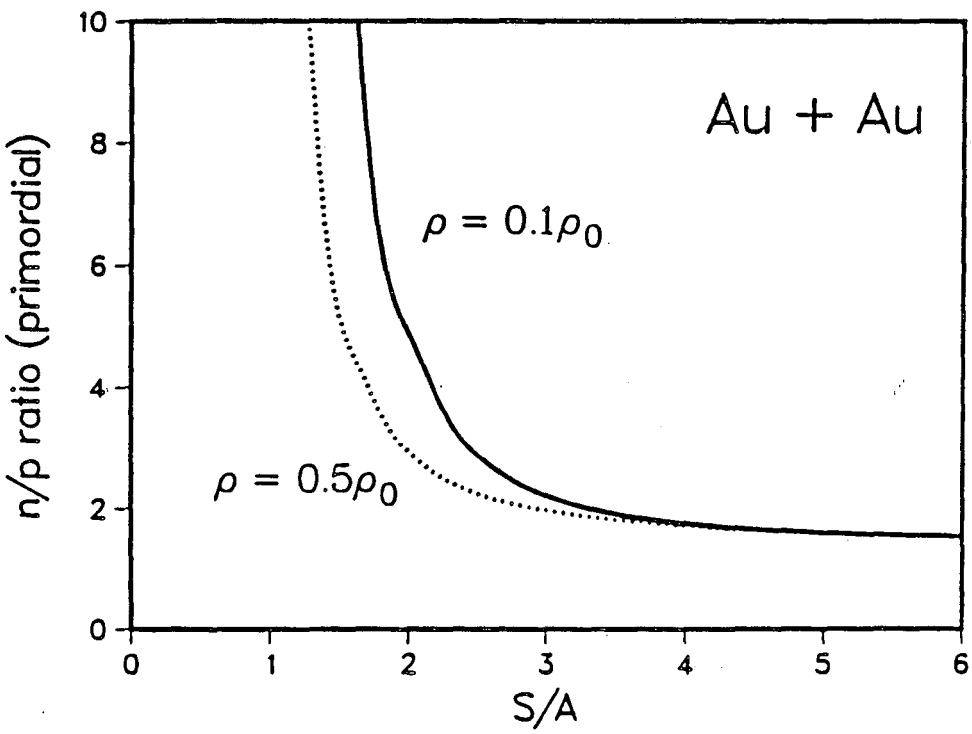

Figure 48b

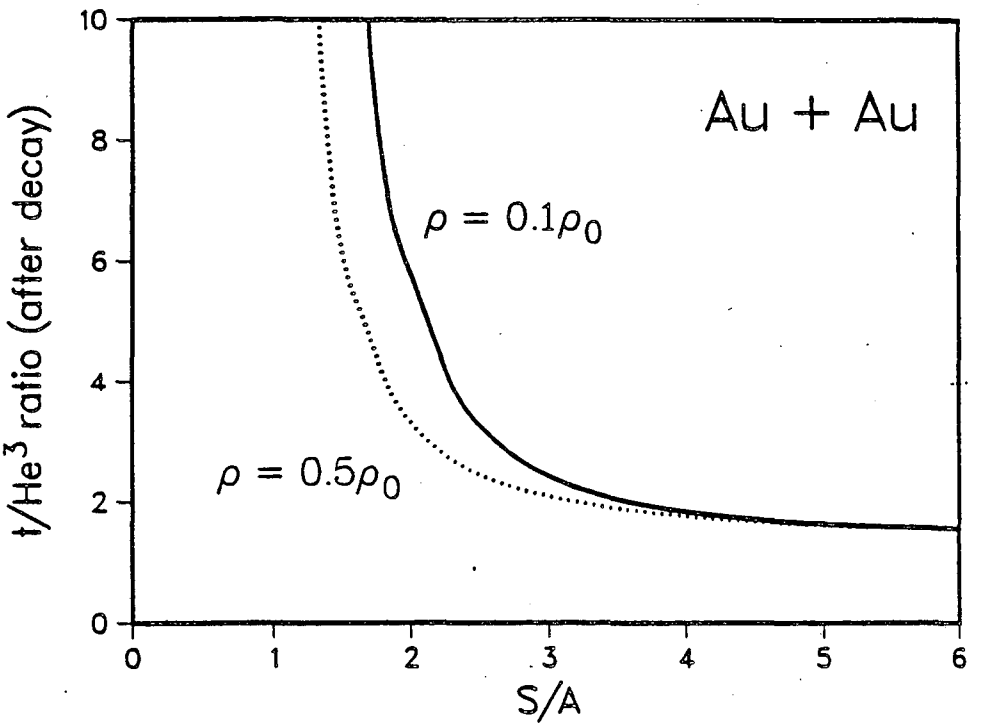

Figure 49

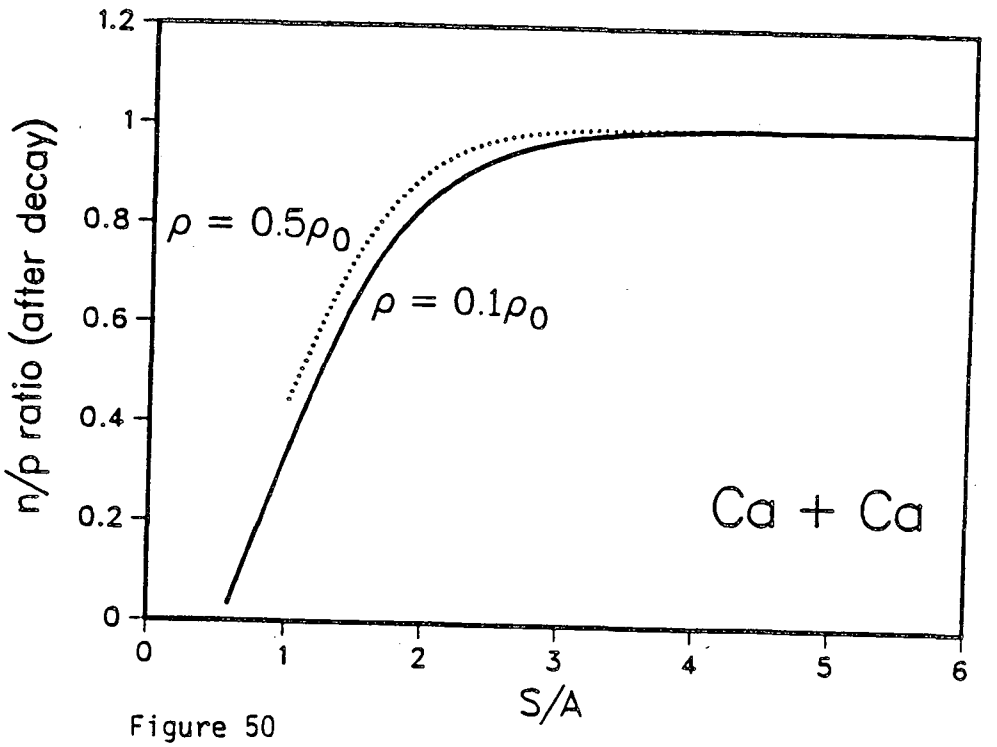

Figure 50

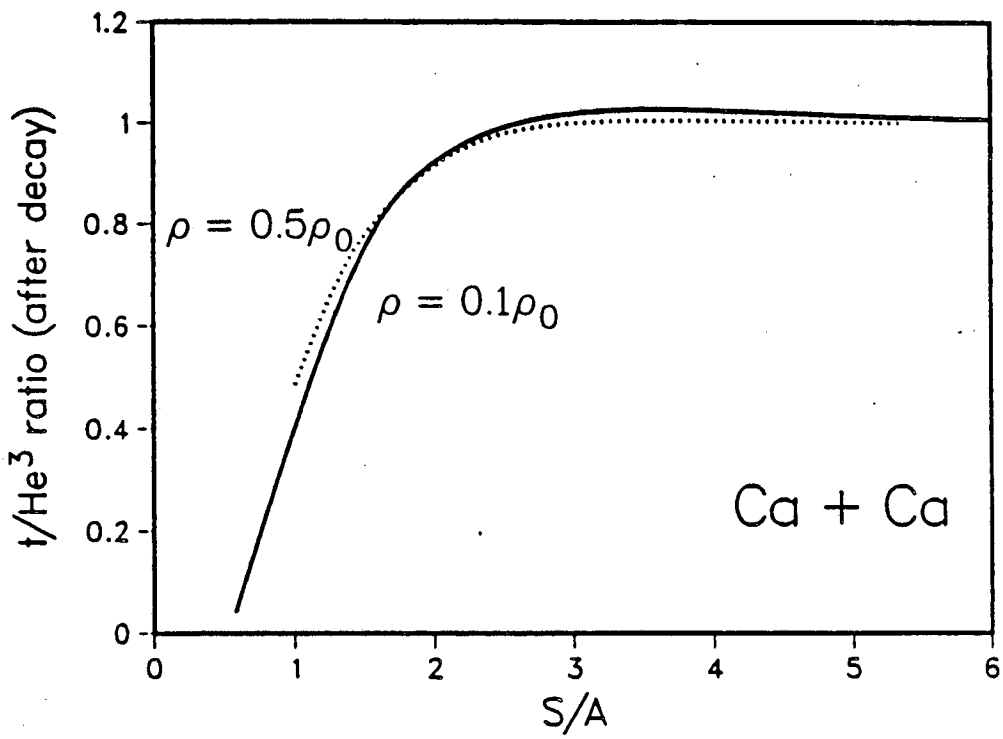
1.2
1
0.8
0.6
0.4
0.2
0
t/He3 ratio (after decay)
ρ = 0.5ρ0
ρ = 0.1ρ0
Ca + Ca
0
1
2
3
4
5
6
S/A

Figure 51

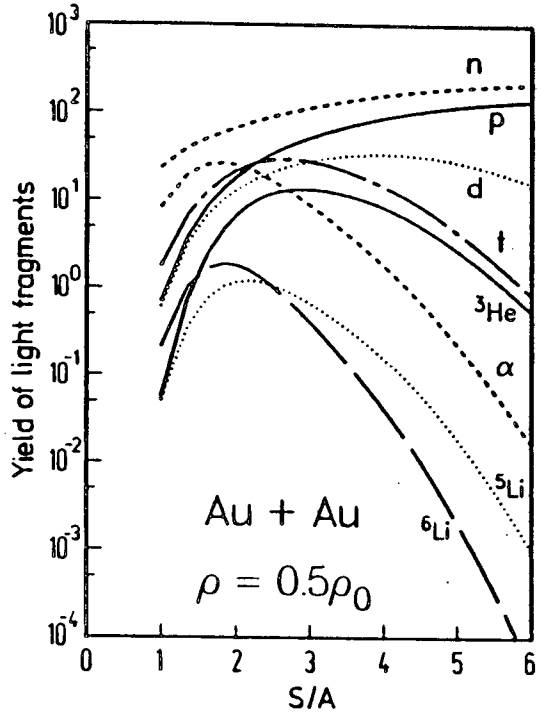

Figure 52a

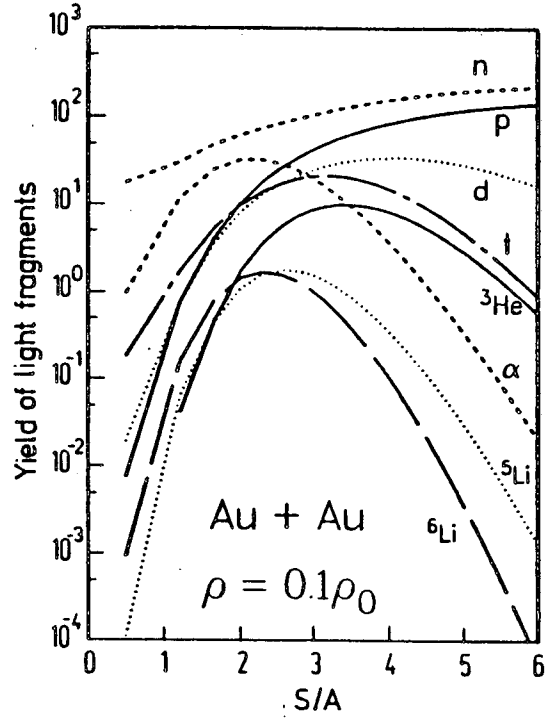

Figure 52b

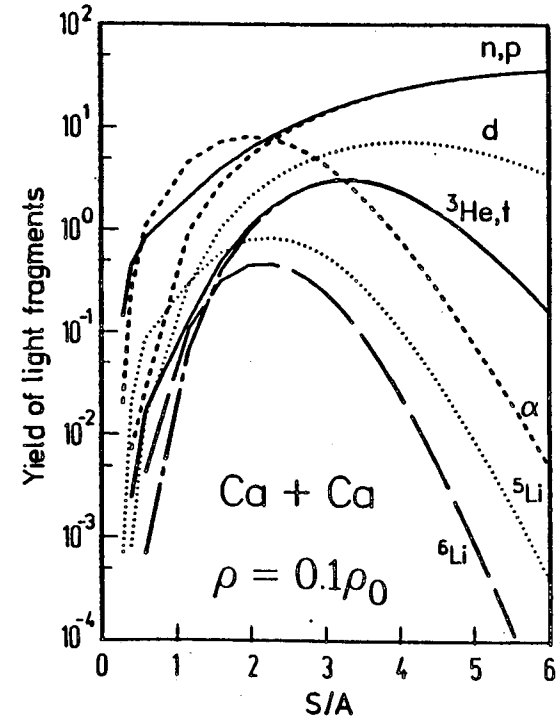

Figure 52c

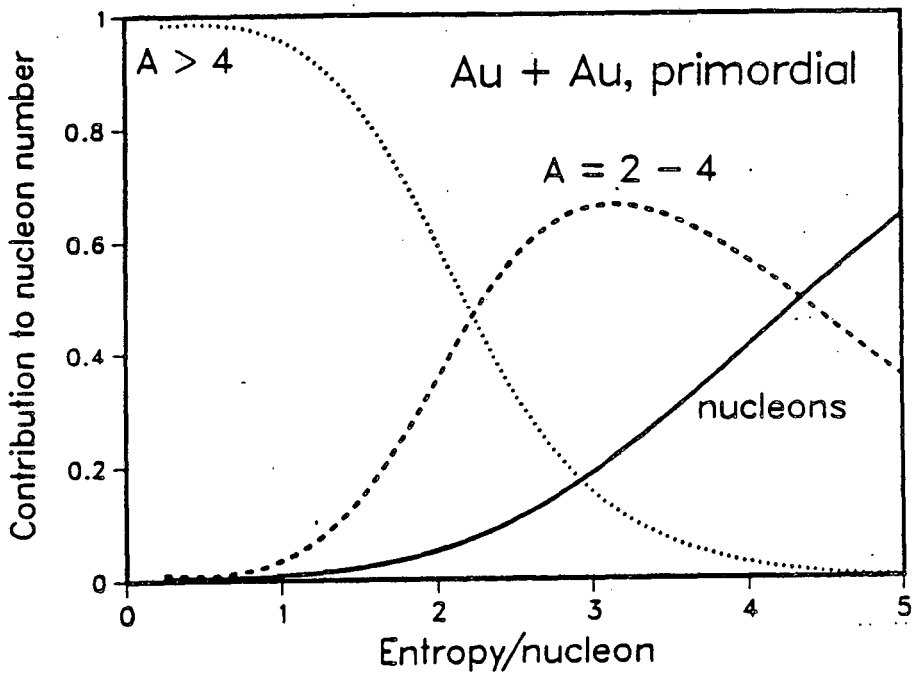

Figure 53a

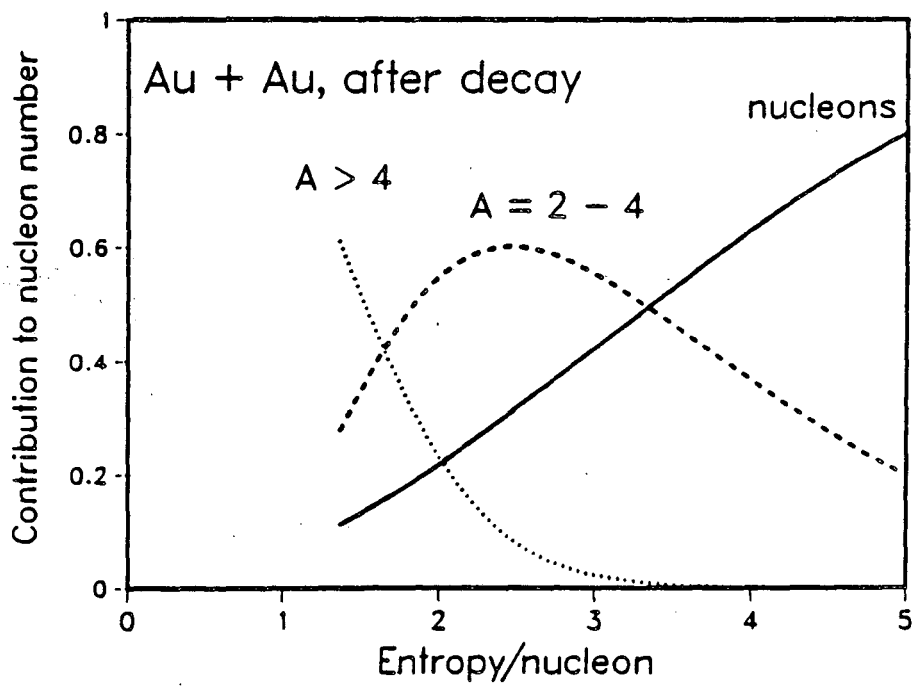

Figure 53b

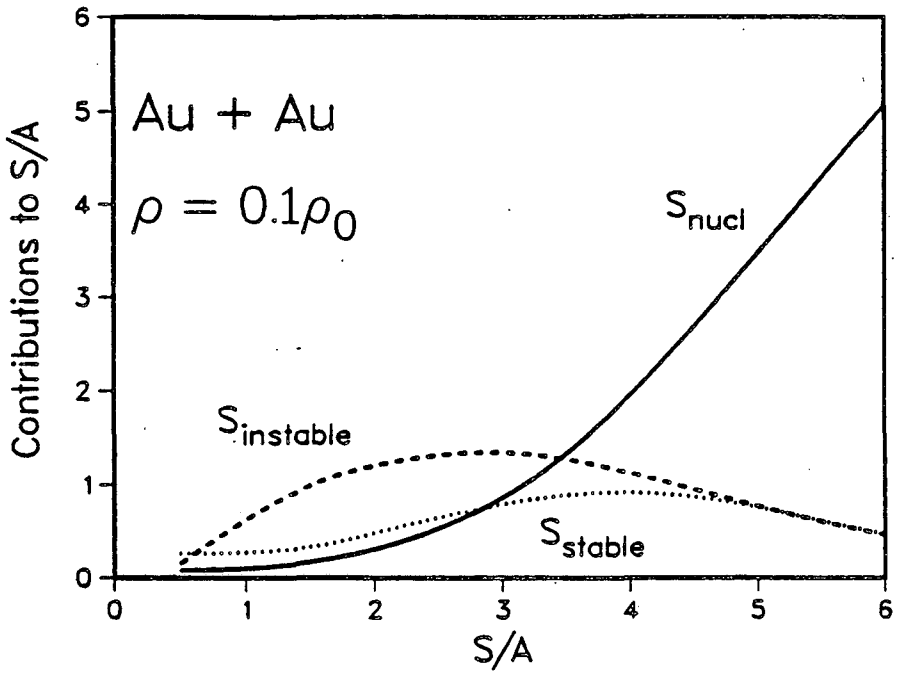

Figure 54a

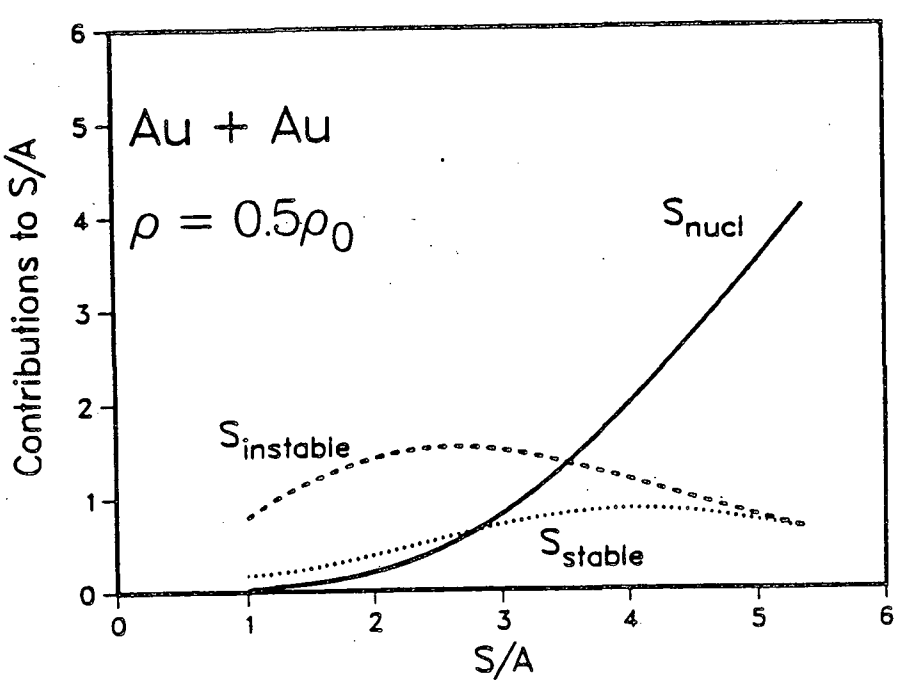

Figure 54b

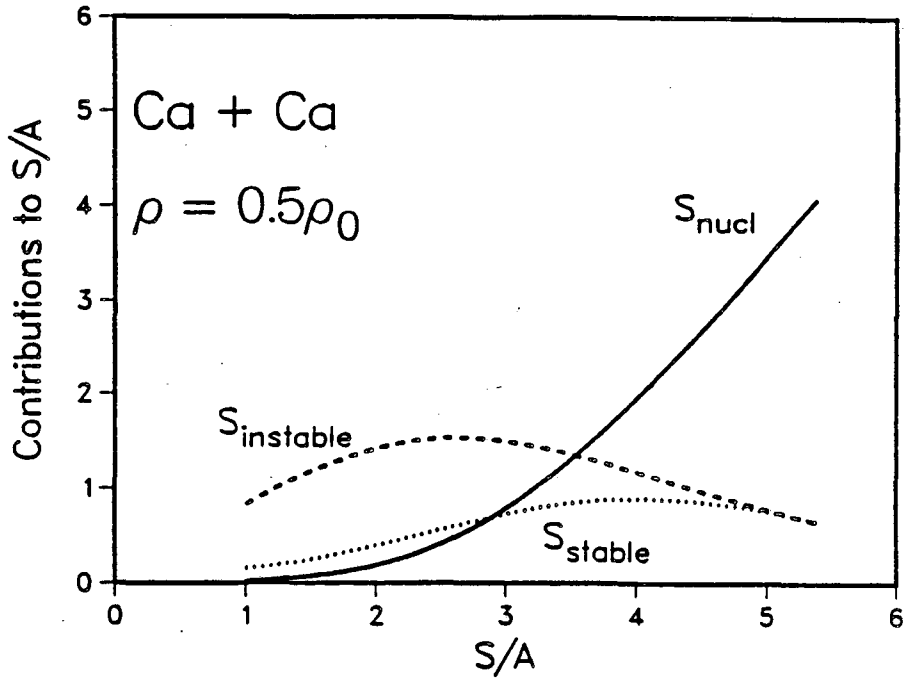

Figure 54c

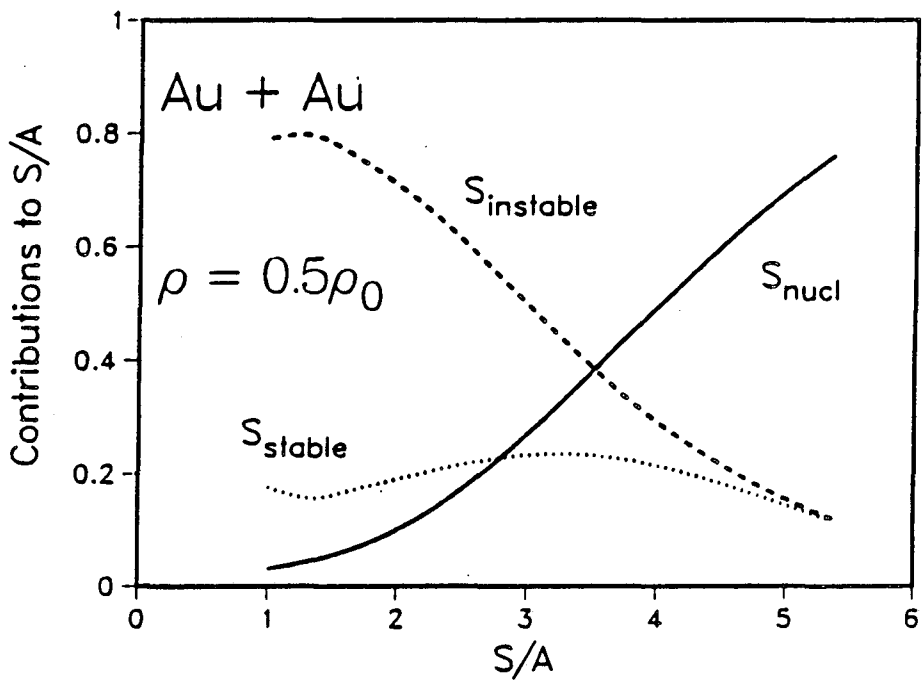

Figure 54d

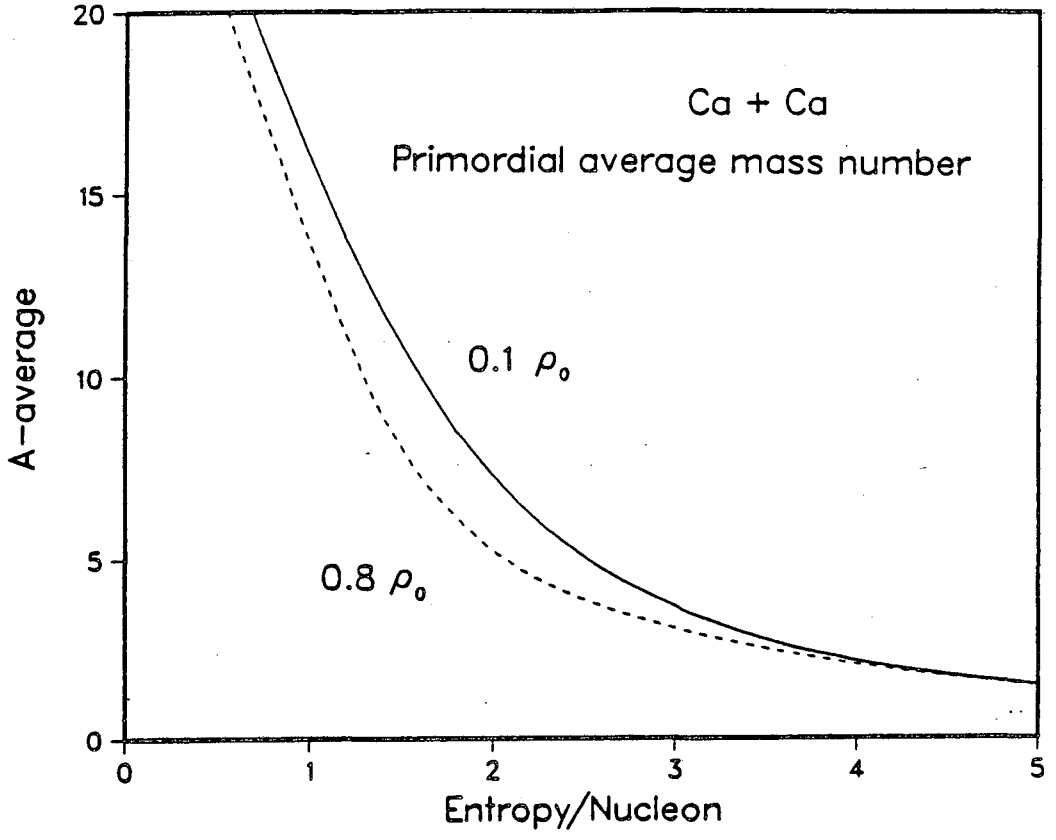

Figure 55a

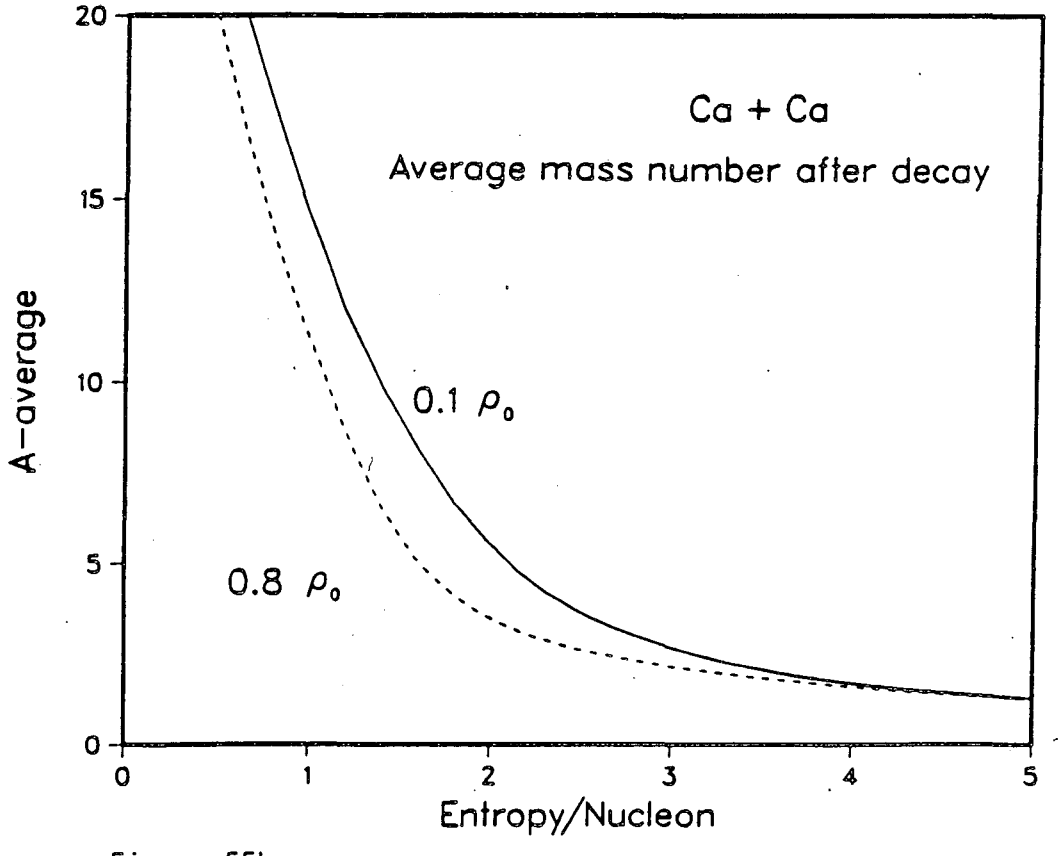

Figure 55b

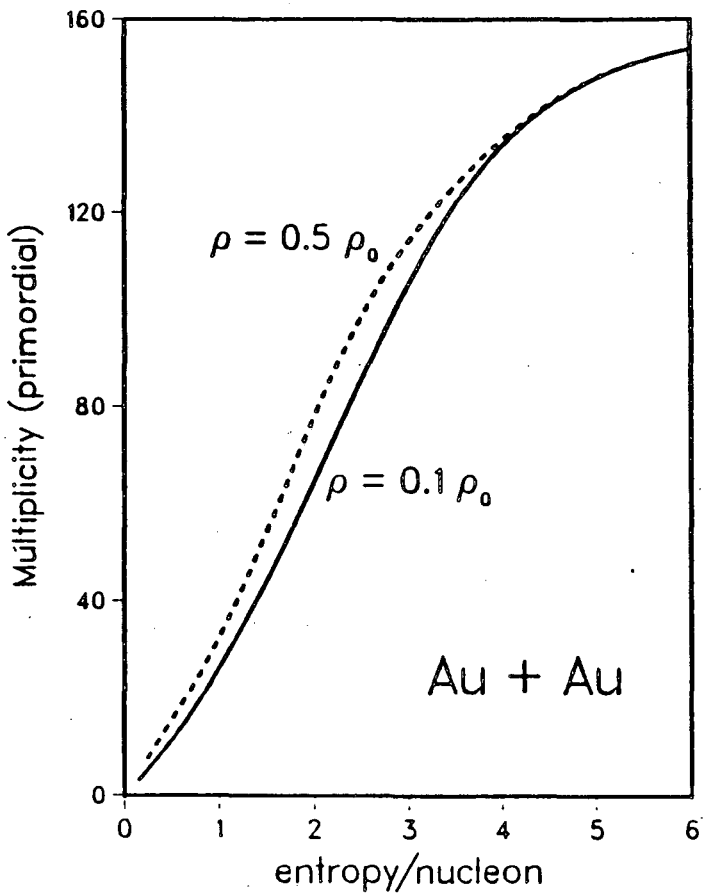

Figure 56a

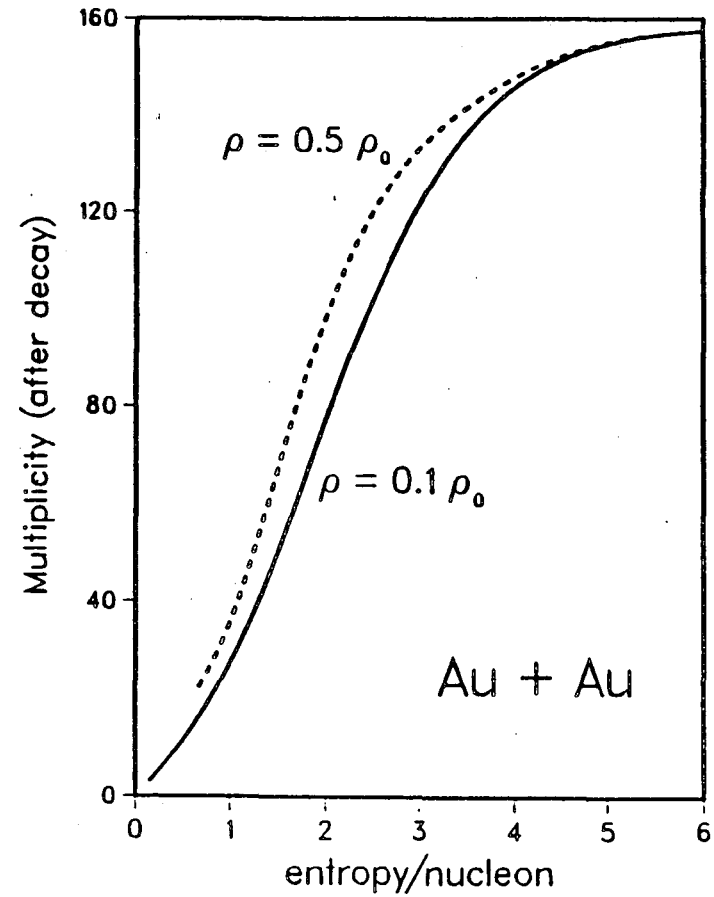

Figure 56b

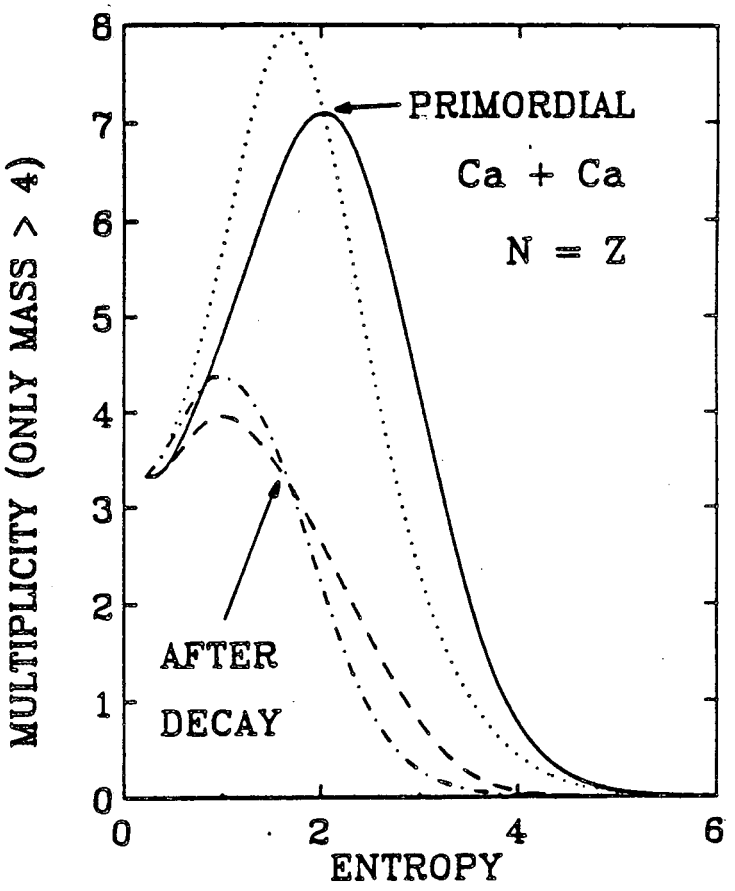
PRIMORDIAL
Ca + Ca
N = Z
AFTER
DECAY
MULTIPLICITY (ONLY MASS > 4)
ENTROPY
0
1
2
3
4
5
6
7
8
0
2
4
6

Figure 57

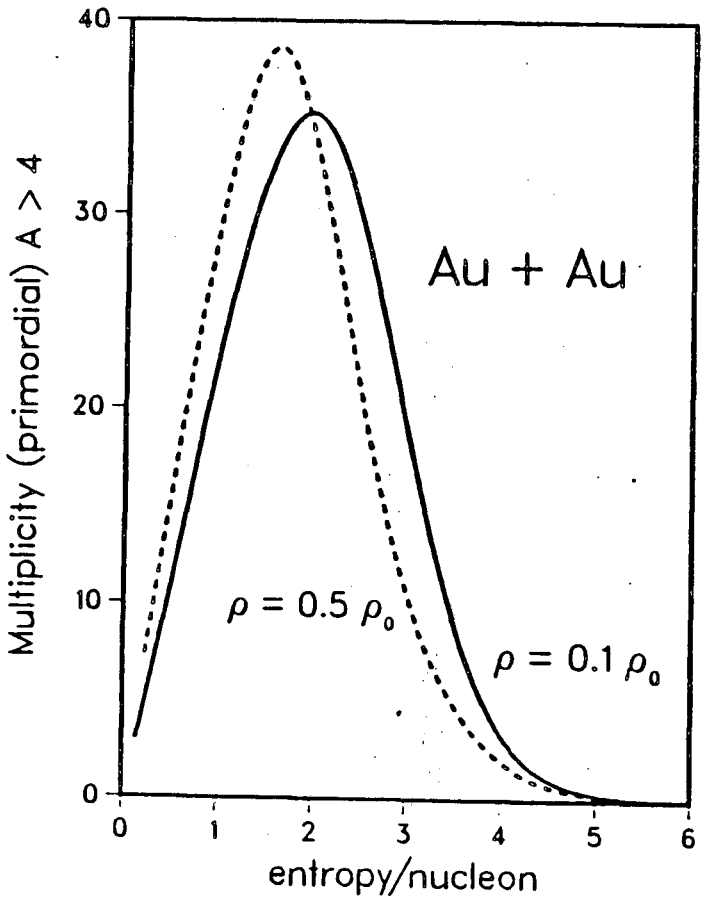

Figure 58a

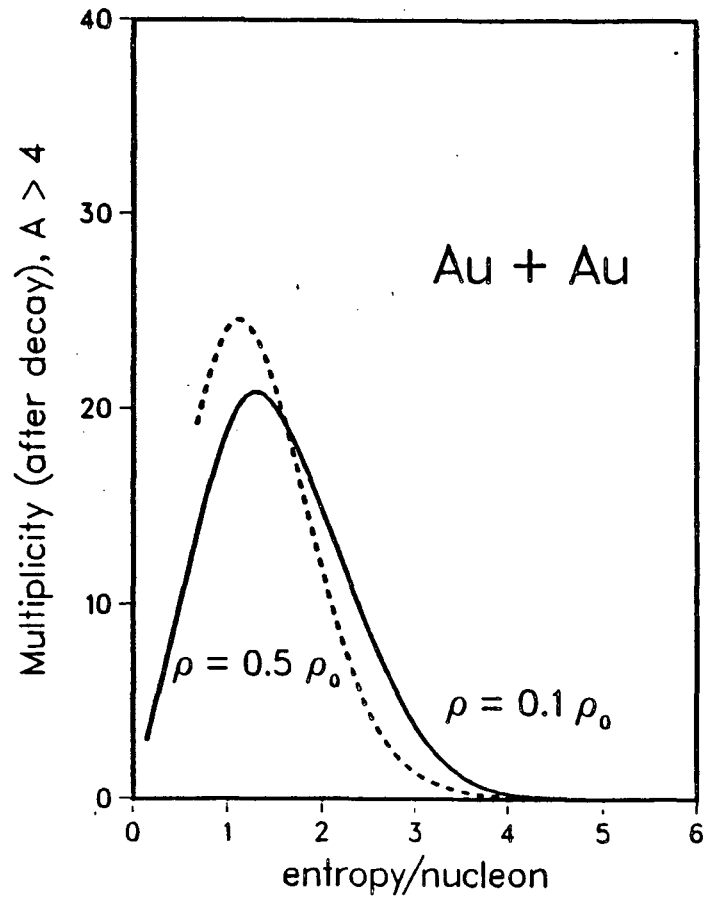

Figure 58b

This report was done with support from the Department of Energy. Any conclusions or opinions expressed in this report represent solely those of the author(s) and not necessarily those of The Regents of the University of California, the Lawrence Berkeley Laboratory or the Department of Energy.

Reference to a company or product name does not imply approval or recommendation of the product by the University of California or the U.S. Department of Energy to the exclusion of others that may be suitable.

LAWRENCE BERKELEY LABORATORY
TECHNICAL INFORMATION DEPARTMENT
UNIVERSITY OF CALIFORNIA
BERKELEY, CALIFORNIA 94720